ION MOBILITY AND MASS SPECTROMETRIC INVESTIGATIONS OF ORGANOPHOSPHATES RELATED TO CHEMICAL WARFARE AGENTS AND PESTICIDES

by

SARAH ELLEN PRICE

A thesis submitted to
The University of Birmingham
for the degree of
DOCTOR OF PHILOSOPHY

School of Physics and Astronomy
The University of Birmingham
June 2010

ABSTRACT

A commercial Ion Mobility Spectrometer (IMS) (Smiths Detection Ltd, GID-M) that is designed to detect Chemical Warfare Agents (CWAs), was modified by the addition of a second ion gate, and connected to a commercial Ion Trap Mass Spectrometer (ITMS) (Finnigan LCQ Classic). The addition of the second gate allows selection of individual ion mobility peaks for m/z analysis in the ITMS. This was demonstrated with the organophosphate DiMethyl MethylPhosphonate (DMMP, a CWA simulant) and two organophosphites. It was found that the modification of the IMS and coupling to an ITMS did not greatly affect the resolution of the GID-M. The Signal-to-Noise Ratio (SNR) of the GID-M, however, was reduced and as such more averaging of the ion mobility spectra was required.

The ITMS was used to perform isolation and fragmentation (MS^n) of the organophosphate and phosphite ions produced in the IMS. For the organophosphates DMMP, DiEthyl MethylPhosphonate (DEMP) and DiisoPropyl MethylPhosphonate (DiPMP), two ion mobility peaks were observed, which through the application of the ITMS were shown to be the ammoniated monomer $M.NH_4^+$ and ammoniated dimer $M_2.NH_4^+$ ions (where M represents the simulants and the empirical formulas have no structural significance). Once isolated and trapped for dwell times of up to 100 ms in the ITMS, the ammoniated monomers were found to predominantly lose neutral ammonia with the parent ion intensity decaying exponentially. The ammoniated dimers of DMMP and DEMP both dissociate to the protonated dimer, and the ammoniated monomer, with different branching ratios. $DiPMP_2.NH_4^+$ dissociates only to the protonated dimer, but it appears that the dissociation never reaches 100%, suggesting two different dimer structures.

Using an ElectroSpray Ionisation - Ion Trap Mass Spectrometer (ESI-ITMS), the fragmentations and subsequent reactions of DiMethyl EthylPhosphonate (DMEP, another CWA simulant) were investigated. The isotopomers of DMEP have unusual fragmentations, and density functional theory calculations were used to aid in the interpretation of the mechanisms involved in these fragmentations. Of note, it is shown that entropy must be taken into consideration, and hence the free energy of the final transition involved in the mechanism, so that the true rate-limiting steps can be determined.

In addition to DEMP, preliminary fragmentations using ESI-ITMS of eighteen other organophosphates (including some nitrogen containing organophosphates) have been undertaken, the results of which are presented. These give an insight as to which fragmentations will require further investigations involving Density Functional Theory (DFT) calculations and deuterated isotopomers to fully understand the mechanisms involved.

ACKNOWLEDGMENTS

Firstly, I'd like to thank Peter Watts for all the telephone conversations, e-mails and visits to try and unravel the mysterious chemistry in my thesis. He is a brilliant man, not just because he has a keen interest in cats, but he has a vast, lifetimes-worth of knowledge of gas-phase chemistry, and for that I am extremely grateful.

Equally as influential in helping me throughout my PhD has been my supervisor, Chris Mayhew. He is so supportive and always ready to lend a hand with experiments (even if you think you're doing OK). Such a character, and a great scientist, thank you Chris for everything.

I am indebted to the support, instrumentation and knowledge from Smiths Detection Ltd (SD), Watford, without which I could not have undertaken this project at all. I have to give special thanks to Neil Thathapudi, Alex McNeish and Jon Atkinson (all of SD) for all their time and effort in trying to fix the GID-M (on more than one occasion).

It has been an absolute pleasure to work in the Molecular physics group over the years with (in order or appearance) Mike, Matt, Margaret, Shane, Dave, Sylvia, Phil, Lyn and another Dave. Special thanks to Dave Howse for all his support with the difficult electronics and for sharing a love of music. Thanks also to Lyn for teaching us all how to knit and to Phil for a good natter and being a great housemate. Thank you all in the group for making this PhD so much more fun.

Lastly, and by no means least, I am so grateful for the support of my husband Dave. He knows what it is like to do a PhD, but is very careful to refrain from telling me how it is done (too much), especially during writing up. Thank you Dave for being generally wonderful.

CONTENTS

ABBREVIATIONS

AChE	Acetylcholinesterase
CAM	Chemical Agent Monitor
CID	Collision Induced Dissociation
CIT	Cylindrical Ion Trap
CWA	Chemical Warfare Agent
CWC	Chemical Weapons Convention
DEMP	DiEthyl MethylPhosphonate
DFT	Density Functional Theory
DiPMP	DiisoPropyl MethylPhosphonate
DMEP	DiMethyl EthylPhosphonate
DMMP	DiMethyl MethylPhosphonate
ESI	ElectroSpray Ionisation
FP	Faraday Plate
FPD	Flame Photometric Detection
GC	Gas Chromatography
IMS	Ion Mobility Spectrometry
ITMS	Ion Trap Mass Spectrometry
LC	Liquid Chromatography
LIT	Linear Ion Trap
MS	Mass Spectrometry or Mass Spectrometer
MS^n or MS/MS	several stages of mass spectrometry, e.g. isolation and fragmentation in an ITMS, or when two or more mass spectrometers are operated in tandem

NAIAD	Nerve Agent Immobiliser Agent Detector
OP	OrganoPhosphate
PTR-MS	Proton Transfer Reaction Mass Spectrometry
QIT	Quadrupole Ion Trap
RIP	Reactant Ion Peak
TMPite	TriMethyl Phosphite
TEPite	TriEthyl Phosphite
SAW	Surface Acoustic Wave
SD	Smiths Detection
SIMMS	Selected Ion Mobility Mass Spectrometry
TMIMS	Tuned Mass Ion Mobility Spectrometry
ZPE	Zero Point Energy

List of chemicals used in section 2 designated by Latin numerals

I DMMP

II $[CH_3P(O)CH_3]^+$ (Fragment of **I**.H^+)

III DMEP

IV $[CH_3OP(O)CH_2CH_3]^+$ (Fragment of **III**.H^+)

V $[HOP(O)CH_2CH_3]^+$ (Fragment of **III**.H^+)

1 INTRODUCTION

1.1 Objectives

Two related research projects are described in this thesis. The research objectives for each of these are as follows:

Project 1: Applications of Ion Mobility Spectrometry – Ion Trap Mass Spectrometry (IMS-ITMS)

1. to construct, characterise and develop an IMS-ITMS incorporating a modified ion mobility drift tube for ion mobility peak selection
2. to illustrate the capabilities of this new instrument to further our understanding of the complex ion/molecule chemistry occurring in state-of-the-art commercial IMS systems used for the detection of Chemical Warfare Agents (CWAs) and other threat agents, using organophosphorus esters as CWA simulants.

Project 2: Applications of Electrospray Ionisation – Ion Trap Mass Spectrometry (ESI-ITMS)

1. to use a commercial ESI-ITMS to aid our understanding of the fragmentation behaviour of protonated organophosphorus esters that relate to CWAs and pesticides.

Each of these projects will have its own section in this thesis with separate abstracts, introductions, experimental details, results, discussions and conclusions. Chapter 4, Section 1 describes project 1, the (non-trivial) coupling of a commercial IMS to an ITMS and subsequent experiments involving organophosphorus esters. Both of these instruments were

provided to the Molecular Physics Group by Smiths Detection Ltd (Watford) as part of a four year EPRSC funded collaborative project: "Fighting Crime, Increasing Security: Fundamentals, Development and Applications of Ion Mobility Spectrometry for Enhanced Trace Detection of Threat Agents" **(**EP/E027571/1). Chapter 5, Section 2 describes the ESI-ITMS experiments of organophosphorus esters (in collaboration with DSTL, Porton Down, Salisbury, and with support from the EC "Reactive Intermediates" Research Training Network.[1])

In addition to these two major projects, and in parallel to the development of the IMS-ITMS, an IMS-quadrupole mass spectrometer (IMS-quad) has been constructed. Although my major assignment was the IMS-ITMS project, I was also involved in the assembly and operation of the IMS-quad. In these investigations, the IMS-quad has been used to substantiate and further understand the results obtained in our ammonia doped IMS system (see section 4.4.5).

The objective of this first chapter is to provide a brief introduction to the main themes in this thesis. More specific and detailed literature reviews are given at the beginning of each chapter.

1.2 The detection of chemical warfare agents

Fears of terrorism and the requirement to detect dangerous chemicals in low concentrations are leading to an ever-increasing need, within homeland security, for reliable, real-time and sensitive detection of a wide range of substances that are a threat to the safety of our society. The chemicals that need to be detected range from explosives through to narcotics and chemical and biological agents. The ability to quickly and accurately identify

these hazardous compounds, particularly within a complex chemical environment, is vital to any nation's needs for the fight against crime and terrorism.

As mentioned in the objectives of this thesis, the investigations reported here primarily involve a series of organophosphorus esters, which have a similar structure to that of some CWAs. The term chemical warfare agent covers a vast and ever expanding array of chemicals. Since 1997, CWAs have been listed on the Chemical Weapons Convention (CWC) Schedule which prevents all development, production, stockpiling and use of these chemicals. The ability to detect CWAs and all precursors is central to the implementation of the CWC. In any war zone it is important to be able to detect CWAs before they are of any risk. Therefore, what is needed is an easy to use, handheld detector with the ability to detect CWAs in concentrations as low as several parts per trillion by volume (pptv) within a few seconds.

The following describes the major technology currently being used for the detection of chemical warfare agents, namely the IMS, a device used by the military and at airports. The IMS has been commercially manufactured by Smiths Detection Ltd, the largest manufacturer and developer of IMS systems in the world. The IMS has so far proved a success in its ability to detect very small quantities of chemical warfare agents[2] and explosives[3] in real time.

The basic concept of the IMS is relatively simple. The IMS detects ionised sample molecules (e.g. CWAs) by measuring their drift times, at atmospheric pressure, under the influence of a weak electric field (E). This gives an ion mobility coefficient, K, which is the drift velocity of the ion divided by the electric field strength (v_d/E). In the IMS used in this project, reagent ions are created using a small radioactive source of ^{63}Ni (10 mCi). These reagent ions then go on to ionise sample ions. Other ionisation techniques for IMS include electrospray, laser ionisation, surface-ionisation, photon ionisation (from UV lamps) or

corona discharge.[4] However, radioactive ionisation and corona tend to be the most commonly used in commercial instruments.

Despite their worldwide deployment and undoubted success, the present generation of IMS-based instruments should be regarded as 'one-dimensional', i.e. only the mobilities of the product ions are measured. The limitations of the IMS are highlighted in a recent National Research Council report dealing with airport security, where it is stated that "currently deployed systems have limitations specific to the physics and chemistry of their operation" making them unsuitable for addressing a variety of emerging threats.[5] These limitations can cause false positive or even false negative readings of the chemical to be detected. False positives may occur, for example, when an ion of some harmless chemical but of similar mobility to a CWA (or any other threat agent on the IMS's computer database) is detected and an alarm is triggered. This is due to the poor temporal resolution of IMS systems. False negatives occur when an IMS system becomes saturated with a chemical that requires less energy to become ionised than, for example, a CWA. Therefore the CWA will not become ionised and will not be detected even though it might be present in the atmosphere. The history, operational details and theory of the IMS is covered in detail in Chapter 2.

Surface Acoustic Wave (SAW) sensors and spectrophotometric sensors are used in-field to confirm the presence of specific chemical agents. SAW sensors can detect the absorption of chemicals onto the surface of a piezoelectric crystal, but the absorbing films required are very difficult to produce. Spectrophotometric sensors change colour on addition of a specific chemical. Whilst both of these techniques have very low detection limits, they require a few minutes for detection and only have the ability to detect a specific chemical.[6 & references therein, 7, 8]. In contrast, IMS detects a broad range of chemicals.

Immunochemical sensors and electrochemical sensors are also chemical specific. The former uses protein antibodies to bind with the chemical agent and provide some kind of response, e.g. fluorescence. The latter uses the hydrolysis products of enzymes that are inhibited by organophosphates (nerve gas). The presence of an organophosphate nerve gas results in a reduction in the concentration of the normal reaction product from the enzymes. This drop in concentration can be detected using graphite electrodes. This was the basis for the British NAIAD (Nerve Agent Immobiliser Agent Detector) developed in the 1970s for military use.[9] The NAIAD was portable, detected nerve gas agents in matter of minutes and could run continuously for up to 12 hours at a time. In contrast, immunochemical sensors can take up to 2 hours to provide a response and have proved to be less successful in the field than electrochemical sensors which take tens of seconds.

One of the most common and powerful laboratory based methods of detecting CWAs is gas-chromatography coupled with a mass-spectrometer (GC/MS).[6, 10] This two dimensional method provides very accurate screening of CWAs down to a few ppbv. Although the technique has been mainly laboratory based so far, there is promising research into field devices.[11] GC has also been combined with ion trap mass spectrometers to provide the ability to perform isolation and fragmentation of ions (MS/MS). This of course increases specificity and can therefore be used to identify chemical agents in increasingly complex mixtures.[12] The main problem with GC use in the field to detect threat agents is that it is very bulky, and is therefore never likely to become a handheld or highly portable detector. Liquid chromatography (LC) is also a powerful tool in analysis of chemicals and can be combined with MS. However, as suggested by the name, the chemicals must be in liquid phase and, because of this, the technique is much slower than gas-chromatography.

Flame Photometric Detection (FPD) techniques are often used in combination with GC in the laboratory. Air is drawn into a chamber containing a hydrogen-rich flame and the light emitted by the burning sample is a fingerprint for the elements that make up the molecules in the air. Phosphorous and sulphur are present in many nerve gas CWAs and therefore FPD can be used to detect these chemicals. The French company, Proengin (Saint Cyr l'Ecole, France) has developed a range of FPD handheld instruments.[13] FPDs provide real-time detection of nerve agent concentrations of ppbv. However, these devices are not chemical specific, only element specific and are therefore prone to false positives.

1.3 Ion trap mass spectrometry

The Ion Trap Mass Spectrometer (ITMS) is an ideal candidate to perform analysis of gas phase ions. Not only does it provide an m/z spectrum, but it can also provide structural information for the ions through isolation and fragmentation (known as MS^n). The ITMS uses a 3D quadrupolar field to trap, isolate and excite ions. There are various ionisation methods, as for the IMS, however the most commonly used is ElectroSpray Ionisation (ESI). A brief history and theory of ESI and ITMS is covered in Chapter 3.

Two commercial ITMS systems were used in the investigations described in this thesis, an LCQ Classic (Finnigan Co, now Thermo Scientific) for coupling to an IMS (as described in Section 1) and an LC Esquire (Bruker Daltonics) with ESI for analysis of organophosphorus ester fragments (as described in Section 2).

An ITMS lends itself particularly to coupling with an IMS due to its ability to accumulate and trap ions for several seconds, and therefore maximising the ion signal from the IMS.

1.4 Organophosphates

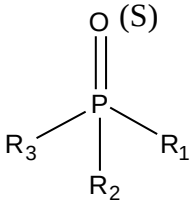

Organophosphates (OPs) all have the basic structure as shown on the left where R_1, R_2 and R_3 are all functional groups. The S in brackets indicates that a sulphur atom exists instead of the oxygen in some of these organophosphates (see Appendix A for examples). Some of these OPs act on the enzyme acetylcholinesterase (AChE). AChE plays a vital role in the transmission of nerve impulses[14] in insects, humans and many other animals. The type of functional groups dictates the action on AChE and therefore there are a whole range of OPs with a variety of biological and chemical properties.[9] Some of the less toxic OPs are used as pesticides (mainly insecticides), for example in sheep-dips, the more toxic OPs include Sarin and Soman, which are nerve gas CWAs that were developed by the Nazi government in the 1930s.

Due to the acute toxicity of some of these OPs, researchers often use substitute organophosphorus esters with similar chemical structures, but that are not so harmful. DiMethyl MethylPhosphonate (DMMP) in particular is one of the most widely used chemicals in research as a substitute or analogue for nerve gas CWAs.[7, 8, 15] Nerve gas agents and their analogues are now recorded under the Chemical Weapons Convention (CWC) in three schedules. Schedule 1 chemicals have few or no uses apart from CWAs, schedule 2 chemicals have legitimate small-scale applications and schedule 3 chemicals have large-scale uses. For the interest of the reader, and for comparison with the organophosphorus esters studied in this thesis, the chemical structures of some of the most common OPs, from insecticides to CWAs, are shown in appendix A.

OPs tend to break down upon exposure to sunlight, air and soil and therefore it is important to not only be able to detect OPs and their fragments, but also to understand what these fragments might be and the chemical mechanisms behind these fragmentation processes.

Fragmentation of a range of organophosphorus esters is achieved, throughout the experiments in this thesis, by Collision Induced Dissociation (CID) in an ion trap mass spectrometer. Chapter 5, Section 2 investigates a specific fragmentation mechanism of DMEP using ESI-ITMS.

In summary, results obtained within this thesis could be of significant importance to homeland security. The IMS is at the forefront of CWA, explosive and narcotic detection. Therefore, its constant development and improvement is vital to the security of any nation. Similarly, the understanding of the fragmentation patterns and possible degradations of CWAs and other OPs is important to improving detection of such chemicals.

2 ION MOBILITY SPECTROMETRY

2.1 Introduction

The Ion Mobility Spectrometer (IMS) is a device that identifies ions by measuring their mobility. Mobility is related to the time it takes (known as the drift time) for an ion to travel a certain distance in an electric field through a buffer gas, at a specific temperature and pressure. The drift time for an ion (at constant temperature, pressure and electric field), depends upon the mass of the ion and of the neutral molecules in the buffer gas, the collision cross-section and charge of the ion, and can be measured using an IMS. IMS systems have poor resolution when compared with mass spectrometers and several ions can appear to have the same mobility. However, they are among the most sensitive ion detection systems in the world and have proved to be invaluable to the international military for detection of Chemical Warfare Agents (CWAs).

Most of the details on the major developments of modern commercial IMS systems have not appeared in the open literature due to the huge military and security interests. There are over 60000 Chemical Agent Monitors (CAMs) in use globally in the military today. These are ion mobility systems designed and produced by Smiths Detection Ltd, (formerly Graseby Dynamics). CAMs were used extensively by UN inspectors, looking for chemical weapon production and storage in Iraq after the Gulf War.

2.2 Operational aspects of ion mobility spectrometry

The IMS is comprised of a drift-tube that is made up of a series of ring shaped electrodes. These electrodes are electrically connected via a series of high resistance resistors. A voltage is applied at the same end of the drift tube where ions are being produced. This creates a

linear voltage gradient down the drift tube, resulting in a uniform electric field. The potential gradient is usually of the order of 200 - 300 V cm^{-1}. A schematic cross-section of a typical IMS is shown in figure 2.1. Ions are formed in the reaction region prior to an ion gate. These ions are introduced into the drift region under the influence of the electric field in very short pulses, produced by opening and closing the ion gate very quickly. The ions separate according to their mobility and are detected at the end of the drift region.

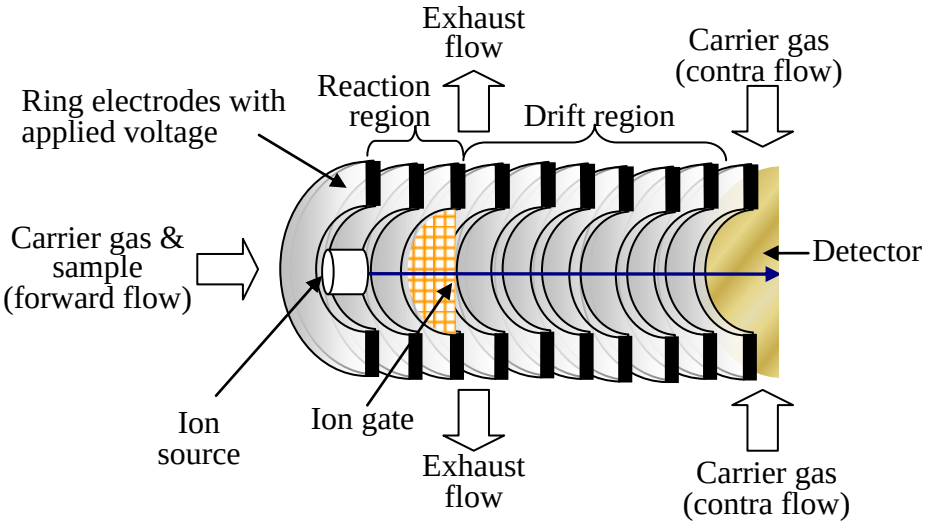

Figure 2.1 Cross section schematic of a typical ion mobility spectrometer. Ions are formed in the ion source and are emitted into the drift region in short pulses using the ion gate. An electric field is applied via a series of ring electrodes around the drift tube guiding the ions towards the detector. Ions with a lower mobility will take longer to reach the detector, therefore different ions are identified by their mobility.

Primary ions are produced via an ion source within the reaction region. In our system the ion source is a 10 mCi beta radioactive source, ^{63}Ni. The electrons produced by the source have enough energy to ionise many neutral molecules, M, in the following reaction.

$$M + e^- \rightarrow M^+ + 2e^- \quad [1]$$

Reactant ions are produced from the gas in the reaction region (usually air) via a series of reactions with the primary ions. These reactant ions can then go on to ionise the trace sample

molecules if present. This description of ion formation is a generalisation for any IMS system and carrier gas. In this thesis, ammonia doped air is the main carrier gas used. Air is primarily composed of nitrogen, and this will become ionised in the reaction described in [2].

$$N_2 + e^- \rightarrow N_2^+ + e^- \text{ (primary)} + e^- \text{ (secondary)} \qquad [2]$$

Then follows a series of reactions, that ultimately lead to the creation of hydronium ions $H^+(H_2O)_n$. One such reaction series that has been previously studied is shown in equations [3] to [6].[16]

$$N_2^+ + 2N_2 \rightarrow N_4^+ + N_2 \quad [3]$$

$$N_4^+ + H_2O \rightarrow 2N_2 + H_2O^+ \quad [4]$$

$$H_2O^+ + H_2O \rightarrow H_3O^+ + OH \quad [5]$$

$$H_3O^+ + H_2O + N_2 \leftrightarrows H_3O^+H_2O + N_2 \quad [6]$$

When the gas in an IMS system is doped with ammonia, hydrated ammonium ions $(H_2O)_n(NH_3)_mNH_4^+$ can be formed by the reactions described in [7] and [8].[17]

$$H_3O^+(H_2O)_n + NH_3 \rightarrow H_3O^+(H_2O)_{n-x}NH_3 + xH_2O \qquad [7],$$

$$H_3O^+(H_2O)_{n-x}NH_3 + NH_3 \rightarrow H_3O^+(H_2O)_{n-x-y}(NH_3)_2 + yH_2O \qquad [8],$$

where *n*, *m*, *x* and *y* are integers. The form of the final reactant ions depends upon the concentration of ammonia and water in the system. The reactant ions produce the reactant ion mobility peak or RIP on the ion mobility spectra.

Chemicals added to the air react with the hydrated ammonium ions and will then go onto form clusters with ammonia and water. The exact chemical formula of the ions again depends upon the concentrations of ammonia and water in the system. It is hard to ascertain the extent of clustering because clusters are loosely bound structures that fragment easily when transferred from an IMS system to any kind of mass analyzer. If the concentration is sufficiently high, monomer containing sample ions can also react with the neutral monomer to

form dimer ions. This subject is touched upon in the studies described in section 1 using an IMS-Ion Trap Mass Spectrometer (IMS-ITMS).

The sample is carried into the reaction region, prior to an ion gate, via a carrier gas that is introduced in the forward flow direction. The carrier gas, with no sample, is also introduced in the contra flow direction (sometimes known as the drift gas). The contra and forward flows are adjusted such that they approximately meet at the ion gate and are exhausted there. This ensures that minimal neutral sample enters the drift region.

As mentioned previously, an ion gate (or shutter of Bradbury-Nielsen construction) is used to allow a very short pulse of ions into the drift tube from the reaction region. This pulse of ions then migrates down the drift tube as a result of the electric field. The ions are then detected after a drift time, *t*, using a Faraday Plate (FP) detector at the end of the drift tube, with *t* being dependent on the mobility. A mobility spectrum therefore consists of a series of peaks. Ions can be assigned an ion mobility coefficient, $K = v_d/E$, (where v_d is the drift velocity and E is the electric field), which, as explained previously is dependent on the temperature and pressure inside the drift tube. Therefore, in an attempt to create a standard coefficient that is independent of the experimental conditions, a reduced mobility coefficient is used as shown in equation 2.1.

$$K_0 = K \frac{273}{T_{(K)}} \frac{P_{(mbar)}}{1013} \qquad [2.1],$$

where T and P are the measured temperature and pressure in the drift tube respectively. However, this takes no account in variation in the degree of clustering between systems.

The Bradbury-Nielsen gate

The Bradbury-Nielsen gate (or shutter) was originally developed in 1936 as an electron filter.[18] It consists of two grids of fine wires, electrically isolated from each other, that are placed such that the wires alternate (see figure 2.2). A voltage is applied to each grid, most commonly this is a DC voltage, although in the original Bradbury-Nielsen experiments, this was an RF voltage. When the grids are at the same potential ions influenced by a linear potential gradient will move through the gate unhindered. When a potential of around ± 50-100 V is applied between the grids, the ions are deflected and are prevented from continuing down a drift tube.

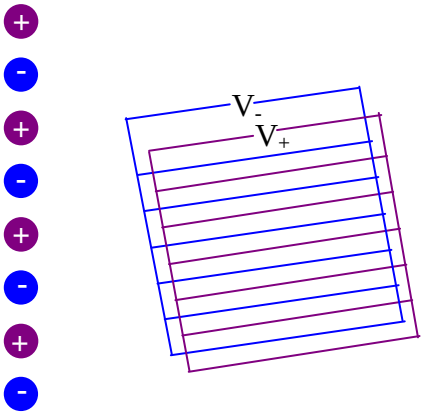

Figure 2.2 A schematic of the two grids in a typical ion shutter. The diagram to the left is a cross sectional representation of the grids. Here the gates are closed to ions as they have a potential applied between them. Wires are ~ 0.05 - 0.1 mm diameter and ~ 0.5 - 1 mm apart (centre to centre).

A Bradbury-Nielsen ion shutter spans the cross-section of the drift-tube in an IMS. The wires are less than 0.1 mm in diameter and approximately 0.5 to 1 mm apart (centre to centre).

2.3 A brief history of ion mobility spectrometry

The concept of an IMS is very simple, and was used as far back as the late 19th century by Rutherford [19] and Roentgen [20] who measured the ion mobility of air molecules that were ionised by radiation. Much work on investigating ion mobilities was subsequently carried out, and it was discovered that mobility coefficients of ions depended greatly on conditions in the drift tube, including temperature, pressure, electric field, buffer gas etc. The role of clustering between the ions and the neutral carrier gas was also recognised at an early stage.[21]

The first commercial ion mobility spectrometers were available in the early 1970s.[22] Many patents for the IMS are held by Cohen and his co-workers, who worked for Franklin GNO and were funded by the military for research into chemical monitoring.[16, p17] These IMS systems developed by Franklin GNO contained a drift tube that had an open construction. Although the whole drift tube was sealed in a container, the gaps between the ring electrodes were not sealed. This meant that gases could flow around the outside of the gate and react with ions in the drift region. The work done, in particular by Karasek et al,[23-25] during the 1970s showed to the scientific community that ion mobilities, especially of more complex ions, were not reproducible. This is not the case with more modern drift-tubes due to their enclosed design or the addition of flow blockers around the ion gate.

At roughly the same time, between 1965 and 1985, there existed military development programmes for the IMS. It was to become a vital piece of military equipment in both the UK and the US. The IMS was reduced in size to a handheld instrument used for detecting CWAs and explosives. The instrument could detect very small quantities of these specific chemicals and also required very little power to operate. Many of the handheld IMS systems, used by military and security forces today, contain two drift tubes, one for negative ions and one for

positive ions. Unfortunately the military research and development into IMS was, and still is, largely confidential and therefore very little of the work is reported in the scientific literature.

The scientific community regained interest in the IMS in the early 1980s when an important improvement was made.[26] A flow of gas in the reversed direction (contra flow) to the sample and carrier gas was introduced, flowing from the detector towards the ions source. This small addition reduced the amount of the neutral carrier gas that was allowed to enter the drift region and therefore the extent of clustering between the ions and neutrals in the drift tube. The IMS became more reliable and this resulted in intense research to improve its capabilities. The research was very much biased towards the detection of chemical warfare agents, explosives and drugs.

A mentioned in chapter 1, the probability of false positives, or even false negatives, is an area of concern when detecting toxic and dangerous chemicals with an IMS. One of the first published works on the IMS describes a combined system, GC/IMS/MS (Gas Chromatography/IMS/Mass Spectrometer), to produce the necessary identification of ions. Mass spectrometry coupled with IMS is now common in research,[27] in particular involving quadrupole mass spectrometry.[28, 29] Coupling of an ion trap mass spectrometer (ITMS) to an IMS provides even more dimensions of analysis owing to the MS^n capabilities, where isolation and fragmentation of ions can be performed.

The IMS-Mass Spectrometer (IMS-MS) is not an ideal solution to the deficiencies in selectivity of the IMS, since most MS systems must be operated under high vacuum. This requires vacuum pumps that increase the size and the power required to drive the instrument. This contrasts with the light, versatile, handheld IMS instruments currently used by the military. However, IMS-MS is an ideal research laboratory instrument which can be used to improve our understanding of the ion/molecule chemistry occurring in current IMS systems.

Characterising and investigating new generations of IMS systems in this way could lead to a reduction in the number of false negatives or positives that occur for future IMS systems.

2.4 Theoretical treatment of ion mobility

As ions migrate down a drift tube under the influence of an electric field, diffusion occurs. If the density of ions is low enough that Coulomb repulsions can be neglected then ions will flow from regions of high concentrations to regions of lower concentrations at a rate that is proportional to the concentration gradient, ∇_n ($mol\ m^{-4}$). The velocity of ions, v ($m\ s^{-1}$), caused by diffusion is given by,

$$v = -\frac{D}{n}\nabla_n \qquad [2.2]$$

where n is the number of ions per unit volume and D is the diffusion coefficient ($m^2 s^{-1}$).

If a weak, uniform electric field, E, is applied along the drift tube then the ion swarm flow will have a drift velocity $v_d = KE$, where K is the mobility coefficient. The relationship between the diffusion coefficient and the weak-field ion mobility coefficient is given by,

$$K = \frac{eD}{kT} \qquad \text{(Einstein's equation)} \ [2.3]$$

where e is the ion charge, k is the Boltzmann constant and T is the gas temperature. This equation only stands for ions that are 'thermalised' i.e. they possess a Maxwell-Boltzmann thermal energy distribution. This condition applies in IMS drift tubes at atmospheric pressure as many collisions occur thereby thermalising the ions.[16]

An ion will be accelerated in a field until it hits a gas molecule and loses all or part of its momentum. Increasing the electric field will increase the drift velocity, but increasing the neutral gas density will have the opposite effect on the ion swarm. Therefore ion motion by

the electric field is governed by the ratio of *E/N*. *K*, will only be independent of *E/N* if the energy the ions acquire from the electric field is much less than their thermal energy; i.e.

$$\left(\frac{m}{M}+\frac{M}{m}\right)eE\lambda << kT \qquad [2.4]$$

m = mass of the ion, *M* = mass of neutral and λ is the mean free path between collisions.

For an ideal gas λ can be approximated to be $1/N\sigma$, where σ = collision cross section. Therefore,

$$\frac{E}{N} << \frac{kT\sigma}{e(m/M + M/m)} \qquad [2.5]$$

E/N is commonly given in units of townsend, 1 Td = 10^{-17} V cm^2. The low field condition holds in an IMS as long as *E/N* < 2 Td.

The ion swarm will move in the direction of the electric field but the drift velocities are small due to the high frequency of collisions and small mean free path. Normal diffusion processes cause the swarm to expand as it travels down the tube and therefore result in a broadening of the peak width of the pulse, which limits resolution.

Ion/neutral interaction models

There are many models that describe these interactions, some better than others. The rigid sphere model, is a very simple model that treats ions and neutrals as if they were rigid spheres that are equally likely to be scattered in any direction upon collision. This produces an expression of the ion mobility coefficient, *K*, which is inversely proportional to the square root of the temperature and the reduced mass. Unfortunately this contradicts experimental findings under the conditions used in an IMS.

The hard-core potential model simulates the short-range attractive and repulsive forces that occur simultaneously as the ions approach the neutral drift gas. Attractive forces lead to

an increase in ion-neutral interactions and therefore mobility is decreased – repulsive forces give the opposite effect. This is a much more refined model than the rigid sphere model and provides good agreement with experimental data. These and other models are described in full in 'Transport properties of Ions in gases' by McDaniel and Mason.[30]

A commonly used equation to describe the mobility coefficient is shown below,[16]

$$K = \frac{3e}{16N}\sqrt{\frac{2\pi}{\mu k T_{eff}}}\frac{1+\alpha}{\sigma(T_{eff})} \qquad [2.6]$$

where, N = density of neutral molecules, e = charge of ion, μ = reduced mass of the ions and neutrals, k = the Boltzmann constant, T_{eff} = effective temperature of the ions (which, in a one-temperature approximation, is equal to the temperature of the neutrals), σ is the collision cross section and α is a correction factor. However, the mobility of ions is often described by an inverse reduced mobility, K_o^{-1} ($cm^2\ V^{-1}\ s^{-1}$), (see equation 2.1) so that the relationship between ion mobility and mass can be more easily correlated.

3 ELECTROSPRAY IONISATION AND ION TRAP MASS SPECTROMETRY

3.1 Electrospray ionisation

Electrospray Ionisation (ESI) is a method by which sample molecules are transferred from solution to gas phase and ionised simultaneously. It is the ionisation technique employed for all the experiments reported in Chapter 5, Section 2 of this thesis, and was used in conjunction with the Ion Trap Mass Spectrometer (ITMS). ESI is a fairly recent invention[31] and one that has revolutionised liquid sampling and ionisation methods. The process involves applying a very high voltage to the end of a small capillary through which the liquid, a mixture of solvent and sample, is forced. This creates a high potential difference between the electrospray tip and a grounded counter electrode (usually the electrospray casing). The liquid is converted into multiply-charged droplets on exiting the capillary as depicted in figure 3.1. A heated carrier gas such as nitrogen flows down either side of the capillary to aid in nebulisation and evaporation of the solvent from the droplet. As the evaporation occurs the sample ions remaining become closer together until Coulombic repulsion overcomes the surface tension and the droplet explodes into smaller multiply-charged droplets. The process is repeated until only the gas-phase ions remain.

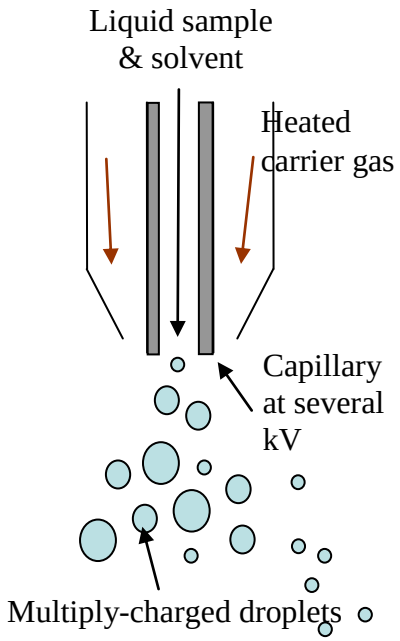

Figure 3.1 Schematic of Electrospray Ionisation. Ionisation and nebulisation occur at the tip of the capillary, which is at a potential of several kilovolts.

ESI has many advantages over other liquid sampling techniques. Most importantly it deposits

very little energy into the sample. Previous techniques often involved heating a substance until it evaporated, or used laser ablation. ESI is therefore ideal for molecules that are very fragile in nature, e.g. biological molecules. It provokes very limited fragmentation in molecules that maintain their structure from liquid to gas phase. The Nobel Prize in Chemistry was awarded to Tanaka and Fenn in 2002 for their work on "soft desorption ionisation methods for mass spectrometric analysis of biological molecules".

3.2 Ion trap mass spectrometry

The ITMS is essentially a 3-dimensional version of the 2-dimensional quadrupole mass filter, the theory and operation of which are very similar. The ITMS is a device that allows ions in the gas-phase to be selectively trapped by means of strong electric fields. Fragmentation of the ions is achieved by Collision Induced Dissociation (CID). The ITMS also provides mass-to-charge ratio (m/z) spectra of all the trapped ions within milliseconds. In the two ITMS systems described in this thesis, the range of trapped and detected ions is m/z 50 to 3000. It is its ability to isolate and fragment selected ions (known as MS^n) that sets the ITMS apart from other mass spectrometers. This allows for deep insight into the structure and chemical nature of gas-phase ions and is one of the main reasons why the ITMS has been adopted for the majority of the work presented in this thesis. The ITMS has been used previously to fingerprint chemicals, for example chemical warfare agents,[12] insecticides,[32] and the constituents of herbal medicines.[33]

The first patent describing an ion trap mass spectrometer was submitted by Paul and Steinwedel in 1960.[34] The main focus of the patent was the first operational details of a quadrupole mass filter; the ion trap was simply "another electrode arrangement". It was Paul

and his colleagues at the University of Bonn, Germany who first appreciated the use of strong-focussing fields for the manipulation and trapping of ions. Subsequently, the most commonly used form of the ion trap is also known as the 'Paul' trap. There are several types of ion trap including the cylindrical ion trap (CIT),[35] the linear ion trap (LIT)[36] and the quadrupole ion trap (QIT) which is the original Paul trap. Both the ITMS systems described in this thesis are quadrupole ion traps.

An ITMS consists of one ring electrode and two end cap electrodes, all having hyperbolic surfaces, see figure 3.2. The ions may be produced in a variety of ways. The method of choice for fragmentation investigations involving Chemical Warfare Agents (CWAs) is ESI (as described previously). Ions then travel though a capillary and are focused using a series of skimmers and octopoles into an ion beam that enters the trap through a hole in the end cap

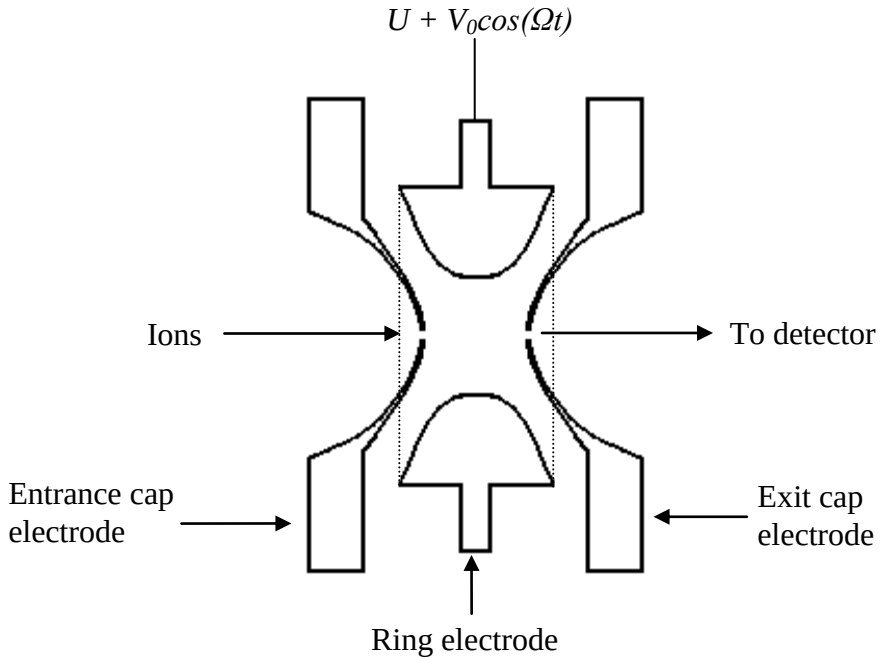

Figure 3.2 Cross-section schematic of a typical ion trap mass spectrometer. *U* is the D.C. voltage and $V_0 cos(\Omega t)$ is the RF potential applied to the ring electrode. The end caps are commonly kept at ground.

electrode as shown in figure 3.2. In the simplest set-up, the end cap electrodes are grounded, and a combination of RF and DC potentials are applied to the ring electrode.

Initially, ions are pulled into the trap through a hole in one of the end cap electrodes, by a small positive potential. The RF voltage applied to the ring electrode then provides the quadrupolar trapping field in which the ions oscillate. The force on an ion in the field increases linearly with the distance from the centre of the trap. Therefore all ions are pushed towards the centre of the trap. Whether the trajectory of an ion remains stable within the trap is determined by the Mathieu equations as shown in the next section (3.3). An ion trajectory can be manipulated by varying the DC and RF applied potentials, so that it becomes unstable in the axial direction and is consequently ejected out of the hole in the other end cap electrode. Ions are then picked up by a detector situated directly outside the trap, this is often an electron multiplier.

The very earliest ion traps used widely differing methods of ion detection. The traps developed by Paul and co-workers used a technique know as 'mass selective resonance detection'.[34] Using this technique, ions of specific m/z were resonated at their secular frequency, using a small AC voltage applied to the end cap electrodes. The secular frequency is the frequency at which an ion of particular m/z travels around inside the ion trap. The ions were detected by the absorption of energy when they came into resonance with the AC potential applied between the endcap electrodes. The mass range, sensitivity and resolution of this early ITMS was severely limited.

Later, in 1970, Dawson and Whetten filed a patent[37] for a novel mass selective storage technique in which ions were trapped, one m/z at a time, then ejected into an external detector by applying a short voltage pulse to one, or both, or the endcap electrodes. This technique is very slow to produce an m/z spectrum since, for each data point, ions had to be accumulated,

stored and emitted for the range of m/z required. However, it did light the way to the development of a new technique of mass scanning that made the ITMS commercially viable. The 'mass selected instability mode' was pioneered by Finnigan MAT Corporation, one of the first commercial manufacturers of the ITMS, in collaboration with John Todd at the University of Kent, Canterbury.[38] The RF and DC voltages are ramped at a particular ratio so that ions of increasing m/z become unstable in the axial direction. As they do so, they are detected externally to the trap. The time at which a particular ion is emitted from the trap identifies its m/z according to the ramp rate of the RF potential.

Helium buffer gas is added to the trap to reduce the kinetic energy of the ions through collisional cooling.[39] This further reduces the trajectory of ions towards the centre of the trap. The work by the team from Finnigan MAT Co. with Todd showed that the addition of helium at relatively high pressures greatly increased trapping efficiency.[38] Further studies from the same collaboration, this time including Louris and Cooks from Purdue University, Indiana, showed that the addition of helium can also be used for CID, the method by which fragmentation of the ions occurs in the trap.[40]

Fragmentation can be induced by increasing the kinetic energy of ions of a selected m/z for a specific amount of time, referred to throughout this report as the 'fragmentation time'. This is achieved by applying an AC voltage of a few millivolts to any of the electrodes at a frequency equal to the secular frequency of the ions. This same AC voltage when applied at several volts can be used to assist in destabilising selected ions and ejecting them from the trap. Heavier buffer gases have been tested in ion traps, but these tend to result in too much kinetic energy being supplied to the ions on collision and eject them from the trap. However, they do prove useful for larger ions which require a much higher internal energy to fragment.[41]

Figure 3.3 shows an example of how the voltage varies for a typical MS^n scan of an ITMS, including accumulation of ions in the trap, isolation, fragmentation and finally mass scan. The diagram is from the users manual of a Brucker LC-Esquire ion trap mass spectrometer, which is the ion trap used in Section 2 experiments. The auxiliary RF is equivalent to the AC voltage as discussed above, and in this case is applied to one of the end-cap electrodes. The primary RF is applied to the ring electrode and the DC voltage is set to ground so that the ITMS operates along the $a = 0$ axis of the Mathieu stability diagram (see figure 3.4).

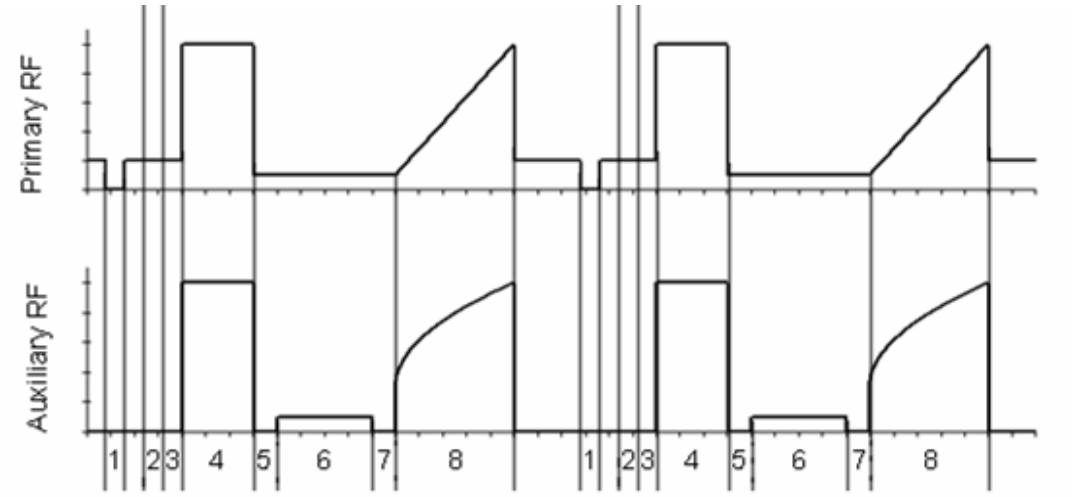

Figure 3.3 RF amplitudes for a typical MS^n scan of an ITMS. 1: Clear all ions from trap. 2: Accumulation of ions. 3: Isolation delay. 4: Isolation. 5: Fragmentation delay. 6: Fragmentation. 7: Scan delay. 8: Mass scan. The amplitude shown is voltage peak-to-peak of the auxiliary and primary RF voltages applied to the end-cap and ring electrodes respectively.

Generally, most commercial ion traps are quadrupole ion traps that use the mass selective instability mode to perform m/z scans and use helium as a buffer gas. Since the work during the 1970s and 80s of the Finnagan MAT Corporation, the Department of Chemistry at Purdue University and the Chemical Laboratory at The University of Kent there have been few major advances in the operation of quadrupole ion traps. However, resolution and mass range have been extensively improved since the ion traps were first invented in 1960, mainly due to

advances in modelling techniques which have led to a better understanding of the fields and ion trajectories within an ion trap.

3.3 Theory of ion trap mass spectrometry

It must be noted at this point that the following theoretical treatment of ion motion in a quadrupole ion trap only applies to a single ion in a trap, neglecting all background gases that may be present. This is not of course a realistic scenario and many more detailed calculations are necessary to model, for example, field effects due to other ions present, or collision effects from buffer gases. However, the model is a good enough approximation to give a basic understanding of ion motion. There are many different methods of modelling the true ion motion in an ion trap, the most predominant of which is the pseudopotential well model as developed by Dehmelt in 1967.[42] These models require detailed explanation that shall not be covered here.

Referring to figure 3.2, a combination of RF and DC voltages is applied to the electrodes, to produce a quadrupolar potential within the trap. The potential at coordinate position *r, z* within the trap is denoted by $\phi_{r,z}$ and can be deduced from the potential applied to the electrodes,[43] providing the Laplace condition is satisfied,

$$\nabla^2 \phi_{r,z} = 0 \qquad [3.1]$$

The general form for the quadrupolar electric potential inside an ion trap can be written as,

$$\phi_{r,z} = A(r^2 - 2z^2) + C \qquad [3.2]$$

where *A* and *C* are terms that can be calculated from the potential applied to the electrodes. It is important to note at this point that the potential in the radial direction is not coupled with the potential in the axial direction. Therefore it is possible to treat the motion along the two axes separately.

The terms A and C are deduced by defining ϕ_o as the difference between the potentials applied to the ring and end-cap electrodes, ϕ_{ring}-ϕ_{endcap}, then $\phi_{ring} = Ar_o^2+C$ and $\phi_{endcap} = -2Az_o^2+C$. Solving for A, the quadrupolar potential is then described by,

$$\phi_{r,z} = \frac{\phi_o(r^2 - 2z^2)}{2(r_o^2 + 2z_o^2)} + \frac{\phi_o}{2} \qquad [3.3]$$

where r and z are the polar coordinates in radial and axial directions respectively.

The motion of ions in the electric field inside an ion trap mass spectrometer is governed by the second-order linear differential equations as postulated by Mathieu in 1868.[44,45] Mathieu's original equations described the unstable and stable regions in elliptical vibrating membranes in fluids. To confirm that the Mathieu equations do in fact describe the movement of ions in a QIT, they need to be compared with and equated to the equations of force, thus giving the Mathieu trapping parameters a_u and q_u.

The canonical form of the Mathieu equation is,

$$\frac{d^2u}{d\xi^2} + (a_u - 2q_u \cos 2\xi)u = 0 \qquad [3.4]$$

where u is the displacement, ξ is a dimensionless term and is equal to $\Omega t/2$ (Ω = frequency and t = time), a_u and q_u are also dimensionless and are known in ITMS theory as trapping parameters.

The force acting on an ion by an electric field is equal to the charge of the ion multiplied by the electric field at that point. The components for motion of the ion in the axial and radial directions can be considered independently of one another. Therefore it can be shown that,

$$F_z = m\left(\frac{d^2z}{dt^2}\right) = -e\left(\frac{d\phi_{r,z}}{dz}\right) = e\frac{4\phi_o z}{r_o^2 + 2z_o^2} \qquad [3.5]$$

where *m* is the mass of the ion. In commercial ion traps, the endcap electrodes are held at ground, and the potential $\phi_o = (U+V\cos\Omega t)$, is applied to the ring electrode. Inserting this into equation 3.5, the motion of the ion can be written as,

$$\frac{d^2z}{dt^2} = \left[\frac{4eU}{m(r_o^2+2z_o^2)} + \frac{4eV\cos\Omega t}{m(r_o^2+2z_o^2)}\right]z \quad [3.6]$$

where *U* is the DC voltage and *V* is the zero-to-peak amplitude of the RF potential oscillating at an angular frequency of Ω. It is then trivial to compare equation 3.6 to the Mathieu equation (3.4), and the trapping parameters a_z and q_z can be derived.

$$a_z = -\frac{16eU}{m(r_o^2+2z_o^2)\Omega^2} \quad [3.7] \qquad q_z = \frac{8eV}{m(r_o^2+2z_o^2)\Omega^2} \quad [3.8]$$

Similarly it can be shown that $a_z=-2a_r$ and $q_z=-2q_r$. These equations are very important in ion trap physics, since at particular values of a_z and q_z, an ion's trajectory will either be stable or unstable. The parameters such as RF and DC amplitude can be varied so as to manipulate the value of a_z and q_z for a particular m/z. Therefore, one can choose the trajectory to be stable or unstable. This is presented schematically using the Mathieu stability diagrams as shown in figures 3.4 and 3.5.

Both axial and radial dimensions must be combined to define the two dimensional stability regions for an ion in a quadrupolar ion trap. The largest stability region shown in red in figure 3.5 is the most commonly employed. Most commercial ion traps operate in this region since only the lowest DC and RF voltages are required for operation. Further stability regions are also indicated on figure 3.5. There is little or no literature on ion traps operating in these regions. However it is a topic of interest for investigations into quadrupole mass filters.[46, 47]

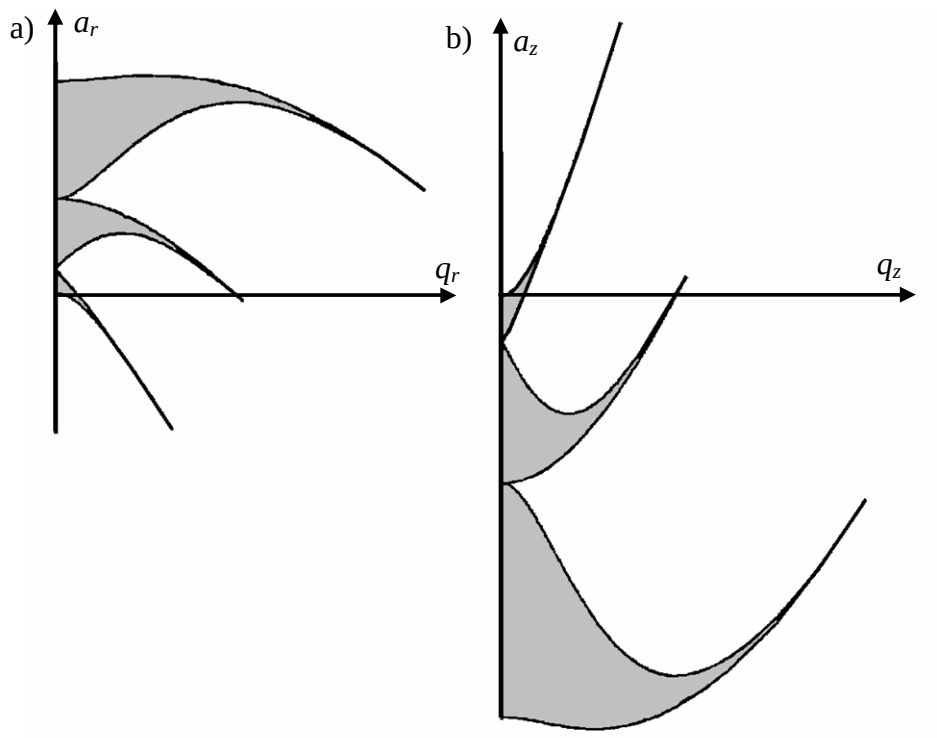

Figure 3.4 Mathieu stability diagrams for ions in a quadrupole ion trap, a) in the radial direction b) in the axial direction. Stable regions are shaded, ions are unstable at all other values of (*a*,*q*) (adapted from Ion Trap Mass Spectrometry, March & Todd[43]).

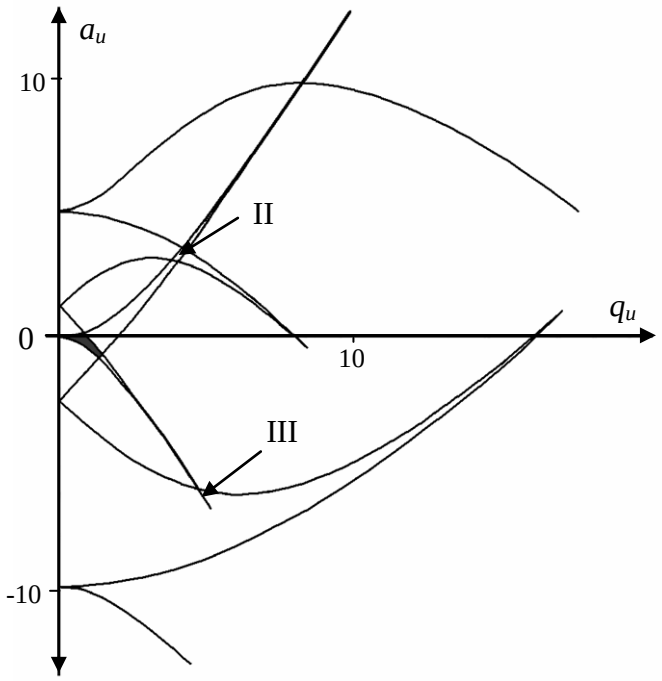

Figure 3.5 2D Mathieu stability diagram for ions in a quadrupole ion trap. Shaded black region is the largest and most frequently used stability region for operation in an ion trap. II and III are further two-dimensional stability regions at higher values of (*a*,*q*) (adapted from Ion Trap Mass Spectrometry, March & Todd[43]). *u* is used to denote *r* or *z*.

Producing an m/z scan in an ion trap mass spectrometer

As described above, an m/z scan can be achieved by ramping the RF voltage at a certain ratio, the ions will therefore become unstable with increasing mass to charge ratio. This can also be explained using the Mathieu stability diagram as shown in Figure 3.6. This shows the most commonly used stability region, where an ion will become unstable when it has trapping parameters of q_u= 0.91 and a_u= 0. Many commercial ITMSs operate m/z scans with a_u = 0, i.e. there is no DC voltage applied to the electrodes. This means that as the RF voltage is ramped up, ions of increasing m/z will approach a q value of 0.91 and at this point will become unstable in the axial direction. They are ejected from the trap through a hole in the end cap electrode and are detected using some form of electron multiplier.

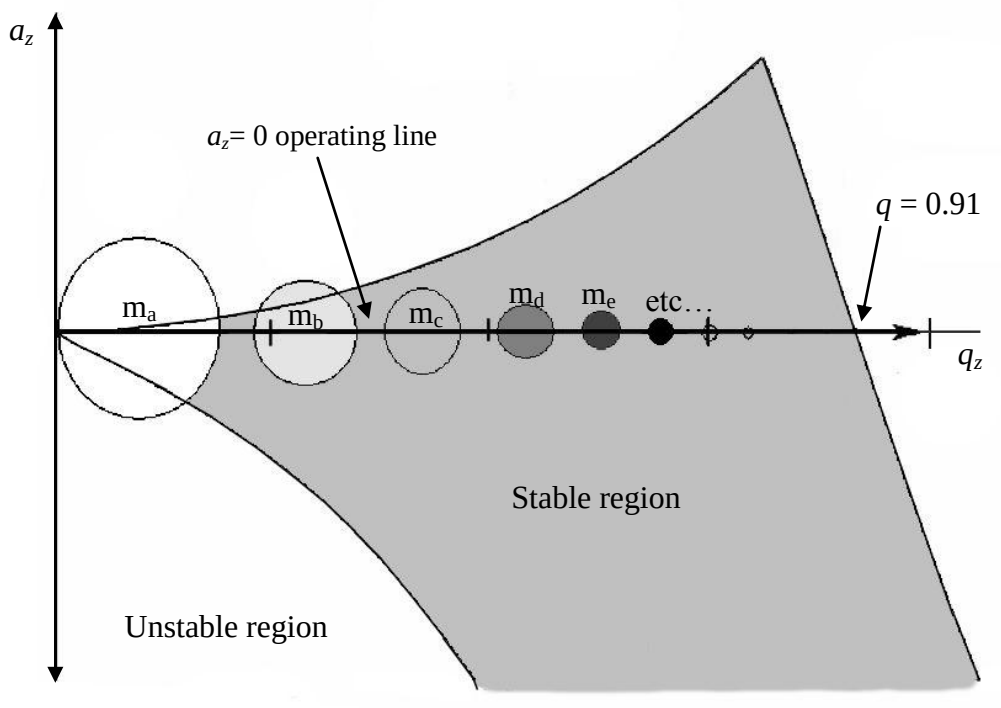

Figure 3.6 m_a is an ion with m/z greater than m_b, $m_b > m_c$ and so on, the size of the circle is intended to represent the m/z of the ion. Commercial ITMS systems are commonly operated with $a_{r,z}$ = 0, so that the RF voltage may be ramped up shifting ions of increasing m/z towards a q value of 0.91 where they will become unstable and are ejected axially out of the trap and detected. This is the basis of an m/z scan.

4 SECTION 1

The development of an ion mobility spectrometer-ion trap mass spectrometer to investigate ion chemistry occurring in ion mobility systems used in the detection of threat agents

4.1 Abstract

A commercial ammonia-doped Ion Mobility Spectrometer (IMS) (Smiths Detection Ltd, GID-M) that is designed to detect Chemical Warfare Agents (CWAs), has been modified by the addition of a second gate (a Bradbury-Nielson ion shutter) and connected to the front end of a commercial Ion Trap Mass Spectrometer (ITMS) (Finnigan LCQ Classic) via a capillary. Importantly, the second gate allows selection of individual ion mobility peaks for m/z analysis in the ITMS. The modification of the IMS and coupling to an ITMS did not greatly affect the resolution of the GID-M. The Signal-to-Noise Ratio (SNR) of the GID-M, however, was reduced and as such more averaging of the ion mobility spectra was required.

The ITMS adds an additional dimension over that of the usual IMS-quadrupole mass spectrometer system in that it has the ability to undertake MS^n studies, thereby allowing information to be obtained about the structure of the product ions. To demonstrate the application and potential of this new instrument, results are presented for a series of nerve gas CWA simulants; namely the organophosphates DiMethyl MethylPhosphonate (DMMP), DiEthyl MethylPhosphonate (DEMP), DiisoPropyl MethylPhosphonate (DiPMP) and the organphosphites TriMethyl Phosphite (TMPite) and TriEthyl Phosphite (TEPite).

For DMMP, DEMP and DiPMP, two ion mobility peaks are observed, which through the application of the ITMS are shown to be the ammoniated monomer $M.NH_4^+$ and ammoniated

dimer $M_2.NH_4^+$ ions (where M represents the simulants and the empirical formulas have no structural significance). Once isolated and trapped for dwell times of up to 100 ms in the ITMS, the ammoniated monomers are found to predominantly lose neutral ammonia with the parent ion intensity decaying exponentially. The ammoniated dimers of DMMP and DEMP both dissociate to the protonated dimer, and the ammoniated monomer, with different branching ratios. $DiPMP_2.NH_4^+$ dissociates only to the protonated dimer, but it appears that the dissociation never reaches 100%, suggesting two different dimer structures.

TMPite and TEPite have more complicated ion mobility spectra than the organophosphates. The ion mobility peaks for TMPite and TEPite are interpreted by selecting individual ion mobility peaks using the second gate and performing mass analysis in the ITMS. MS^n studies (isolation and fragmentation) of the ions seen in the m/z spectra are also performed with the ITMS, to confirm their structures.

4.2 Introduction

IMS is the base technology in a wide range of CWA, drug and explosive detectors, and environmental monitors.[4, 48] IMS systems can be extremely sensitive, but they are not very selective and can produce false positives and negatives. This is due mainly to two factors. Firstly, the gas-phase ion chemistry is complex and needs to be better understood. Secondly, the temporal resolution is often insufficient to distinguish between ionic species of similar mobilities. Selectivity can be manipulated by the introduction of dopants to give different chemistries. For example, ammonia doping generates NH_4^+-based cluster ions, which will only proton transfer to compounds with proton affinities higher than that of the neutral clusters. This can be exploited to filter out a large number of unwanted organic compounds[49] in favour of detecting CWAs,[17, 50] explosives[51, 52] and narcotics.[53]

The ion chemistry occurring in atmospheric pressure IMS systems has previously been investigated by the use of mass spectrometers,[54] including Time-of-Flight (TOF)[55, 56] and quadrupole,[29, 51, 52, 57, 58] coupled to the IMS. The quadrupole mass spectrometer is the most popular and probably the simplest mass analyser. This allows ions present in a mobility peak to be identified, and hence provides critical information which can be used by normal IMS systems to identify the presence of hazardous trace gases. However, whilst the information obtained from such instruments can be detailed and of considerable value, quadrupole and TOF mass spectrometry are limited particularly by the fact that no tandem mass spectrometry (MS^n) is possible. In these instruments only the m/z value of the ions can be determined and therefore no information concerning their structure can be obtained. This limitation can be overcome by the use of an ITMS.

An ITMS offers one more dimension of analysis than most mass spectrometers. Not only does it provide the conventional m/z spectra, but ions can be trapped and then isolated and

fragmented in order to obtain information about their structure. A second advantage over quadrupole and TOF mass spectrometry is that the ITMS can accumulate ions for a long period of time (up to 10s), thereby greatly enhancing the intensity of the ion signal.

To illustrate the applications of the novel IMS-ITMS instrument that we have developed, a series of studies involving the organophosphates DMMP, DEMP, DiPMP and the organophosphites TMPite and TEPite are presented. The molecular structures and masses of these chemicals are shown in figure 4.1. DMMP, DEMP and DiPMP can be used to produce nerve gas CWAs, therefore their production, processing and consumption must be disclosed each year under Schedule 2 of the CWC. TMPite and TEPite can also be used in the production of CWAs, but they also have large-scale industrial applications, for example, they are used for the production of flame retardants, optical brighteners, pesticides, antioxidants, and pharmaceuticals. TMPite and TEPite are listed under Schedule 3 of the CWC.

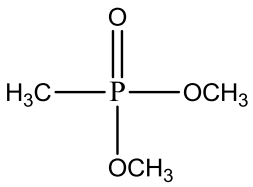

Dimethyl methylphosphonate
124 amu

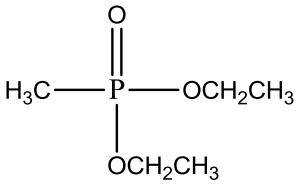

Diethyl methylphosphonate
152 amu

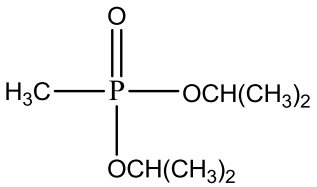

Diisopropyl methylphosphonate
180 amu

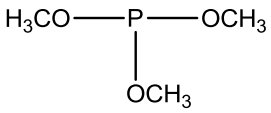

Trimethyl phosphite
124 amu

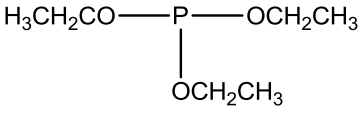

Triethyl phosphite
166 amu

Figure 4.1 Molecular structures and masses of DiMethyl MethylPhosphonate (DMMP), DiEthyl MethylPhosphonate (DEMP), DiisoPropyl MethylPhosphonate (DiPMP), TriMethyl Phosphite (TMPite) and TriEthyl Phosphite (TEPite).

A similar coupling of an IMS with an ITMS has been reported by Clowers and Hill.[59] However there are significant differences in its design and proposed use from that described in this section. In particular, Clowers and Hill are using the IMS section of their instrument to filter peptide and carbohydrate ions produced by electrospray ionisation (ESI) prior to their mass spectrometric investigations.

The results from the investigations using the IMS-ITMS system as described in this section, are substantiated with results from two other instruments available within the Molecular Physics group. These are an IMS-quadrupole mass spectrometer (IMS-quad) (built in the laboratory) and a commercial Proton-Transfer Reaction Mass Spectrometer (PTR-MS). The workings of the PTR-MS shall not be discussed here, since they only form a minor part of the investigations and the data were recorded by my colleagues in the group. For further reading about the PTR-MS, please refer to the comprehensive review by Blake et al.[60] An advantage of the IMS-quad over IMS-ITMS, is that it can be used to produce Tuned Mass Ion Mobility Spectra (TMIMS). This is briefly discussed in section 4.4.5 at the very end of the results section.

4.3 Experimental methods

4.3.1 Instrumentation

A complete schematic cross section of the entire IMS-ITMS system constructed during this PhD is shown in figure 4.2. The IMS and ITMS are described separately below followed by a discussion on how the interface between these two instruments was achieved.

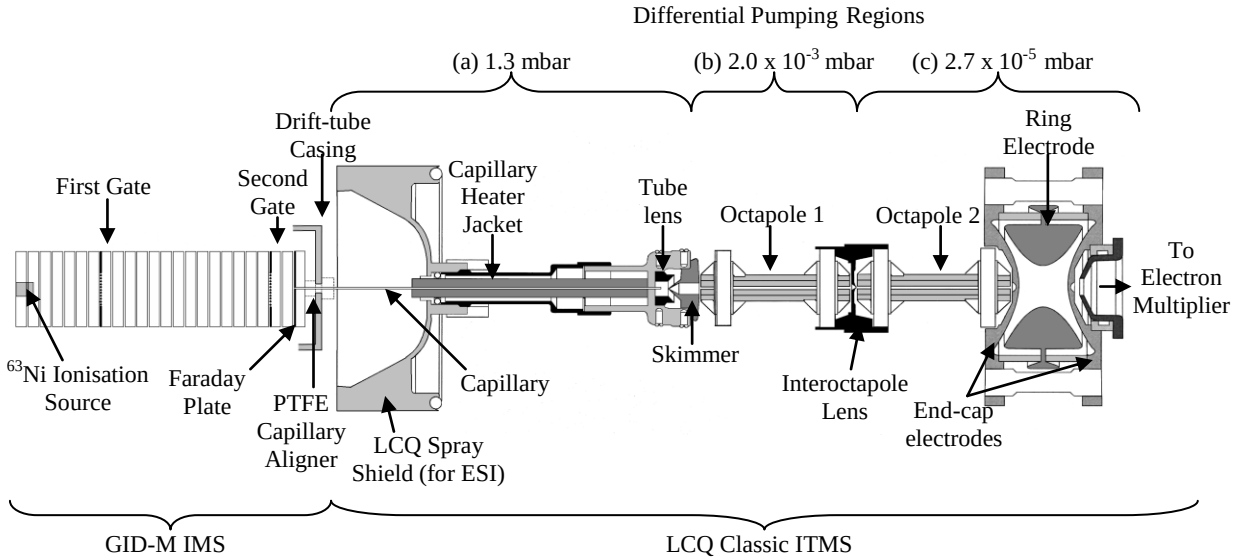

Figure 4.2 Schematic cross section of the IMS-ITMS system consisting of a Smiths Detection GID-M IMS and a Finnigan LCQ Classic ITMS (ITMS schematic was adapted from the LCQ Classic Manual) The gas flows in the IMS are similar to those shown in figure 2.1.

Several problems, both major and minor, were encountered during the development of the IMS-ITMS system, most of which have been addressed. The majority of the difficulties have been with the GID-M, fewer with the interface, and the LCQ Classic has only provided minor issues. Some of the major difficulties with the GID-M and how they were overcome, are described in the IMS section. However, many of the details of the GID-M are confidential and will not be available in the published version of this thesis.

4.3.2 The GID-M ion mobility spectrometer

A commercial military IMS (GID-M) was provided for this project by Smiths Detection Ltd (SD). In the GID-M, ions are generated at atmospheric pressure by a 10 mCi ^{63}Ni radioactive source. A series of ion/molecule reactions then occur to form the reactant ions, which are dependent on the type of dopant used. The GID-M includes a built-in ammonia-doped sieve pack as well as various membranes that filter and dope the air before entering the reaction and drift regions. Due to the ammonia doping, the reactant ions formed are mainly ammonia cluster ions (see results section for discussion of the reactant ions formed in this system). These reactant ions transfer charge (assuming the energetics are favourable) to sample molecules injected into the system (see Chapter 2, 4.2 for examples of these ion/molecule reactions). These processes all occur in the reaction region of the drift tube before the first gate.

The drift tube consists of a series of gold plated electrodes that are electrically connected by an external resistor chain. The ions are pulsed via a Bradbury-Nielsen type ion gate and are detected at the Faraday Plate (FP) (figure 4.2). The ion gate can be operated either in pulsed mode as described above, or in DC mode, i.e. where the gate is permanently open. The latter mode is used to maximise the transmission of all ions through the IMS, and therefore to significantly increase the signal in the ITMS.

Since the GID-M is a commercial military device, it is normally enclosed in a protective casing surround. However, in order to couple the IMS to the ITMS, the GID-M (with the associated molecular sieve pack) had to be removed from this casing. All electronics remained inside the protective casing and break-out cables were used to connect them to the IMS. The GID-M usually operates with two drift-tubes, one for negative ions and the other for positive ions. Only one drift tube was used for this study due to the nature of the capillary

interface between the IMS and ITMS. The GID-M has been modified such that it can be operated in both positive and negative modes using the same drift tube, by interchanging the cables.

After removing the GID-M from its protective casing, several modifications were made to the drift tube. In particular, an objective of this project is to have the ability to select specific ion mobility peaks for m/z analysis. To achieve this, a second gate was installed near to the FP (see figure 4.2). Identical to the first gate, the second gate could either be left open to allow all ion pulses to proceed to the FP and hence to the ITMS, or could be pulsed to only allow through ions associated with a particular ion mobility peak for m/z analysis. To select an ion mobility peak of interest for m/z analysis, the second gate pulse is delayed with respect to the first gate pulse by a required amount of time, such that the second gate is open when the ion mobility peak to be selected has reached it. To illustrate this, the first and second gate pulse patterns are shown in figure 4.3. The electronics for the second gate were designed and produced by Smiths Detection Ltd, Watford.

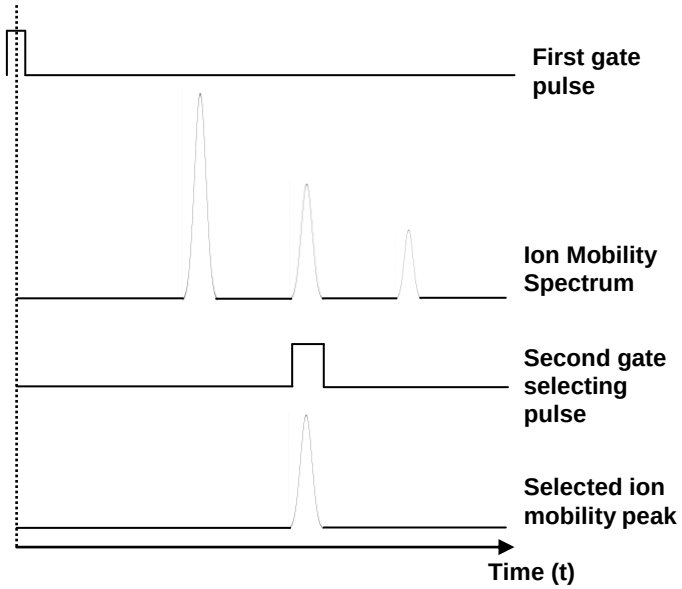

Figure 4.3 Schematic representations of the temporal positions of the first and second gate pulses, illustrating the ability to select subsequent ion mobility peaks for m/z analysis. The ion mobility spectra represent that as detected by the Faraday plate.

The second gate pulse is detected on the Faraday Plate (FP) through capacitative coupling, and therefore can be easily positioned over a mobility peak. In reality, due to the finite distance between the second gate and the Faraday plate, the ions take a short time to travel this distance and be detected, whereas the second gate pulse is an instantaneous signal pick-up. In practice this means that the second gate pulse has to be positioned to slightly shorter drift times than the required mobility peak. This is advantageous as the mobility peak can still be seen and the intensity optimised during the adjustment of the second gate position. To illustrate this, the ion mobility spectra, with the second gate positioned in order to select the Reactant Ion Peak (RIP) are shown in figure 4.4. In DC mode, the second gate pulse is actually inverted rather than switched off completely. This means that all ions are allowed through the second gate apart from a very small period where the gate is pulsed shut.

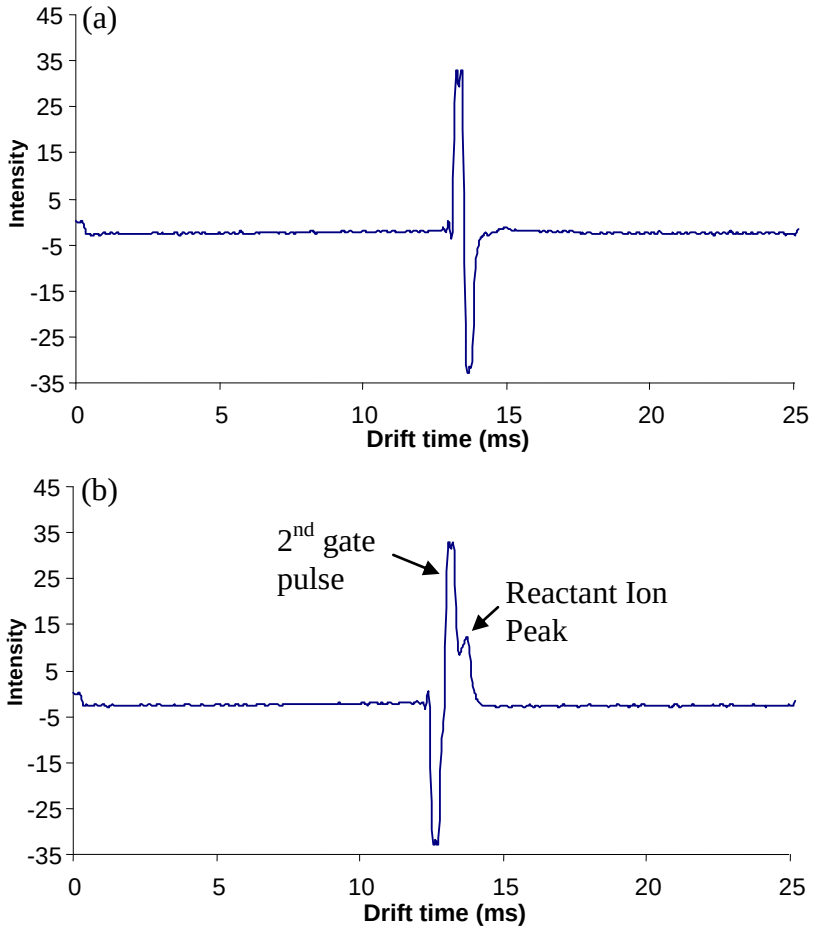

Figure 4.4 (a) The second gate pulse is positioned over the RIP and is closed, letting all ions through except those making up the RIP. (b) The second gate pulse is open over the RIP, therefore letting through only ions that produce the RIP.

4.3.3 The LCQ Classic ion trap mass spectrometer

The ITMS used in this study is an LCQ Classic (Finnigan Co, now Thermo Scientific) that was operated without any modifications, with the exception of the ion formation and inlet system. The original ElectroSpray Ionisation unit (ESI) was removed entirely and the inlet capillary was replaced with a longer one (see interface section for more details). One difficulty associated with this removal was that the auxiliary gas flow used for the ESI unit requires a minimum pressure in the gas line for the LCQ Classic to operate. To overcome this problem the end of the line was simply blocked and maintained at a specific pressure using compressed air. The ESI high voltage supply (usually at ~4 kV) was disconnected, reduced to 0 kV and sealed with insulating tape for safety.

The LCQ Classic is a typical quadrupole ITMS with three pumping regions. The capillary inlet and tube lens are situated in the first differential pumping region figure 4.2 (a) that is pumped only by a rotary pump, and the ion optics, quadrupole trap and ion detection system are situated in the high-vacuum regions, figure 4.2 (b) and (c), that are pumped by a turbo pump. Helium gas is added to the trap to a partial pressure of 1 mTorr. Note that the pressure is higher inside the ion trap than the region in which the ion trap sits.

The trap itself has internal dimensions of z_0 = 0.783 cm and r_0 = 0.707 cm in the axial and radial dimensions respectively,[61] where r_0 is the distance from the centre of the trap to the nearest point on the ring electrode, and z_0 is the distance from the centre of the trap to the nearest point on the end cap electrodes. The LCQ Classic applies a radio frequency (RF) voltage of 760 kHz and 0-8500 V (zero-to-peak) to the ring electrode in order to trap, isolate, excite (for fragmentation) and eject (for m/z scanning) ions. In addition to this, the LCQ classic also applies supplementary resonance RF voltages to the end-cap electrodes during the isolation, excitation and mass scanning periods, which increases the sensitivity and resolution

of the instrument. Figure 4.5 shows the typical amplitudes applied to the main RF and the supplementary (axial) RF during an MS^n scan in the LCQ classic.

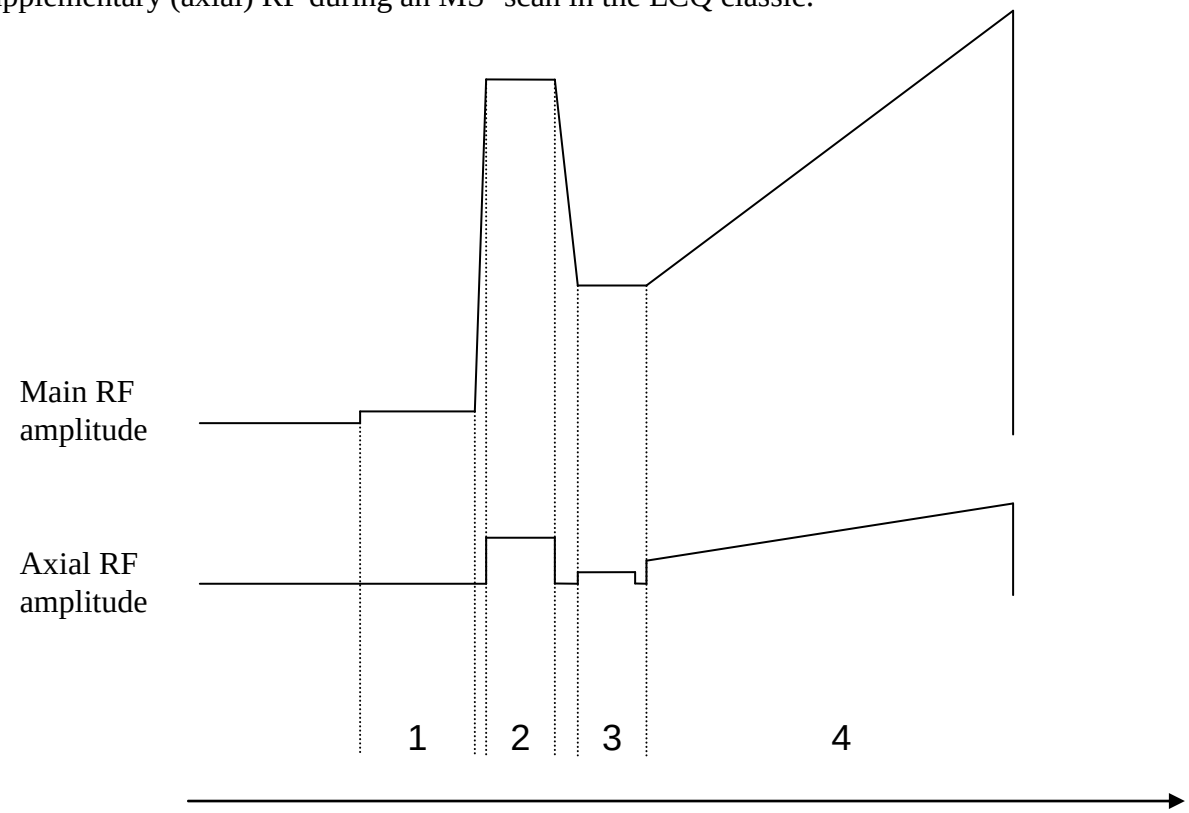

Figure 4.5 RF voltage amplitudes for a typical LCQ ion trap scan including 1, Ion injection, 2, Ion isolation, 3, Excitation/Fragmentation and 4, m/z scan. The main RF voltage is applied to the ring electrode and the axial RF amplitude (sometimes known as the supplementary RF) is applied to the end cap electrodes (adapted from LCQ operators course booklet).

The q_z value upon isolation for all masses is set to $q_z = 0.83$ which corresponds to the edge of the stability region in an LCQ Classic. This makes isolation more efficient as all ions of a lower m/z than the isolated ion are no longer stable in the trap and are ejected. A range of RF frequencies are then applied to the end-cap electrodes to destabilise the larger ions.

4.3.4 Interface

The IMS-ITMS interface is shown in the photo in figure 4.6. A purpose-built stainless steel support was designed and produced by Smiths Detection Ltd to enable the GID-M to be

bolted onto the front of the LCQ Classic using the screw holes originally intended to secure the ESI unit. The lens system in the first pumping region of the LCQ classic can be entirely removed, thus giving access to the capillary.

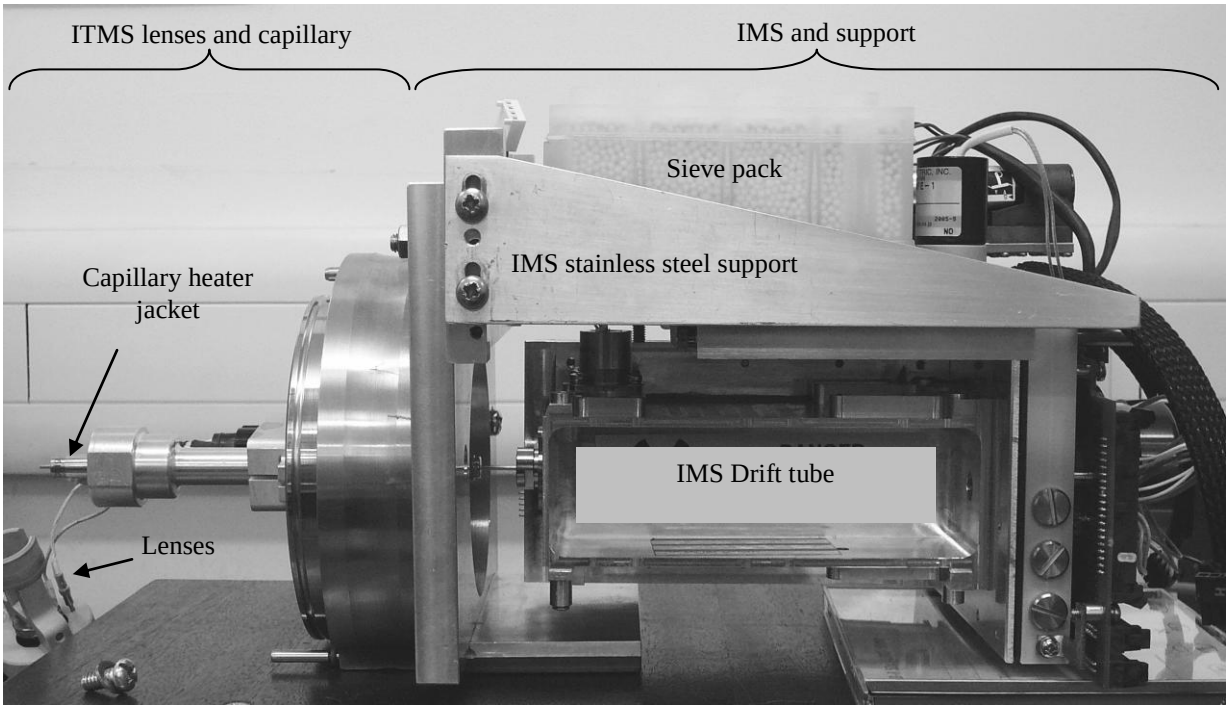

Figure 4.6 Photo of a GID-M drift tube and a purpose built stainless steel support that is bolted to the removable LCQ lens system. The capillary is threaded right through this lens system and into the back of the GID-M drift tube to the Faraday plate.

A longer capillary is required to allow it to extend out of the front of the LCQ Classic and into the back of the Faraday plate of the GID-M (see figure 4.2). The following describes the modifications required to fit the capillary to allow ions to flow from the drift region of the GID-M to the LCQ classic lens system. The new capillary is 190 mm in length and has a 380 μm internal diameter, which is the widest that is possible without compromising the vacuum system in the ITMS. The original capillary could be capped with a septum and this was always in place when starting up the vacuum pumps in the ITMS to minimise the strain on them. The new capillary cannot be capped once fitted into the IMS, and the capillary must be fitted before being inserted into the ITMS. The original capillary had a diameter of 508 μm,

however, a suitable vacuum could not be reached if this diameter of capillary was left uncapped. Therefore, a smaller diameter had to be used for the new capillary.

One end of the new capillary was tapered so as to allow for correct alignment with a 500 μm hole drilled through the back of the FP. The FP consists of a sheet of metal mounted onto a thin ceramic plate. The external diameter of the capillary is 1600 μm which ensures that the capillary does not protrude through the FP and make contact with the metal surface at which the ions are detected. The capillary is also supported and aligned at the FP end with a PTFE aligner fixed on the back of the FP of the GID-M. The PTFE aligner was glued in place using a low emission epoxy resin (Scotch Weld EPX^{TM} DP760). A Proton Transfer Reaction - Mass Spectrometer (PTR-MS) was used to investigate potential emissions of the hardened epoxy resin. No volatiles, whose proton affinities are higher than that of water, were being emitted by the hardened resin.

The capillary passes through a 7 mm diameter hole in the casing of the GID-M that is concentric with the hole drilled in the FP. This was achieved by using a 7 mm PTFE coated silicon septum with a hole drilled through the middle through which the capillary was inserted. This also allowed more flexibility for small adjustments of the capillary without having to unfasten bolts and screws.

The original capillary (of 114 mm in length) in the LCQ Classic was permanently sealed into a heater jacket. Therefore, a new heater jacket without a capillary was acquired to enable the new longer capillary to be easily slotted into position. The new capillary required additional sealing nuts and O-rings that were fitted at the point where the heater jacket and capillary protrude from the LCQ classic.

The GID-M, capillary and ion lenses could be assembled externally (as is illustrated in the photograph of figure 4.6) to the LCQ Classic to ensure correct alignment of the capillary.

Correct alignment ensures that the capillary is not bent or forced in any direction when passing from the LCQ classic lens system to the GID-M. This whole system fits into the LCQ Classic and sits neatly on the sliding support designed for the ESI unit.

4.3.5 Operation of the ion mobility spectrometer-ion trap mass spectrometer

The two parts of the instrument (the IMS and ITMS) are operated independently. The GID-M is controlled using Trimscan© software (Smiths Detection Ltd, Watford) from a PC, via a rocket port. The LCQ Classic is controlled via a separate PC using Xcalibur™ v1.1 software, (Finnigan Corp). The IMS-ITMS system was operated in Selected Ion Mobility Mass Scan (SIMMS) mode, where both of the gates are pulsed, or in DC mode, where both gates are held open to obtain m/z spectra independent of mobility.

The LCQ classic was operated with the Automatic Gain Control (AGC) off as we found that this improved the sensitivity of the instrument significantly, in agreement with findings from the Clowers & Hill IMS-ITMS.[59] When the IMS-ITMS system was operated in DC mode, all m/z spectra with neither isolation nor fragmentation, were obtained as one off 10 s scans. This is the maximum allowable scan time that is dictated by the injection time. The isolation and m/z scan periods add only fractions of a second to the total scan time. For isolation of parent ions in DC mode, spectra were recorded for between 10 seconds (1 scan) to 4 minutes (24 × 10 s scans) per m/z spectra, depending upon the ion intensity. Recording m/z spectra for SIMMS gave the lowest ion intensity, and therefore spectra were recorded for up to 30 minutes (180 × 10 s scans). The GID-M completes one mobility scan in 86.25 ms and therefore during a single 10 s m/z spectra in LCQ classic, approximately 116 mobility scans would have taken place in the GID-M.

For isolation of trapped ions in the LCQ Classic, a very wide isolation window of 12-18 m/z was required to maintain the intensity of the ion peak compared with no isolation. This has been noted previously in the LCQ Classic although no explanation is given.[62] However, it could be because the LCQ Classic, when isolating, operates at the edge of the region in which ions have stable trajectories in the trap. Therefore a wider isolation window brings the q value of the required ion further within the theoretical stability region, and therefore the ion is less likely to be ejected from the trap due to non-linear fields, space-charge effects and is less likely to incur boundary-activated dissociation.[63] This wide isolation window is not a concern in these experiments since no other ions lie within ± 9 m/z of the parent ion.

The studies involving DMMP, DEMP and DiPMP required the use of a dwell time. Initially we expected to have to use an excitation voltage to cause dissociation of the ammoniated parent ions. However, we found that sufficient energy was imparted to the ions by storing them in the ion trap. The dwell time is the amount of time that the ions are stored in the trap after isolation and prior to m/z analysis. This was achieved by altering the 'Activation' (or excitation) time in the Xcalibur software, but with the activation energy set to 0 %. The q_z value for each parent ion during this dwell time was set to 0.25. A typical scan cycle for the dwell time experiments in the ITMS can be summarised as follows. The ions are injected into the trap (for a set time, typically 10 s in this system). The required parent ion is then isolated at a q_z value of 0.83. The parent ion is then allowed to dwell in the trap at a reduced q_z value of 0.25, where ions with a range of m/z are stable. The m/z scan then follows where the RF voltage amplitude is ramped up on both the end-cap and ring electrodes to eject ions of increasing m/z that will then be detected at the conversion dynode detector.

The operating conditions used in this study for the GID-M and LCQ Classic, including voltages applied to the ion optics in the LCQ (all labelled in figure 4.2) are provided in table 4.1.

Table 4.1 Operating parameters for the IMS-ITMS system. The various lens and octapole voltages described in the ITMS section are all part of the ion optics system between the IMS and the ion trap.

GID-M Ion Mobility Spectrometer	
Drift tube temperature	299-301 K
Drift tube pressure	903 – 938 mbar
Potential between 1st gate and FP	2260 V
LCQ Classic Ion Trap Mass Spectrometer	
Pressure in ion optics region	1.55 mbar
Pressure in trap region	1.5×10^{-5} mbar
Capillary voltage	-4 V
Capillary temperature	308 - 310 K
Tube lens offset	-39 V
Octapole 1 offset	-5 V
Interoctapole Lens	-11.9 V
Octapole 2 offset	-14.1 V
Octapole RF	640 V_{p-p}
Electron Multiplier	-1200 V

The capillary in the LCQ classic is usually heated to around 200 ºC when using ESI. In this study, it was found that ion transmission fell to zero when the capillary was heated above the ambient temperature, which is slightly above room temperature (~31 ºC) due to heating

from the operating turbo pumps inside the LCQ classic casing. The voltages applied to the ion optics were individually optimised to produce maximum total ion count when the IMS-ITMS system was operated in DC mode.

The pressure in the drift tube of the GID-M varies with atmospheric pressure, our system runs at 60-90 mbar below atmospheric pressure due to the additional airflow out of the drift tube through the capillary, which is being pumped from the first pumping region of the LCQ Classic. A typical operating pressure of 915 mbar gives an E/N value of 1.27 Td for the GID-M drift region

4.3.6 Chemical samples

All chemicals were commercially purchased and were used with no further purification. Dimethyl methylphosphonate (Sigma-Aldrich Company Ltd. Dorset, England. 97 %) (DMMP), diethyl methylphosphonate (Sigma-Aldrich 97 %) (DEMP) diisopropyl methylphosphonate (Alfa Aesar, Lancashire, England. 95 %) (DiPMP), trimethylphosphite (Sigma-Aldrich 99+ %) (TMPite), triethylphosphite (Sigma-Aldrich 98 %) (TEPite). DMMP, DEMP and DiPMP, must be registered under Schedule 2 of the Chemical Weapons Convention (CWC).

4.3.7 Sample injection

The organophosphorus ester samples were injected using a simple syringe system. Several drops of the sample were added to a small amount of cotton wool placed in a 30 ml glass syringe that was subsequently filled with lab air. The sample flow was controlled by the use of a syringe drive. The amount of flow required was judged by the relative intensity of the RIP, monomer and dimer peaks (see section 4.4.1 for identification of the monomer and dimer

peaks) in the mobility spectrum. The concentrations were varied such that the monomer or dimer peak dominated the mobility spectrum for monomer and dimer studies respectively. Actual concentrations were not required for these studies. The syringe drive was generally used at a rate of 300 ml/hr (maximum setting) to ensure a good ion count in the ITMS.

The GID-M has an inlet flow rate of 750 ml/min, the syringe needle was placed inside the inlet tube of the GID-M so that the sample was introduced into the GID-M along with lab air. The GID-M is designed to sample air, so no dry nitrogen or other gas is needed for sampling in this case. All cleaning and drying of the air is performed internally within the GID-M.

4.3.8 Resolution and signal-to-noise ratio

Before recording any mass spectrometric data, investigations of resolution and Signal-to-Noise Ratio (SNR) of the IMS were conducted, the results of which are shown in figure 4.7. Importantly, these data were taken once all modifications were completed and the GID-M was connected to the ITMS. This is in order to make comparisons between the system created as described here with other IMS systems, including the unmodified GID-M.

The spectra used to calculate the data presented in figure 4.7 were an average of 16 mobility spectra taken from Trimscan© with a rolling average of 5 spectra applied on top of this. These are the data that are viewed in real time under normal IMS-ITMS operating conditions; each of the above averaged spectra takes less than a second to generate. IMS systems may be operated with a range of gate widths. The final gate width is often chosen as a compromise between resolution and signal intensity. To investigate the effect of the gate width on resolution and SNR, the first gate width was increased from 100 to 600 μs in steps of 50 μs.

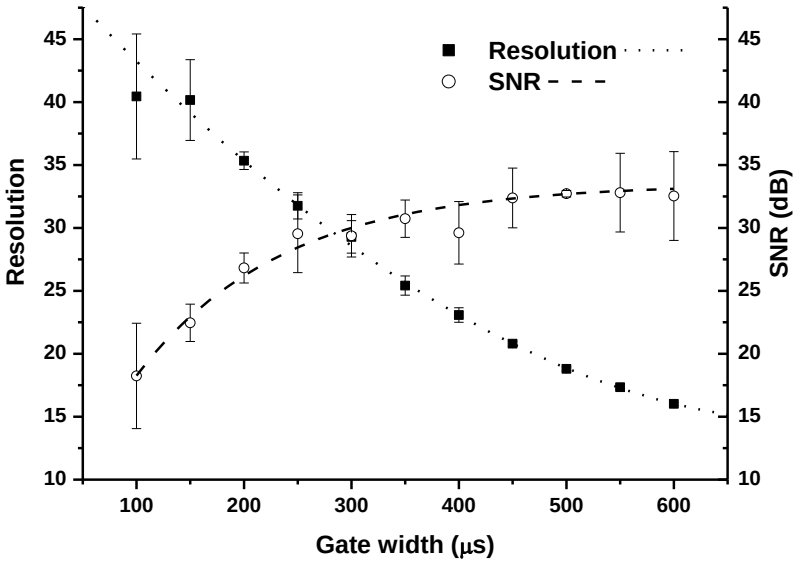

Figure 4.7 The Signal-to-Noise Ratio (SNR) and resolution of the ammonia based Reactant Ion Peak (RIP) of the GID-M as a function of the gate pulse width of the first gate in the drift tube. The lines of best fit are to guide the eye only.

The resolution, *R*, of an IMS has been calculated as follows

$$R = t_d/t_{FWHM},^{64}$$

where t_d is the drift time of the ion mobility peak and t_{FWHM} is the full width at half the maximum peak height. As expected, the resolution increases as the gate width is decreased. There are a number of factors that affect resolution including temperature,[65] voltage gradient in the drift region,[66] chemistry, length of the drift tube and space charge effects.[67] The maximum resolution obtainable in our system is 41 ± 5 which is fairly low in comparison to other IMS research systems,[56, 66, 68, 69] but is more than sufficient in our investigations owing to the large separation between the ion mobility peaks of the organophosphorus esters used in this study. Interestingly, the ion signal at low gate widths is far greater than in the Clowers & Hill IMS-ITMS system: for example, no data were obtained for cocaine at ion gate pulse widths below 0.2 ms.[59] The resolution, however, in our system is lower in comparison, most

probably because the drift tube is less than half the length of the drift tube in the Clowers and Hill system.

The SNR has been calculated as follows

$$SNR\ (dB) = 20\ \log_{10}(RMS_{signal}/RMS_{noise}).^{70}$$

In contrast to the resolution, the SNR increases with increasing gate width, but the curve flattens off towards higher gate widths as the signal intensity reaches it maximum.

It must be noted that the noise was far less before the drift tube was modified, this is thought to be due to the loosening of the electrodes at the FP end of the drift tube after modification. The electrodes are only secured at the base by a thin layer of solder and a considerable amount of force is applied when the capillary is inserted into the FP. The loose FP and electrodes are then more likely to vibrate and pick up noise from the surrounding pumps. Furthermore, the addition of the second gate reduces the transmission of the ions and therefore the maximum ion mobility peak intensity. The GID-M was operated with a gate width of 250 μs for the following studies. An unmodified GID-M which, under normal conditions, would also operate with a gate width of 250 μs, has a resolution of 35, which is comparable to the modified system. However, a typical SNR of 43 is higher than that of the modified GID-M, as expected

4.4 Results and discussion

Independent of the mode of operation of the IMS-ITMS, no ions from the RIP were observed in the ITMS m/z spectra. This is thought to be because the ammonia ion clusters produced in the GID-M dissociated to a low m/z[71] (< m/z 50), upon leaving the drift tube, which the LCQ Classic used in this study is not capable of detecting. This dissociation is partly due to the potentials applied to the ion optics and partly during the extended ion injection and trapping time in the ITMS. However, to identify the type of reactant ions being produced in the IMS, the molecular sieve pack was attached to the inlet of an IMS-quadrupole mass spectrometer (IMS-quad). The IMS-quad was being developed in parallel with the IMS-ITMS system. Although the IMS in the IMS-quad, being built in the Molecular Physics laboratory, is different from the GID-M, it was maintained at a similar temperature and E/N to the GID-M. The quadrupole mass spectrometer does not have any restriction in low m/z. The resulting spectrum of the RIP was dominated by m/z 35 ions corresponding to $NH_4^+.NH_3$. The IMS-quad also has a series of ion optics that will cause fragmentation, similar to the ITMS. Therefore, it is not possible to accurately realise the identity of the dominant ions that contribute to the reactant ion peak, from these m/z spectra. More detail about the IMS-quad system can be found in section 4.4.5.

4.4.1 Selected ion mobility mass spectra of organophosphates

Upon the introduction of the organophosphates DMMP, DEMP and DiPMP (figure 4.1), the ion mobility spectrum obtained using the GID-M showed three mobility peaks. This is illustrated for DMMP in figure 4.8. The first mobility peak is the RIP, the second and third peaks result from neutral DMMP reacting with the ions that make up the RIP. The identification of these peaks can only be made through mass spectrometric analysis.

However, it is expected that these are associated with the DMMP monomer and dimer ions respectively. This was confirmed later by application of Selected Ion Mobility Mass Spectra (SIMMS) measurements. DEMP and DiPMP produce very similar ion mobility spectra, presenting two ion mobility peaks other than the RIP. The DEMP ion mobility peaks have a longer drift time than the DMMP peaks, and similarly for DiPMP with respect to DEMP. This is expected as mobility is related to the cross-sectional area of the ion. DEMP has bigger functional groups than DMMP, and DiPMP has bigger groups than DEMP, therefore their collisional cross sections should also follow the same trend.

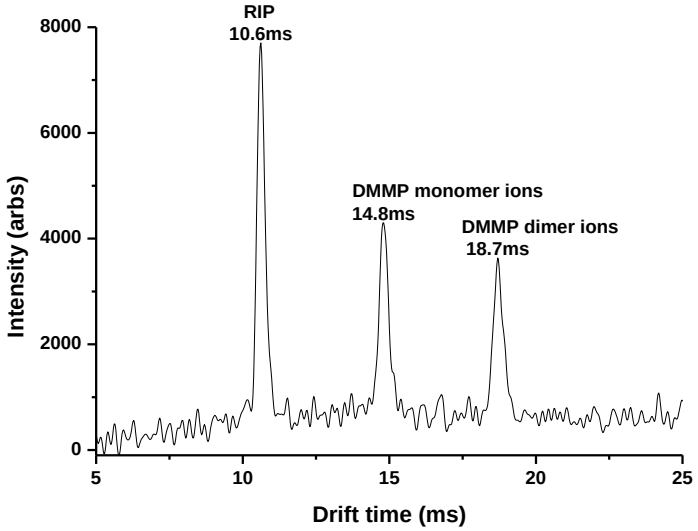

Figure 4.8 Ion mobility spectrum of DMMP using a 250 µm gate width and associated assignments of the peaks.

An ITMS m/z spectrum of DMMP taken in DC mode is shown in figure 4.9 (a), this shows four peaks corresponding to the protonated and ammoniated, monomer and dimer ions of DMMP (i.e. $M.H^+$, $M.NH_4^+$, $M_2.H^+$ and $M_2.NH_4^+$ where M is DMMP). It is evident that both the protonated monomer and dimer are present at m/z 125 ($DMMP.H^+$) and m/z 249 ($DMMP_2.H^+$), respectively, as are the ammoniated monomer and dimer at m/z 142 ($DMMP.NH_4^+$) and m/z 266 ($DMMP_2.NH4^+$). This does not imply that the protonated species are present in the drift tube. They are almost certainly formed after exiting the drift

tube due to the series of voltage gradients in the lens system of the ITMS that, in the higher pressure region, could fragment the ammonia from the parent ion via collision induced dissociation (CID).[71] There may also be fragmentation caused by simply trapping the ions for the extended periods used in this paper (i.e. 10 s). This is consistent with the observed symmetry of the ion mobility peaks as one would expect to see at least a broad asymmetric peak if both the protonated and ammoniated ions are present in the drift tube. This is also consistent with data from the IMS-quad system as briefly described in section 4.4.5.

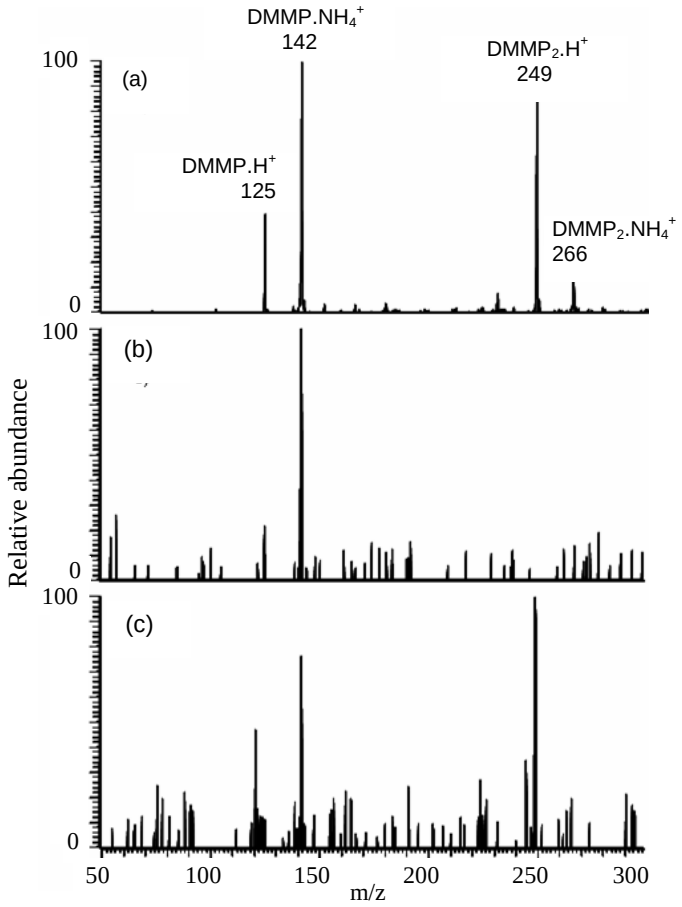

Figure 4.9 (a) is the mass spectrum of DMMP taken in DC mode and (b) and (c) are the second gate mobility peak selection of the second and third mobility peaks as shown in the example mobility spectra in figure 4.8.

SIMMS for DMMP were obtained using the technique as described by figure 4.3, for the second and third mobility peaks, as shown in figure 4.9 (b) and (c), respectively. These SIMMS data were obtained with a first gate width of 250 µs and the second gate width of approximately 500 µs (maximum gate width). Only the DMMP monomers are present upon selection of the second ion mobility peak as expected.[72] Upon selection of the third ion mobility peak, both the monomer and dimer ions are observed in the m/z spectrum. The presence of the monomer ions in these spectra is most probably due to fragmentation in the ITMS as explained above. Similar results have been obtained for the other simulants when selecting the second and third ion mobility peaks in the IMS spectrum of DEMP and DiPMP.

Air from the forward and contra flow is constantly circulated through the molecular sieve pack. A fresh ammonia-doped molecular sieve pack on the GID-M removes the neutral sample very quickly from the GID-M drift tube. This means that every time the syringe drive is stopped and refilled (~ every 6 minutes at the maximum injection rate), the sample concentration in the GID-M drops almost instantaneously. Refilling the syringe with air to start injection again takes ~ 30 seconds. During the recording of a 30 minute SIMMS spectra in the ITMS, this can reduce the total possible ion intensity achieved by up to 10 %. However, it was found that no dimer ions could be detected at all using a new ammonia doped molecular sieve pack when performing SIMMS in the ITMS. Conflictingly, the dimer ion mobility peak intensity recorded on the Faraday plate of the IMS is higher with a new ammonia doped sieve pack than with a more depleted one. It is not clear why this might be.

A higher ion intensity during the recording of SIMMS data was achieved in the ITMS, by using an old, more depleted sieve pack (with at least 6 months continuous use, Smiths Detection recommend the sieve pack in the GID-M is changed every 6 months). The effect is that the RIP is shifted to longer drift times, most probably due to a higher concentration of

water in the system. This leads to ions combined with large water clusters, for example $[M(NH_3)_n(H_2O)_m]H^+$ where n and m = 0, 1, 2, 3… and M is the sample. m would be higher for a more depleted sieve pack. The monomer ion peaks of DMMP, DEMP and DiPMP were also shifted to longer drift times, but to a lesser extent than the RIP, and the dimer peaks were unaffected.

Ions clustered with water were not observed in the m/z spectra, most probably due to their dissociation whilst passing from the GID-M to the ion trap (similar to the dissociation of the DMMP dimer and the possible dissociation of the RIP ions as explained previously). The ratio of ammoniated parent ions to protonated parent ions for any of the chemicals in the m/z spectra was unaffected. Therefore, it is considered that the ammonia concentration of a more depleted sieve pack has not significantly dropped. This also meant that the m/z spectra were essentially the same, independent of the run time of the sieve pack, even if the ion mobilities shifted. A depleted molecular sieve pack does not refer to a lack of ammonia, but to the reduction in its ability to remove water from the system.

Although we used a depleted sieve pack, it is more useful to quote reduced mobilities, K_0, ($cm^2\ V\ s^{-1}$) of DMMP, DEMP and DiPMP for a new ammonia doped molecular sieve pack (see table 4.2). Firstly they are more representative of a GID-M, as used in the field, and secondly, the effect of water in the system can be ruled out. This is valuable since there is no current method of measuring the humidity in the GID-M and therefore comparing the water content of the drift tube with other apparatus.

Table 4.2 Reduced mobilities of DMMP, DEMP and DiPMP 1st and 2nd ion mobility peaks, as well as the RIP recorded in each ion mobility spectra. The 1st ion mobility peaks are considered to be due to monomer ions and the 2nd due to the dimer ions of each chemical (see figures 4.8 and 4.9).

± 0.005 $cm^2 V s^{-1}$	RIP	1st ion mobility peak	2nd ion mobility peak
DMMP	2.19	1.58	1.25
DEMP	2.19	1.44	1.10
DiPMP	2.19	1.35	0.99

4.4.2 Ion mobility spectrometry-ion trap mass spectrometric studies of organophosphates

Operating in DC mode, the ammoniated monomer ions of each of the three chemicals, DMMP, DEMP and DiPMP, were isolated in the ion trap. After isolation, the dissociation of ammonia from these monomer ions was followed as a function of dwell time in the trap. During the dwell time all ions within a specified m/z range have stable trajectories in the trap before an m/z scan is produced. Figure 4.10 (a), (b) and (c) show the relative intensity of the ammoniated and protonated monomer ions with increasing dwell time for DMMP, DEMP and DiPMP respectively. The plots are fitted with exponential curves from 10 ms onwards. Each data point corresponds to measurements taken from between four and eight m/z spectra from which the associated errors are obtained (to one standard deviation). The main source of experimental error in these data is due to the very low intensity of ions in the ion trap, this is particularly the case with the dimer ions.

Dissociation rates were determined from plots of $-\ln[A_0^+]/[A^+]$ versus dwell time (t), where $[A_0^+]$ is the initial parent ion concentration and $[A^+]$ is the parent ion concentration at a specified dwell time. The normalized parent ion signal intensity as a function of dwell time for ammoniated DMMP, DEMP and DiPMP are shown in figure 4.11. Only the linear portion

of the data is plotted, corresponding to dwell times greater than 10 ms, as before this time, equilibrium of the internal energy distribution has not been reached. The delay in the onset of the dissociations will be discussed later in this report. The first order dissociation rate coefficients, k, are equal to the gradients of these plots and the following values have been obtained: $DMMP.NH_4^+$ k = 50 ± 1 s^{-1}, $DEMP.NH_4^+$ k = 47 ± 2 s^{-1} and $DiPMP.NH_4^+$ k = 51 ± 3 s^{-1}. The error in the gradient of the linear fit, and therefore k, is weighted by the experimental error in the data. To within experimental errors the dissociation rates are identical. Although these dissociation rates have been calculated with a low error, it is not possible to make any more assumptions about the decay of these monomers apart from that fact that they appear to be of a first-order rate. This is due to the insufficient information regarding the detailed operation of the LCQ Classic.

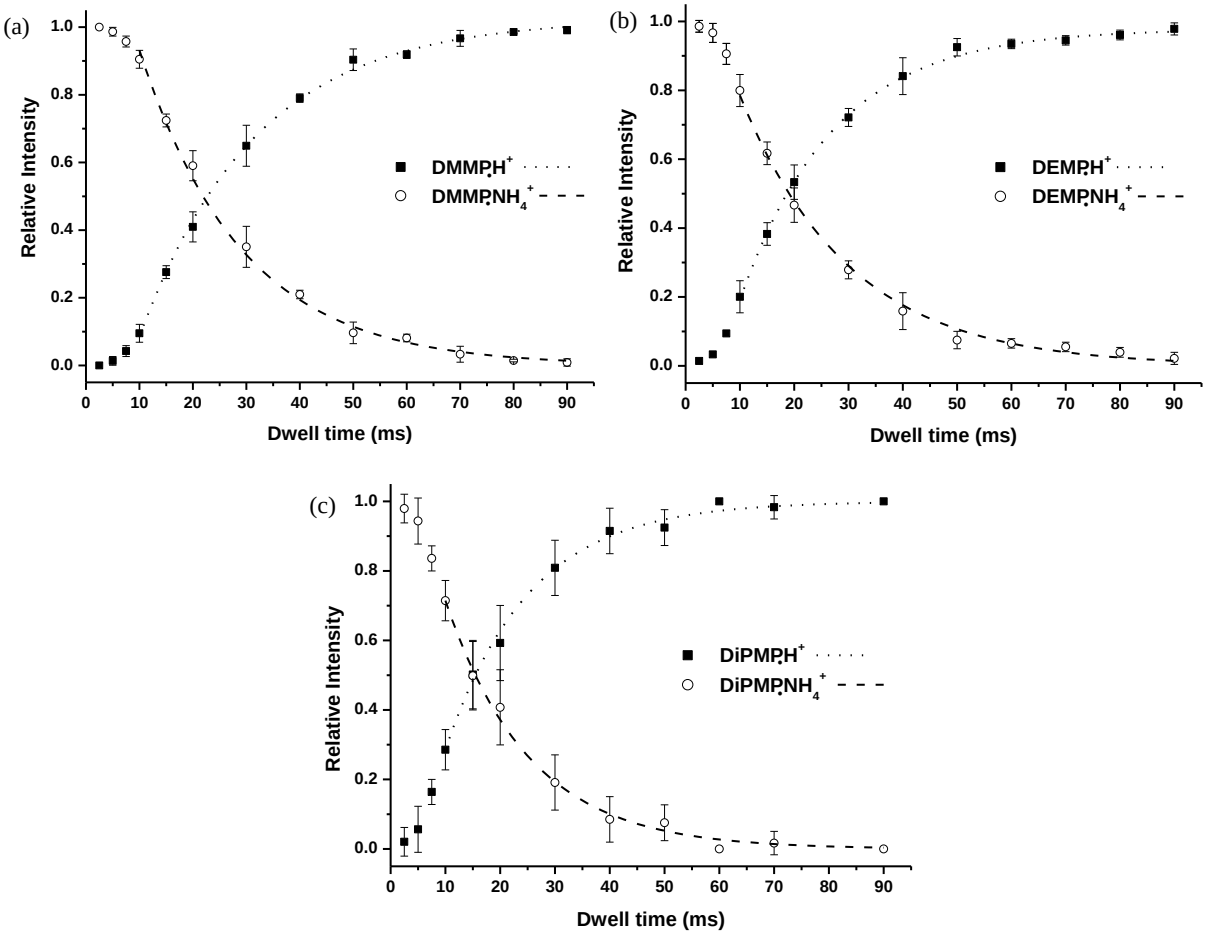

Figure 4.10 Graphs (a), (b) and (c) respectively show the relative intensities of the protonated and ammoniated monomers for DMMP, DEMP and DiPMP plotted against dwell time in the trap after isolation of the ammoniated monomer.

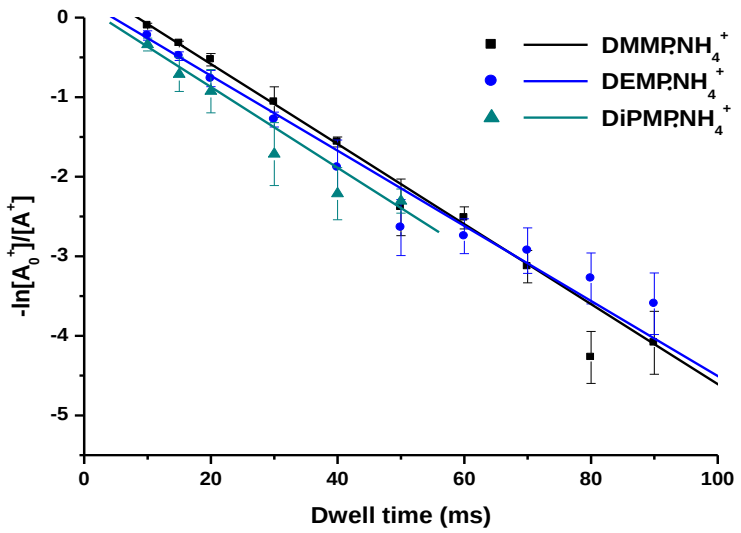

Figure 4.11 Kinetic data for the dissociation of ammonia from the ammoniated monomers of DMMP, DEMP and DiPMP.

The ammoniated dimers of DMMP, DEMP and DiPMP were also isolated with increasing dwell times and are shown in figure 4.12 (a), (b) and (c) respectively. $DMMP_2.NH_4^+$ dissociates into $DMMP_2.H^+$ and $DMMP.NH_4^+$ in equal quantities (within experimental error) as a function of time. $DEMP_2.NH_4^+$ dissociates to $DEMP_2.H^+$ and only a small amount of $DEMP_2.H^+$ is observed (< 10 % relative intensity at 100 ms dwell time). Finally, $DiPMP_2.NH_4^+$ dissociates only to $DiPMP_2.H^+$. The rate coefficients derived from the slopes of the $-\ln[A_0^+]/[A^+]$ plots have too high an error associated with them to be meaningful, and therefore they will not be included.

The branching ratios of $DMMP_2.NH_4^+$ and $DEMP_2.NH_4^+$ could possibly be explained by calculating the energetics of each of the fragmentation pathways. However, for $DiPMP_2.NH_4^+$, this is not the case. $DiPMP_2.NH_4^+$ never reaches 100% intensity relative to the product ion $DiPMP_2.H^+$. If there were two structures of $DiPMP_2.NH_4^+$, one that fragments into $DiPMP_2.H^+$ with the rate as shown in figure 4.12 (c), and another structure that will not fragment under the conditions in the trap during the dwell time, this could explain the results

observed. Similarly, it is also possible that $DEMP_2.NH_4^+$ and $DMMP_2.NH_4^+$ also have two different structures, one that preferentially fragments to the protonated dimer and the other that fragments to the ammoniated monomer.

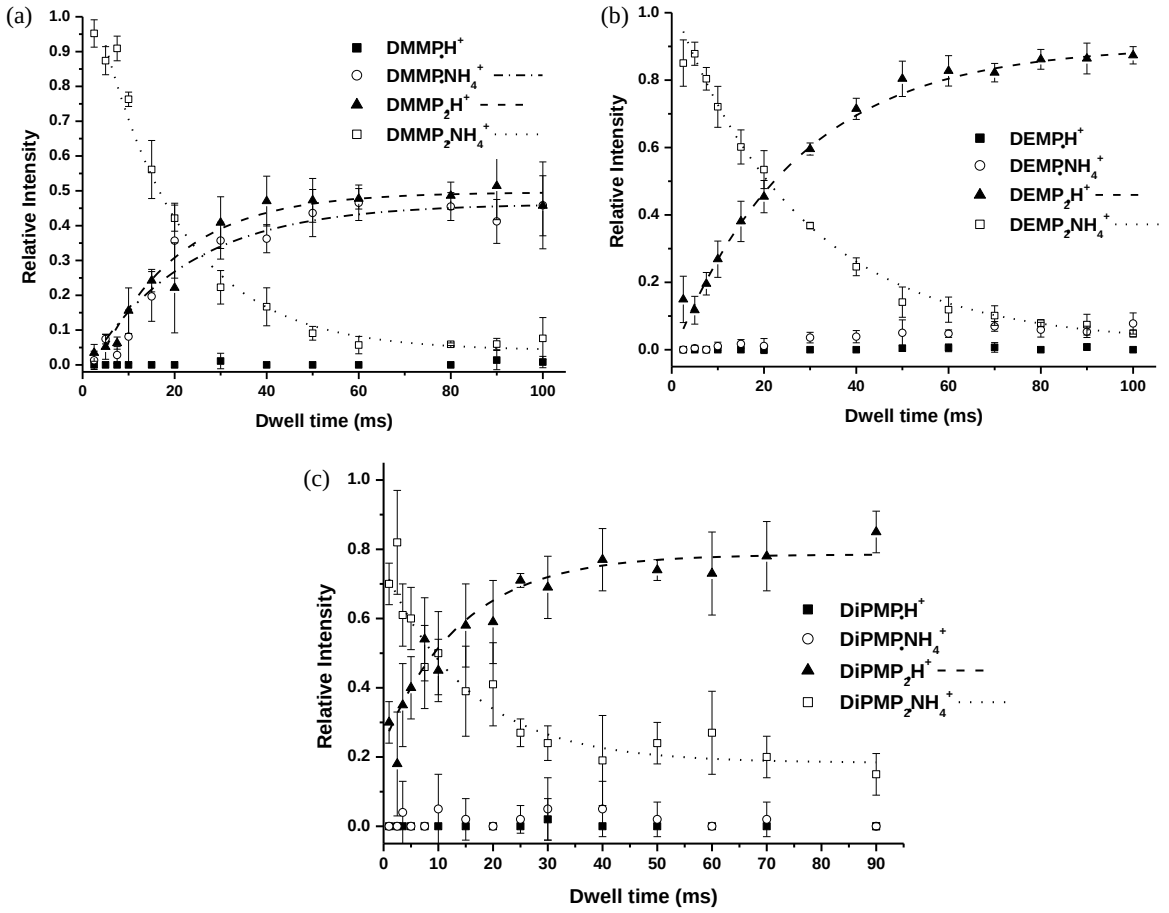

Figure 4.12 (a), (b) and (c) respectively show the relative intensities of the ammoniated and protonated monomers and dimers of DMMP, DEMP and DiPMP with varying dwell time, after isolation of the ammoniated dimer in the ITMS.

There is a slight curve of the data points before the onset of the exponential decay curves, particularly for the monomer ions. This can be seen before approximately 10 ms dwell time for all three monomers, but it is most pronounced in the decay of $DMMP.NH_4^+$. A possible explanation for this is that there is a ramp in the voltages applied to the ring electrode that lasts approximately 3 ms. During this time the voltages are changed such that ions with a

range of m/z have stable trajectories in the trap, rather than just the parent ion (as in the isolation period). This would mean that the product ions (the protonated monomers) would not be 100 % stable in the trap until 3 ms has passed, thus apparently delaying the onset of the loss of ammonia from the parent ion. However, it is difficult to explain why the actual delays seen are significantly more than this.

Similar 'S' shaped decay curves have been observed in ion trap mass spectrometers and have been associated with what is known as an 'induction period'. This is when a cloud of ions is slowly heated so that their internal energy distribution is shifted from an initial state to a final state, where some of the ions will have gained enough energy to dissociate.[73-75] However, this theory is applicable when a resonant excitation voltage is applied to the end-cap electrodes to cause CID of the parent ion. In written and verbal communications with Finnigan (now Thermo Fisher) I have had conflicting descriptions of the voltages applied in the LCQ Classic during the dwell period with an activation amplitude of 0%. It is not clear therefore, to what extent the ions are being 'excited'.

Research undertaken by McLuckey et al. shows that it is possible to compare the decay rate coefficients of relatively high mass ions (> m/z 400), provided they are trapped at low *q* values (< 0.5). In this limit, they should not gain significant amounts of energy (known as rf heating) from an RF trapping field applied to the ring electrode.[76] Therefore, the ions will be close to the temperature of the helium buffer gas in the ion trap.

Since it is not clear what is happening in the LCQ classic, if the ions are simply trapped, or in fact how these trapping voltages are applied to the electrodes, I can unfortunately make no further comments about this data. I have documented the relevant theories that might be applied if one were working on an ITMS system where all these details were known.

4.4.3 Ion mobility spectrometry-ion trap mass spectrometric studies of organophosphites

TEPite shows similar properties to DMMP, DEMP and DiPMP in that their ammoniated parent ions dissociate to the corresponding protonated ions when trapped in the ITMS for a dwell period of several ms. The ammoniated TMPite parent ions do not dissociate to the protonated monomer in the trap with increasing dwell time. TMPite and TEPite have mobility spectra that depart from the usual three ion mobility peaks, for example, of DMMP, i.e. RIP, monomer sample ion and dimer sample ion (as shown in figure 4.8). It is of interest therefore, to investigate these mobility spectra and to perform MS^n studies of TMPite and TEPite with the ITMS.

Trimethyl phosphite

The ion mobility spectrum for TMPite given in figure 4.13, shows an RIP and two other ion mobility peaks close together. For a nearly new ammonia doped molecular sieve pack (used for results in figure 4.13) on the GID-M, the RIP has a K_0 of 2.06 $cm^2\ V\ s^{-1}$, the two mobility peaks have reduced mobilities of K_0 = 1.57 $cm^2\ V\ s^{-1}$ and K_0 = 1.47 $cm^2\ V\ s^{-1}$ (all ± 0.005 $cm^2\ V\ s^{-1}$). Note that the RIP of this sieve pack has already shifted when compared with the K_0 of the RIP for the DMMP data, with only 1 months continuous use.

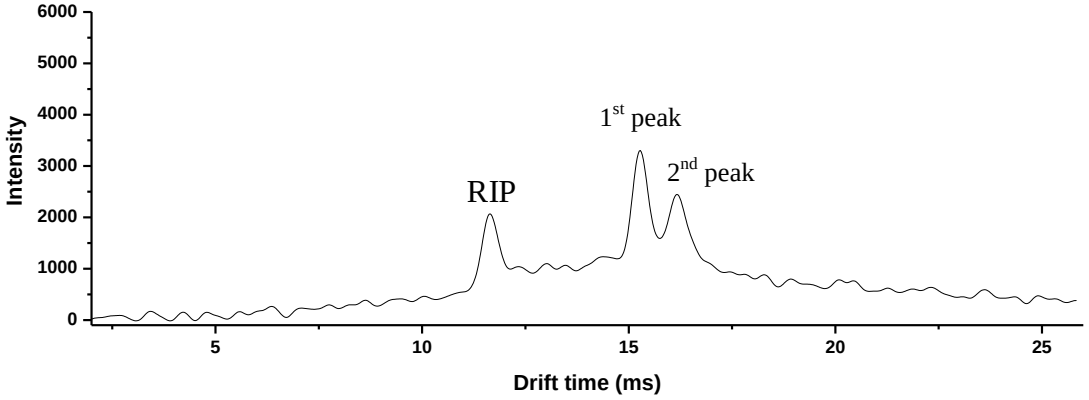

Figure 4.13 Ion mobility spectrum for trimethyl phosphite.

The formation of the second ion mobility peak occurs with higher concentrations of TMPite in the drift tube.

The m/z spectrum of TMPite taken in DC mode is shown in figure 4.14. This is not as straight forward as the m/z spectra for DMMP, DEMP and DiPMP. The most probable chemical formula of the relevant ions are shown in table 4.3 (other small ion peaks that may be present in figure 4.14 are not included in table 4.3 because they are not reproducible between m/z spectra). It must be restated that the empirical formulae suggested here are not intended to imply specific structures of the ions.

The trimethyl phosphate ion (m/z 158) may result from reactions of TMPite with the air in the syringe, or within the GID-M reaction region.

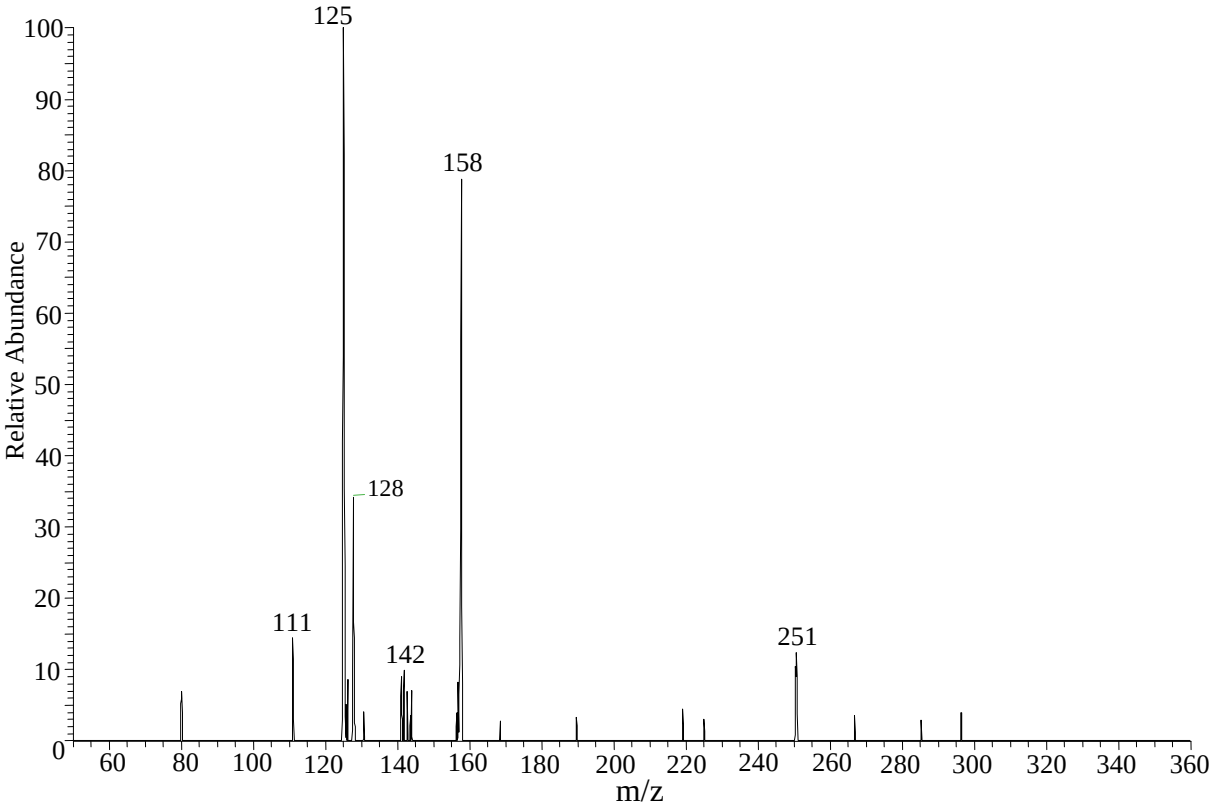

Figure 4.14 m/z spectra of TMPite taken in DC mode in the IMS-ITMS.

m/z	Suggested formula
111	$[(CH_3O)_2P(OH)]H^+$
125	$[(CH_3O)_3P]H^+$
128	$[(CH_3O)_2P(OH)]NH_4^+$
141	$[(CH_3O)_3PO]H^+$
142	$[(CH_3O)_3P]NH_4^+$
158	$[(CH_3O)_3PO]NH_4^+$
251	$[(CH_3O)_3PO][(CH_3O)_2P(OH)]H^+$

Table 4.3 Suggested formula for the ions seen in the spectra in figure 4.14 for a TMPite sample. m/z 125 is the protonated parent ion.

In DC mode, isolation and fragmentation of the above m/z peaks in the ITMS gives a series of fragmentation pathways that agree with the suggested formula in table 4.3. For example, m/z 128 fragments to 111, m/z 142 to 125 and m/z 158 to 141 which all correspond to a loss of NH_3 (as seen with ammoniated DMMP, DEMP and DiPMP). Fragmentation of m/z 251 results in an ion at m/z 141, a loss of m/z 110. This implies that m/z 251 is a protonated dimer of 140 amu and 110 amu. Interestingly, no dimers of the parent ion (TMPite, 124 amu) are seen, these would be expected at the same m/z as the DMMP dimers (m/z 249 and m/z 266), since DMMP and TMPite have the same mass.

SIMMS of the two TMPite mobility peaks were performed and the resultant m/z spectra are shown in figure 4.15 (a) and (b). These m/z spectra are of very low intensity and the peaks are only just above the noise level of ~5 x 10^4 arbitrary units, therefore they must not be taken at face value. To be sure of true identification of the m/z of the ions that make up an ion mobility peak, several aspects must be considered. Firstly, the m/z spectra must be reproducible from one spectrum to the next. Secondly, the m/z values in a SIMMS must correspond to m/z values in the spectra taken in DC mode (i.e. figure 4.14). Finally, the more dominant ion peaks are not necessarily the highest, but tend to be wider than peaks that are a product of noise at the conversion dynode detector in the ITMS.

The first ion mobility peak is due to an ion with m/z of 128 (figure 4.15 a). A suggested formula for this ion is $[(CH_3O)_2POH]NH_4^+$ as shown in table 4.3. There are several possible pathways for its formation. One example is that it could be formed from the parent molecule (TMPite) in the syringe, via loss of a methanol group and subsequent combination with OH in the air. This molecule is then ionized in the GID-M by addition of NH_4^+, giving m/z 128.

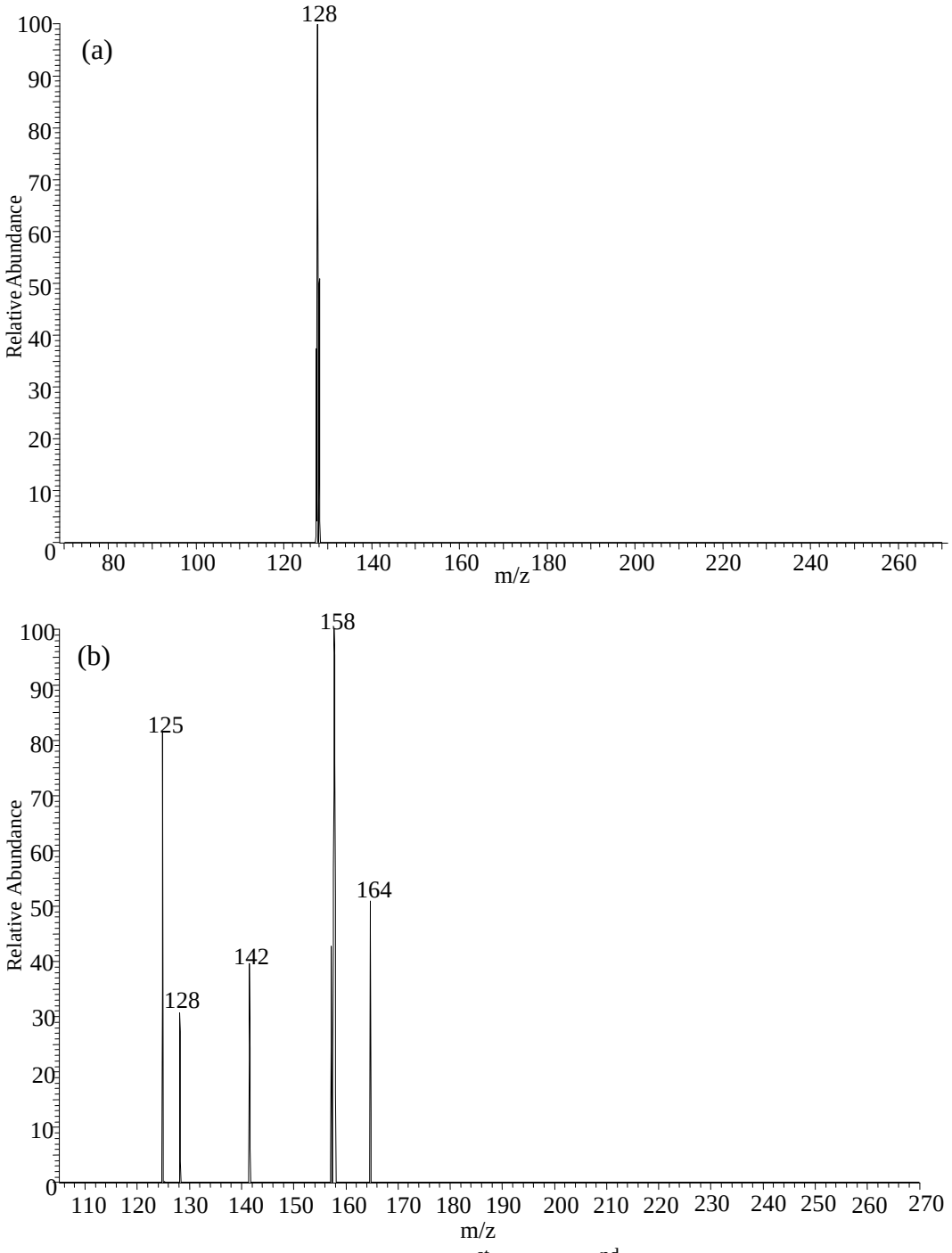

Figure 4.15 SIMMS spectra of the (a) 1st and (b) 2nd ion mobility peaks of TMPite.

The second ion mobility peak has a more complicated mass spectrum (figure 4.15 b)). 158 m/z is the dominant ion, which is ammoniated trimethyl phosphate. The peak at m/z 142 corresponds to the TMPite ammoniated parent ion. m/z 128 and 125 are also present in the m/z spectra. It may be that m/z 128 is from the first ion mobility peak and that the 2nd gate pulse is wide enough to allow some of this peak through since they are so close together. m/z 164 is not reproducible, and does not appear in the spectra in figure 4.14, so it is discounted.

Triethyl phosphite

Similar investigations were undertaken for TEPite as for TMPite. The mobility spectrum for TEPite is shown in figure 4.16. Four ion mobility peaks are evident with the reduced mobilities shown in table 4.4.

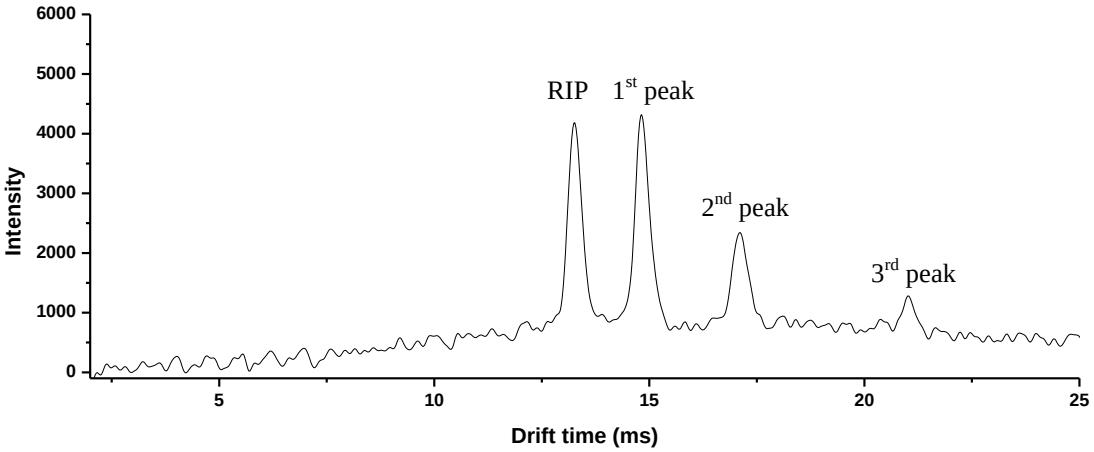

Figure 4.16 Ion mobility spectrum of TEPite

Table 4.4 Reduced mobilities for TEPite ion mobility peaks (figure 4.16) with a depleted molecular sieve pack and a nearly new molecular sieve pack.

± 0.005 $cm^2 V s^{-1}$	Depleted molecular sieve	Nearly new molecular sieve
RIP	1.71	2.06
1st ion mobility peak	1.54	-
2nd ion mobility peak	1.34	1.43
3rd ion mobility peak	1.09	-

The 1st and 3rd ion mobility peaks were not observed in the ion mobility spectra with a nearly new molecular sieve pack. This sieve pack also exhibited symptoms of a blockage somewhere within its flow system and unfortunately, another new molecular sieve pack was not available at the time to calculate the reduced mobilities. Therefore the depleted molecular sieve pack mobility spectrum is displayed in figure 4.16, in contrast to TMPite where better ion mobility spectra were obtained with the nearly new molecular sieve pack (figure 4.13).

The 1st ion mobility peak of TEPite does not appear until a few minutes after the syringe drive is started, the 2nd ion mobility peak decreases in intensity simultaneously. The 3rd ion mobility peak intensity is very low and is often difficult to see above the noise level, however it does not vary much with time. The sample injection method used in these studies may not be the most suitable since it can cause more confusion in interpreting the ion mobility spectra.

The m/z spectrum of TEPite taken in DC mode is shown in figure 4.17 and the most probable chemical formula of the main ions are shown in table 4.5. m/z 321 is the only ambiguous ion since it could be one of a number of adducts, the most likely combination is given in table 4.5. m/z 200 is considered to be triethyl phosphate, the presence of which is consistent with the observation of trimethyl phosphate in the m/z spectra of TMPite. Similar to trimethyl phosphate, triethyl phosphate could be formed in the syringe prior to sample injection by reaction of TEPite with air. Therefore, triethyl phosphate and trimethyl phosphate may be impurities that are only present due to the sampling method used. TEPite was investigated using the PTRMS in section 4.4.4 to try to further understand these results.

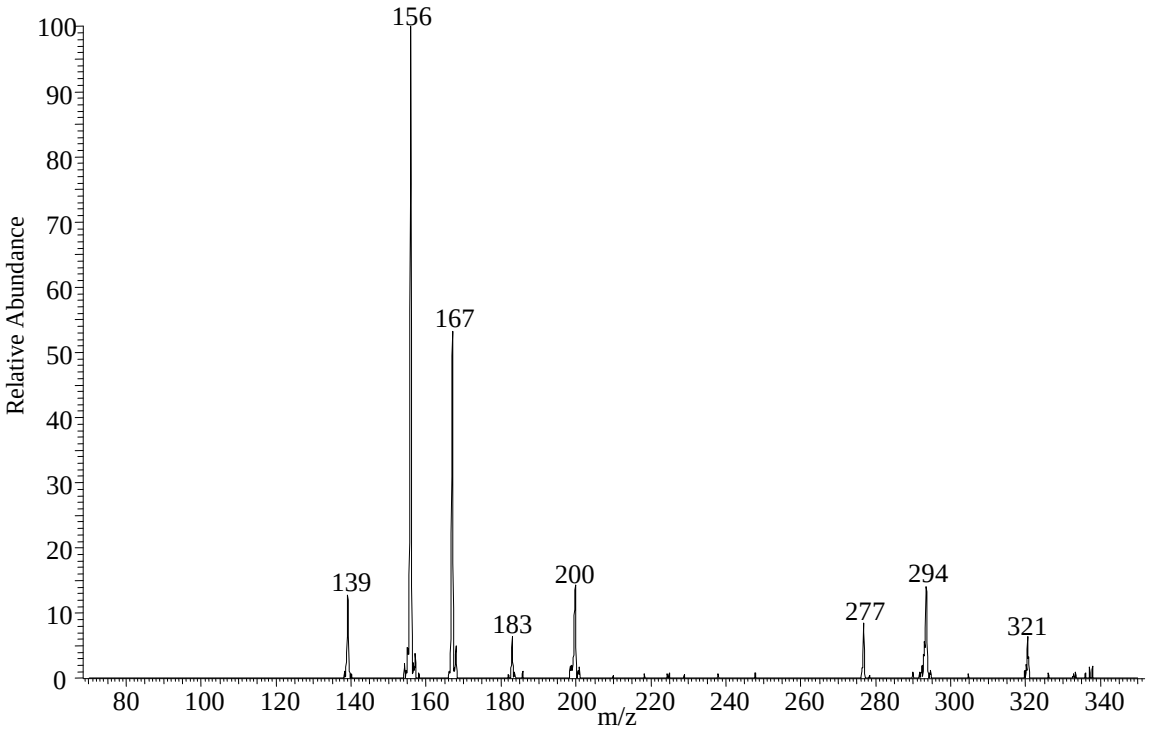

Figure 4.17 m/z spectrum of TEPite recorded with the IMS-ITMS system in DC mode.

m/z	Suggested formula
139	$[(CH_3CH_2O)_2P(OH)]H^+$
156	$[(CH_3CH_2O)_2P(OH)]NH_4^+$
167	$[(CH_3CH_2O)_3P]H^+$
183	$[(CH_3CH_2O)_3PO]H^+$
200	$[(CH_3CH_2O)_3PO]NH_4^+$
277	$[(CH_3CH_2O)_2P(OH)]_2H^+$
294	$[(CH_3CH_2O)_2P(OH)]_2NH_4^+$
321	$[182][138]H^+$

Table 4.5 Suggested formula for the ions seen in the spectrum in figure 4.17 for a TEPite sample. m/z 167 is the protonated parent ion.

The dominant ions in the m/z spectra for TEPite were each isolated and fragmented in the ITMS. The fragmentation pathways, as shown in figure 4.18, observed in the LCQ classic for the above ions are consistent with the suggested formulae. The fragmentation of m/z 156

follows the same pathway as m/z 167, i.e. m/z 139, 111 and 83. This is expected as m/z 156 is simply the ammoniated equivalent of 139 m/z.

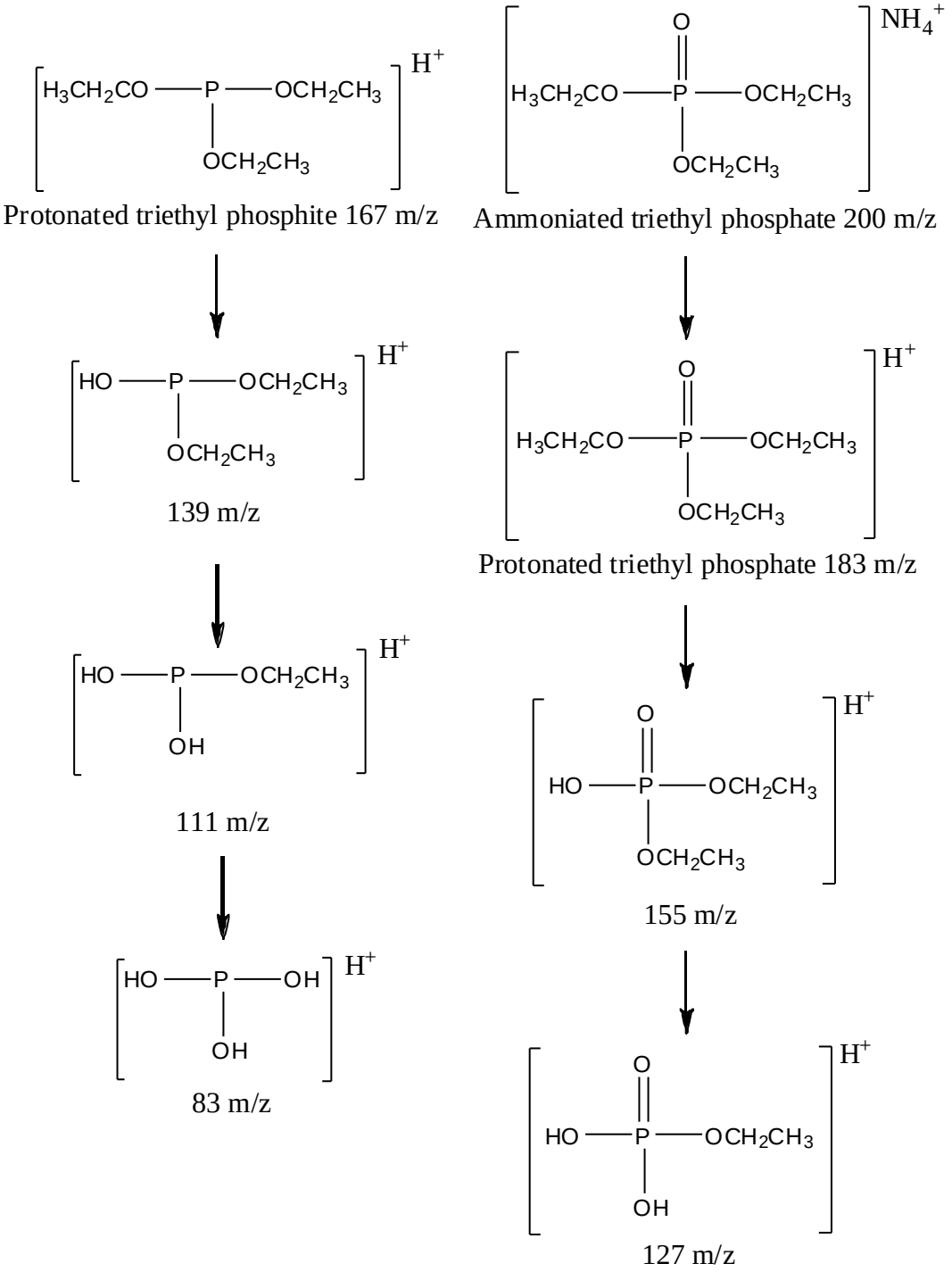

Figure 4.18 Fragmentation pathways as observed in the LCQ classic for a TEPite sample in an IMS-ITMS

SIMMS were taken of the ion mobility peaks of TEPite. However, it was only possible to obtain any ion intensity above zero in the m/z spectra for the 1st mobility peak. Second gate selection of the 1st ion mobility peak gave m/z 167, which is assumed to be the protonated parent ion. SIMMS could not be used to identify the ions in the 2nd and 3rd ion mobility peaks as their intensity was too low.

4.4.4 Proton-transfer reaction mass spectrometric studies of organophosphites

PTR-MS studies were undertaken to investigate further the nature of the m/z spectra of TEPite recorded in the IMS-ITMS system. Vapour from a 10 ml plastic syringe containing two drops of TEPite was injected into a PTR-MS in order to conduct further m/z studies. The syringe was filled with lab air and also injected into a flow of air, simulating the sample injection conditions for the IMS-ITMS system. The m/z spectra were recorded with an E/N in the drift tube of the PTR-MS of 90 Td. This is much higher than the 1.41 Td of the GID-M drift tube. Therefore, one would expect to see more fragmentations occurring. The m/z spectrum from the PTR-MS is shown in figure 4.19.

The PTR-MS is not ammonia doped so obviously there is no m/z 156 or 199 present in the m/z spectra. m/z 139 is more dominant than m/z 167, the opposite to the IMS-ITMS m/z spectra. This is because there is more fragmentation occurring in the PTR-MS. This also explains the presence of m/z 111 and 83. Triethyl phosphate (m/z 183) is present in a much higher quantity in the PTR-MS for this sampling method. However, when the same sample syringe is filled with dry nitrogen, and then injected into a flow of nitrogen into the PTR-MS, the m/z 183 peak is significantly diminished. All of the other m/z peaks remain unaffected. This implies that triethylphosphate is indeed a product of the experimental procedure, and is not formed in the drift-tube of the PTR-MS, or IMS systems, but is predominantly formed in

the sample syringe full of air. The peaks occurring at m/z 93 and 121 are most probably $[(CH_3CH_2O)P(OH)]^+$ and $[(CH_3CH_2O)_2P]^+$ and respectively. These ions are not seen in the IMS-ITMS system because there are more neutral water molecules for them to react with, forming m/z 111 and 139 respectively.

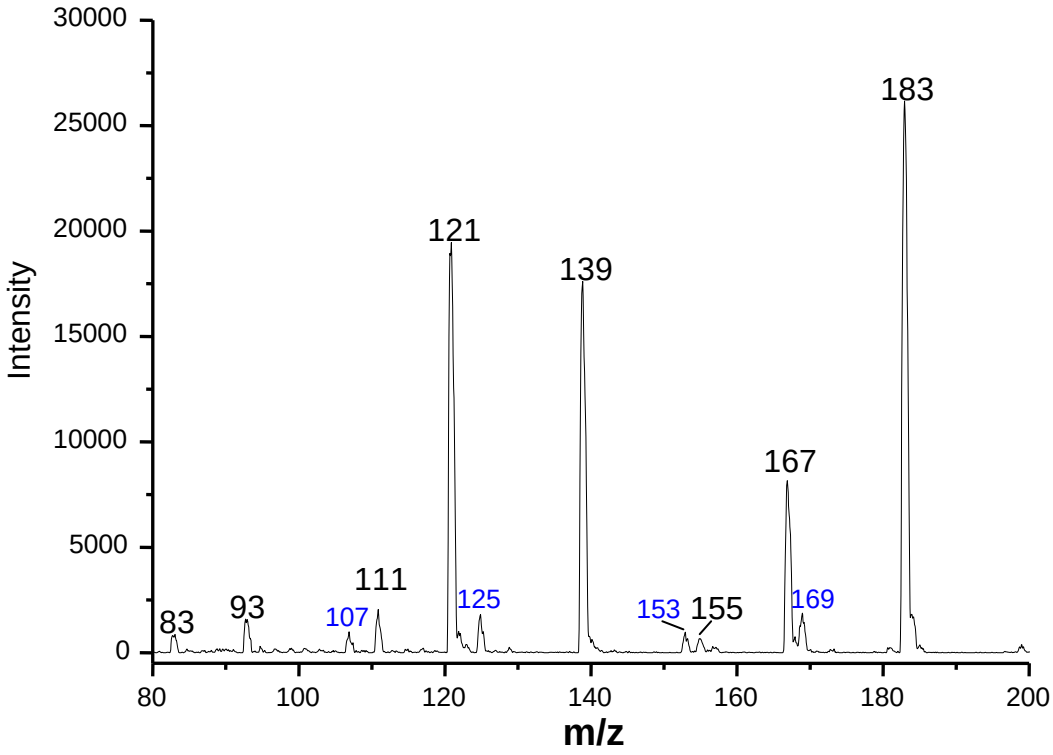

Figure 4.19 m/z spectra taken for TEPite in a proton transfer reaction mass spectrometer.

m/z 169, 153, 125 and 107 highlighted in blue in figure 4.19 are not seen in the IMS-ITMS. They could all be part of a fragmentation series starting from $[(CH_3CH_2O)_2P(CH_2OH)O]H^+$ (m/z 169). They are not of interest here as they are only loosely related to the structure of TEPite.

4.4.5 Ion mobility spectrometer-quadrupole mass spectrometric studies of organophosphates

In parallel with the IMS-ITMS, the group has built and developed an IMS-quad system in order to compare and strengthen the results obtained in the IMS-ITMS system. The IMS-quad is similar in terms of its applications to the IMS-ITMS, the main difference being that the quadrupole cannot trap ions. A simple schematic of the IMS-quad system is shown in figure 4.20. The E/N in the IMS drift tube of the IMS-quad system is 0.94 Td compared with 1.41 Td in the GID-M of the IMS-ITMS system. The IMS-drift tube is maintained at 30 ºC using a temperature controller and is operated at atmospheric pressure. The quadrupole operates at similar pressures to the ITMS.

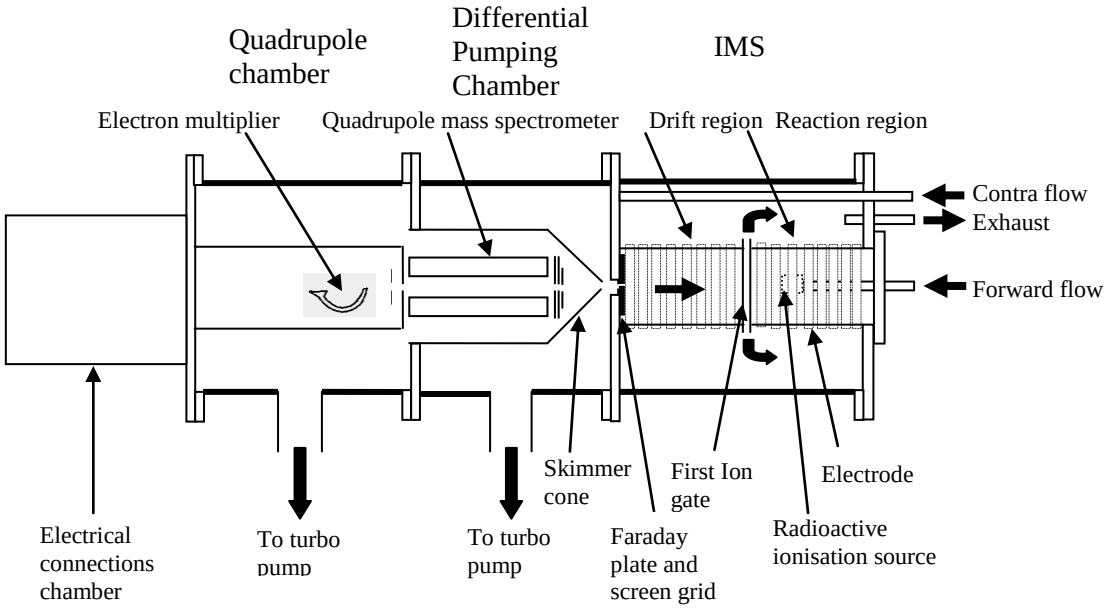

Figure 4.20 Schematic of the IMS-quadrupole system built in the Molecular Physics laboratory. The quadrupole operates at approximately 10^{-5} mbar and the IMS at atmospheric pressure (Adapted from a diagram by David Howse, University of Birmingham)

The most useful function of the IMS-quad system is its capability to perform Tuned Mass Ion Mobility Spectra (TMIMS). This is where the quadrupole is used to record ion mobility data of a specific m/z. First, an m/z spectrum is recorded to find the dominant ions in the IMS

drift tube. Then the quadrupole is set such that only one m/z has a stable trajectory through the quadrupole and is detected by the electron multiplier. An ion mobility spectrum can then be recorded for a specific m/z provided the recording of the data from the electron multiplier is triggered with the opening of the first gate in the IMS drift tube. Ion mobility spectra were also recorded from the Faraday plate of the IMS and m/z spectra were recorded using the quadrupole with the IMS in DC mode, similar to the IMS-ITMS system where the first gate is held open.

A new ammonia doped molecular sieve pack from the GID-M was attached to the forward flow of the IMS-quad system. DMMP, DEMP and DiPMP were subsequently added to the forward flow using a syringe, a similar method to sample injection in the IMS-ITMS. Ion mobility spectra and the corresponding m/z spectra were recorded for each of the chemicals. Then TMIMS were taken of the ammoniated and protonated, monomers and dimers. The m/z spectra, ion mobility spectra and TMIMS are shown in figure 4.21 for DMMP, figure 4.22 for DEMP and figure 4.23 for DiPMP.

For DMMP, the dominant ions are the ammoniated monomer and dimer. This is expected as the molecular sieve pack was new on the day that these data were taken, and therefore the water content was very low. The DEMP and DiPMP spectra were taken on subsequent days and so the concentration of protonated monomer and dimer ions increased as the water concentration increased. The water ions are more likely to proton transfer to sample neutrals, whereas the ammonium ions tend to stay intact when transferring charge. The molecular sieve pack would have become saturated with water more quickly in this experimental set-up than when used in the GID-M as the forward flow through the molecular sieve was unfiltered lab air. In the GID-M only ~10% of the water content of the lab air is transmitted into the drift tube, and therefore into the molecular sieve pack.

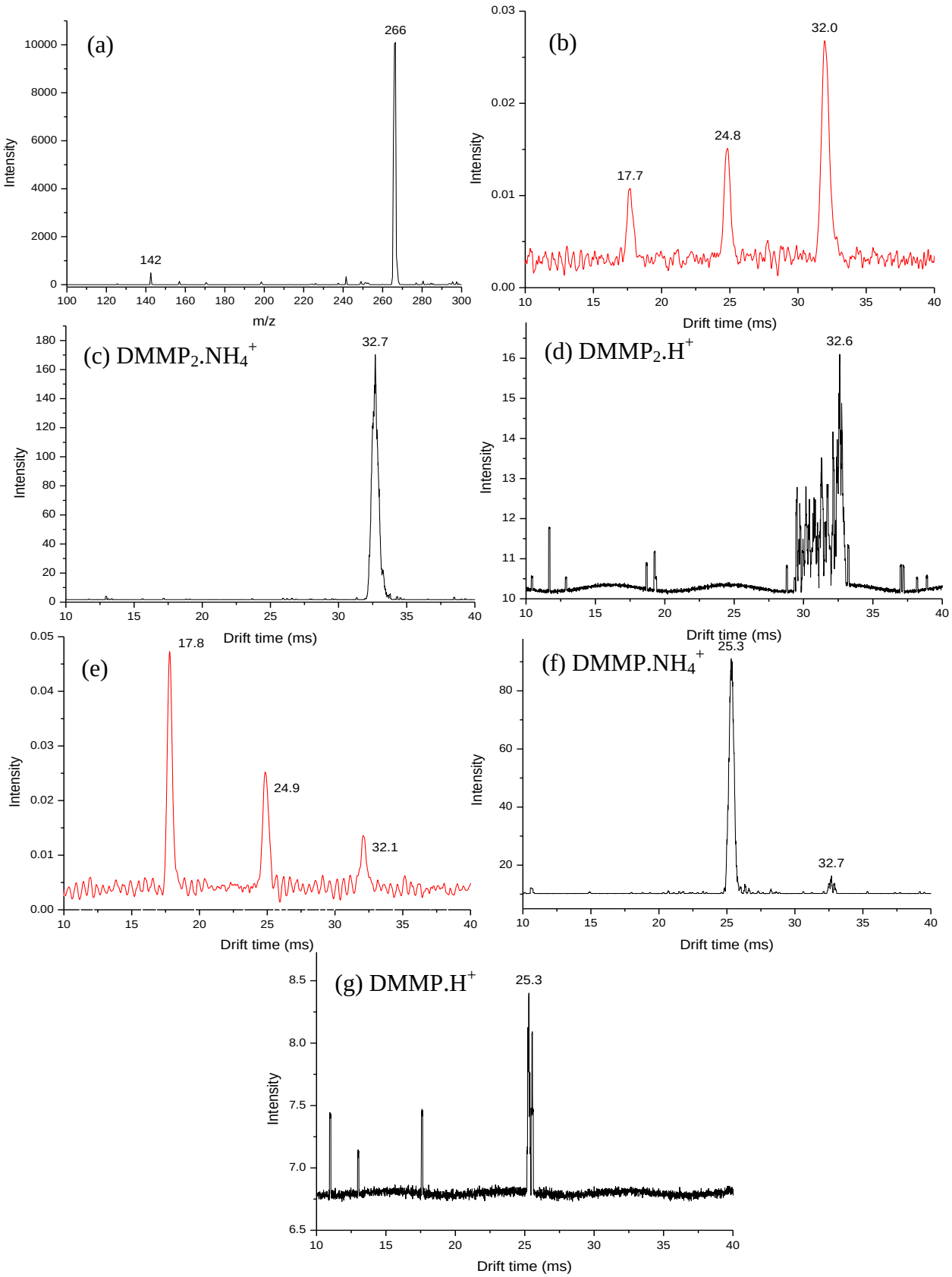

Figure 4.21 Spectra of DMMP as measured in an IMS-quad system with an ammonia-doped molecular sieve pack attached to the forward flow of the IMS. (a) m/z spectrum at a high concentration of DMMP corresponding to the ion mobility spectrum (b). (c) TMIMS of $DMMP_2.NH_4^+$. (d) TMIMS of $DMMP_2.H^+$. (e) Ion mobility spectrum at a lower concentration of DMMP. (f) TMIMS of $DMMP.NH_4^+$. (g) TMIMS of $DMMP.H^+$.

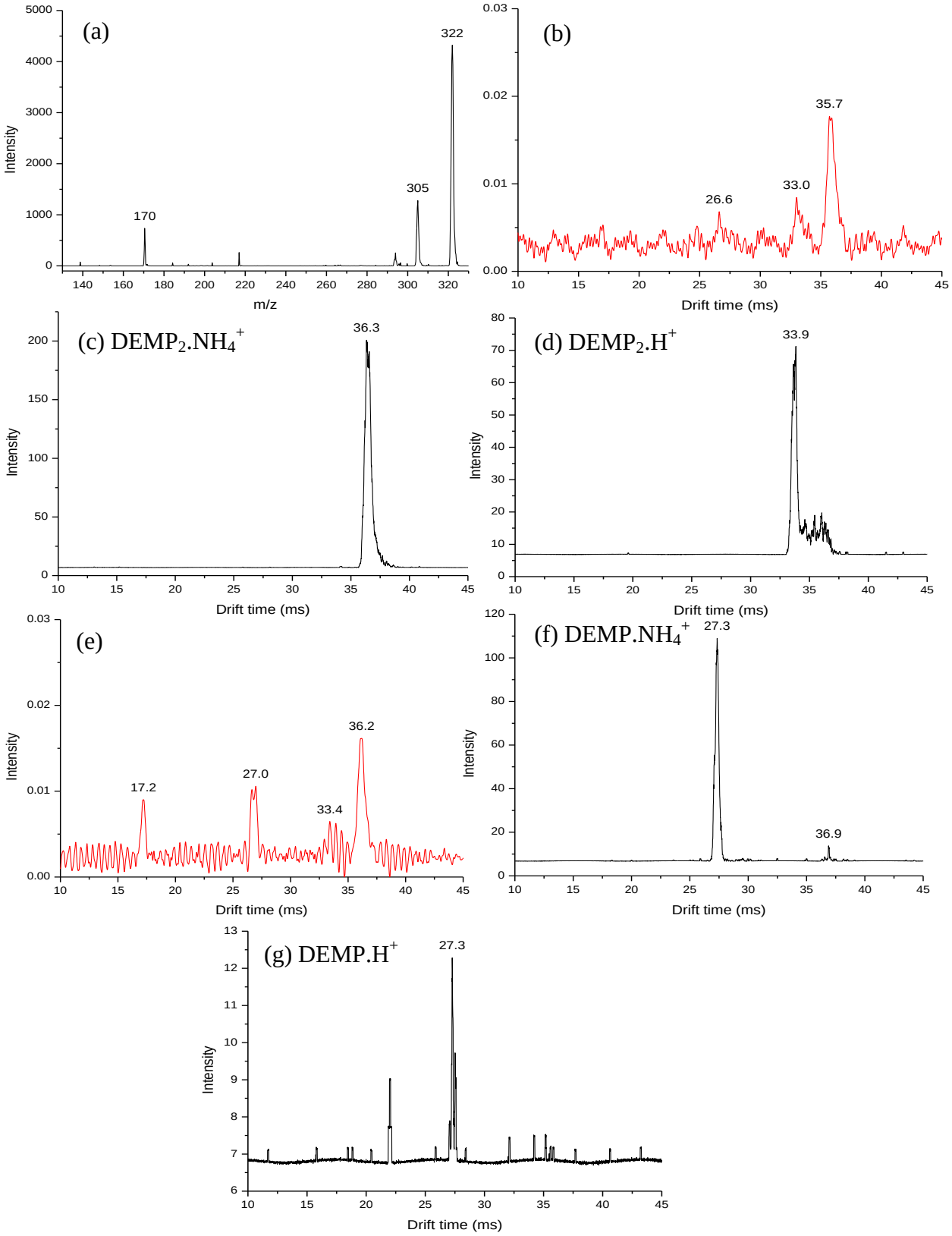

Figure 4.22 Spectra of DEMP as measured in an IMS-quad system with an ammonia-doped molecular sieve pack attached to the forward flow of the IMS. (a) m/z spectrum taken during the period between high and lower concentration of DEMP as shown in the ion mobility spectra (b) and (e) respectively. (c) TMIMS of $DEMP_2.NH_4^+$. (d) TMIMS of $DEMP_2.H^+$. (f) TMIMS of $DEMP.NH_4^+$. (g) TMIMS of $DEMP.H^+$.

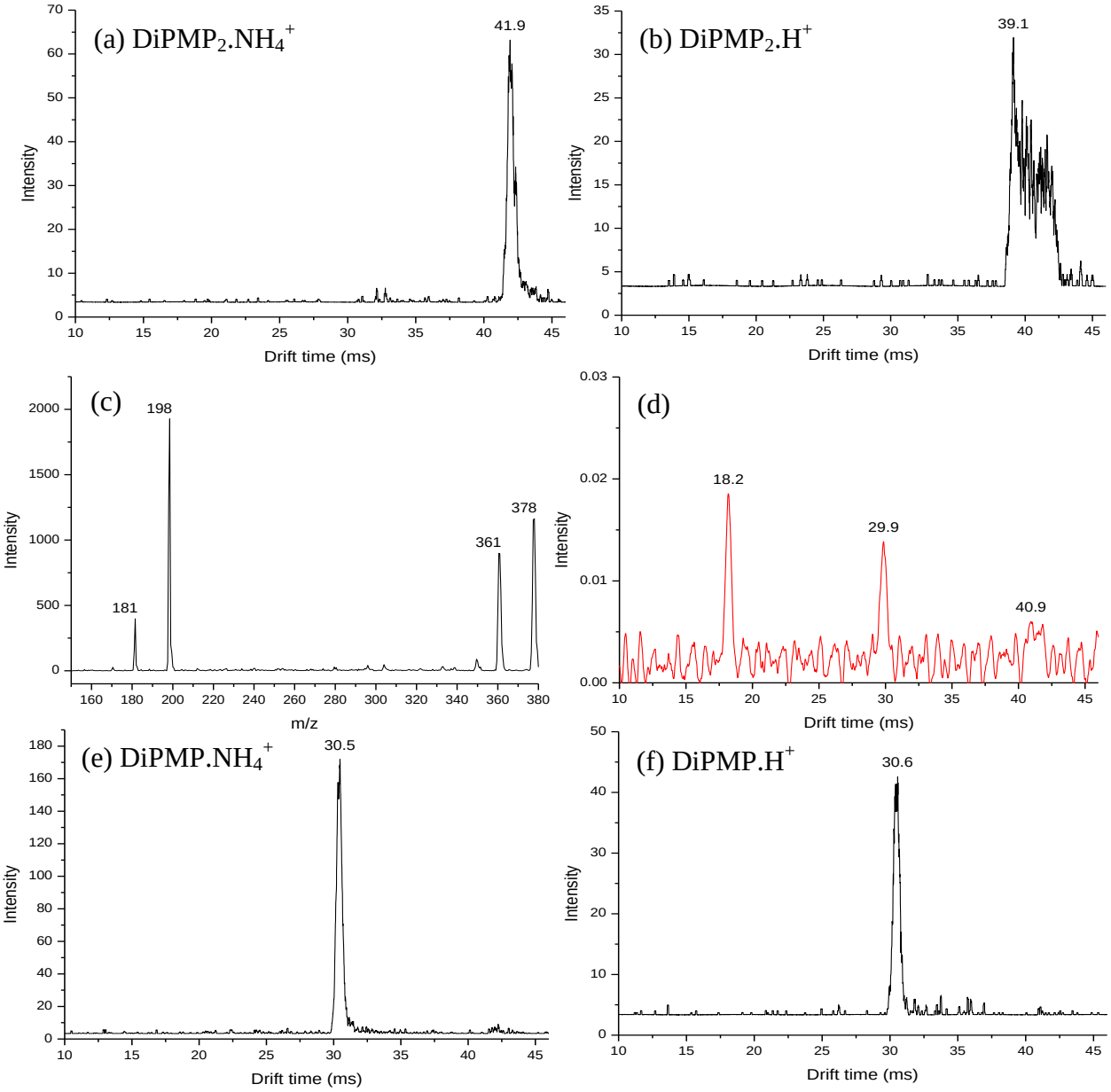

Figure 4.23 Spectra of DiPMP as measured in an IMS-quad system with an ammonia-doped molecular sieve pack attached to the forward flow of the IMS. (a) TMIMS of $DiPMP_2.NH_4^+$. (b) TMIMS of $DiPMP_2.H^+$. (c) m/z spectrum at taken with a low concentration of DiPMP as shown in the ion mobility spectrum (d). (e) TMIMS of $DiPMP.NH_4^+$. (f) TMIMS of $DiPMP.H^+$.

There is a notable time delay between mobility peaks recorded at the FP and those recorded by the electron multiplier at the quadrupole exit. This is due to the time of flight of

the ions through the skimmer and the quadrupole. The delay in drift time varies as a function of m/z of the ions, with their velocities decreasing with increasing m/z. The delay is apparent when comparing the ion mobility spectra with the TMIMS spectra in figures 4.21, 4.22 and 23. Fortunately, it is still obvious which peaks from the TMIMS spectra correspond with which peaks in the ion mobility spectra since they are well separated. The delay is of the order of 0.4 ms for the ammoniated DMMP monomer ion (minimum delay) and approximately 1 ms for the DiPMP ammoniated dimer ion.

It is evident that the protonated and ammoniated dimer ions have different drift times, the ammoniated being slower than the protonated ion. The biggest difference of 2.8 ms is between $DiPMP_2.NH_4^+$ and $DiPMP_2.H^+$ as can be seen in the TMIMS spectra of figure 4.23 (a) and (b). This is consistent with the broad ion mobility dimer peak as seen in figure 4.23 (d). All the chemicals show a large spread of drift times when performing TMIMS of the protonated dimer. This is because some of the protonated dimers are likely to be formed in the drift tube as the ammonia concentration decreases and NH_3 dissociates from the ammoniated dimer ions. NH_3 is lost at various times as the ions are moving down the drift tube. Some are lost very close to the FP and so their drift times will be close to that of the ammoniated dimer ions. Ammonia is not lost from ions in the drift tube of the IMS-ITMS system as both the contra and forward flow are ammonia-doped. Only the forward flow is ammonia doped in the IMS-quad system.

DEMP has a particularly high intensity protonated dimer peak (see figure 4.22 (d)) with a good resolution. This peak is due to $DEMP_2.H^+$ ions that have been formed in the reaction region of the drift tube, prior to the first gate. This could be due to a lower concentration of ammonia and a higher concentration of water in the system, which would give rise to more protonated dimer ions. DiPMP does not exhibit quite as strong a protonated dimer peak.

However, the system was heated up to 90 degrees for at least 24 hours between taking the DEMP and DiPMP spectra, therefore possibly removing some of the water from the system. There is very little protonated monomer in any of the spectra. This is consistent with the ITMS m/z spectra where the ammoniated monomer always has a much higher intensity than the protonated monomer.

The protonated and ammoniated monomer ions do not have different drift times for DMMP and for DEMP. However there is a difference of approximately 0.1 ms between DiPMP.H^+ and DiPMP.NH_4^+. It may be that there is a small difference in mobility for the monomers of DMMP and for DEMP, but the resolution is not sufficient to detect this. The data collected from the IMS-quad show that it is not likely that the protonated dimers are formed in the drift tube of the GID-M. The GID-M has ammonia doped forward and contra flow and therefore the ammonia will not dissociate from the ions until they have exited the drift tube. If the protonated dimer ion was present in the GID-M drift tube, then its mobility peak would also be observed in the ion mobility spectrum detected at the FP, at a slightly shorter drift time to the ammoniated dimer ion mobility peak.

4.5 Conclusions

Two commercial analytical instruments, the GID-M IMS (Smiths Detection Ltd) and the LCQ Classic ITMS (Finnigan MAT) have been successfully interfaced via an extended inlet capillary. The GID-M was modified by the addition of a second gate allowing the individual ion mobility peaks to be selected and mass analysed with the ITMS. The ions making up ion mobility peaks of DMMP and TMPite were identified using this method. The ITMS was also used to perform MS^n (isolation and fragmentation) of DMMP, DEMP, DiPMP, TEPite and TMPite. For TEPite and TMPite, MS^n confirmed the suggested structures of the ions seen in the m/z spectra.

The ammoniated organophosphates (DMMP, DEMP and DiPMP) showed interesting behaviour when trapped in the ITMS for increasing dwell times. Ammonia fragmented from all of the parent ions with no additional excitation and a low q value of 0.25. In addition, the ammoniated dimers of DMMP and to some extent DEMP also decayed into the corresponding ammoniated monomer ions. Although the dissociation rates of DMMP, DEMP and DiPMP cannot be compared, much can be inferred from the branching ratios of the ammoniated dimers. The dissociation of $DiPMP_2NH_4^+$ never reaches completion, and this could be explained by the presence of two different structures. This requires further experimental study along with energetic calculations of the fragmentations of these chemicals.

Further investigations of DMMP, DEMP and DiPMP involving the IMS-quad were conducted, the significant results being that the ammoniated and protonated dimers have different mobilities for all three chemicals. It can therefore be concluded that, although detected in the ITMS m/z spectra, the protonated dimer fragmented after leaving the GID-M drift tube: had it fragmented in the drift tube, another, separate, ion mobility peak would have been observed.

The PTR-MS was also used to substantiate the TEPite results from the IMS-ITMS. The findings agreed well and any minor differences could be attributed to the operating or sampling conditions of the PTR-MS. The presence of triethyl phosphate and trimethyl phosphate in the TEPite and TMPite m/z spectra, respectively, was attributed to the experimental sampling procedure used.

The IMS-quadrupole was used to illustrate that the protonated and ammoniated dimer of DMMP, DEMP and DiPMP each have different drift times. This supports the hypothesis that the protonated ions are not produced in the drift tube of the GID-M IMS, but are a consequence of the potential gradients in the ion trap optics, and the act of trapping the ions.

All the chemicals studied in the IMS-ITMS showed a dependence upon the length of time the syringe had been injecting the sample. The ion mobility and m/z spectra were affected every time the syringe was refilled. Therefore, it is suggested that a continuous sample injection method should be used in future experiments, perhaps using an uninterrupted flow of nitrogen past the inlet of the GID-M, that first passes over a liquid sample, subsequently drawing in the headspace.

The data taken in these IMS-ITMS studies of organophosphorus esters have successfully demonstrated the versatility and powerful analytical features of the ITMS for interpreting ion mobility spectra. These experiments demonstrated the importance of understanding the nature and behaviour of ions within the ITMS that are relevant to the chemical reactions occurring in the IMS. The ITMS may not detect all the cluster ions formed in the IMS. However, detection, isolation and performing MS^n on the core ions is sufficient for their further analysis. Other ion detection instruments, such as the IMS-quad and the PTR-MS, also added valuable information that facilitated the identification of ions formed in the ion mobility spectrometer.

As a whole, this section of the thesis describes a milestone in the EPSRC project “Fighting Crime, Increasing Security…” . The major achievement is the development and application of the IMS-ITMS system that provides a solid basis for further investigations into the chemistry occurring within IMS systems for the detection of CWAs.

5 SECTION 2

Fragmentation studies of organophosphorus esters using electrospray ionisation - ion trap mass spectrometry

Declaration of contribution

My major contribution to the studies described in this section is the experimental work performed on the Electrospray Ionisation-Ion Trap Mass Spectrometer (ESI-ITMS). The Density Functional Theory (DFT) calculations used to help interpret the data were made by Franco Ferrante (Universita, degli Studi di Palermo, Italy). Interpretation and analysis of the DFT calculations were performed Peter Watts (Honorary Staff, University of Birmingham). The work on DiMethyl EthylPhosphonate (DMEP) has been published (see Appendix C for full version of the paper).[1] The majority of this section is a more detailed description of the experimental work undertaken in the paper on DMEP, although more information can be found regarding the chemical theory and subsequent discussions in the paper. Further ESI-ITMS investigations involving other organophosphorus esters can be found at the end of this section, again all the experimental data was performed by myself, as well as much of the interpretation of the fragmentation pathways for these chemicals.

5.1 Abstract

This section of the thesis focuses on the fragmentations and subsequent reactions of a group of organophosphorus esters relating to nerve gas Chemical Warfare Agents (CWAs) and pesticides, using ESI-ITMS. In particular, the fragmentation of DMEP shows elimination of methanol followed by ethene. The isotopomers of DMEP, deuterated in the α and β positions of the ethyl group, give intriguing fragmentations that involve elimination of hydrogen from both the α and β positions. DFT calculations are used to explore the mechanisms of this fragmentation. However, from these calculations, excluding entropy, a unitary branching ratio for α- and β-elimination is predicted. This does not agree with the experimental observations. Only by taking entropy into consideration, and hence the free energy of the final transition involved in the mechanism, can the true rate-limiting steps be determined. It is therefore free energy, and not enthalpy that determines the course of gas phase ion processes.

Preliminary fragmentations of other organophosphorus esters have been undertaken. These also indicate some fascinating fragmentation pathways that show possibility of hydrogen elimination from the α, β and even γ carbons on the alkyl group attached to the phosphorus. These will require further investigations involving DFT calculations and deuterated isotopomers.

5.2 Introduction

The following study on DMEP described here (and in the paper in Appendix C)[1] was performed as a result of several previous investigations on the fragmentation of protonated DMMP (**I**).[77-79]

In an initial investigation into the electrospray ionisation ion trap mass spectrometry of simple organophosphorus esters by Peter Watts et al. from dstl, Salisbury,[77] it was reported that the Collision Induced Dissociation (CID) of protonated DMMP (figure 5.1), resulted in the loss of methanol and the formation of the $CH_3P(O)OCH_3^+$ ion, **II**, which in turn fragmented under appropriate CID conditions to lose CH_2O.

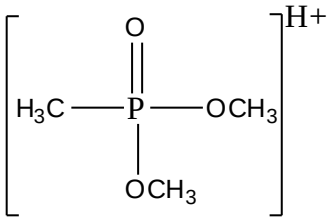

Figure 5.1 **I**.H^+ Protonated dimethyl methylphosphonate (DMMP), m/z 125.

It was observed that fragmentation of the deuterated ion $CD_3P(O)OCH_3^+$, formed from an isotopomer of **I**, **I**a (figure 5.2) produces a mixture of CH_2O and CD_2O, indicating that a scrambling of the methyl groups is involved during fragmentation. More detailed studies of

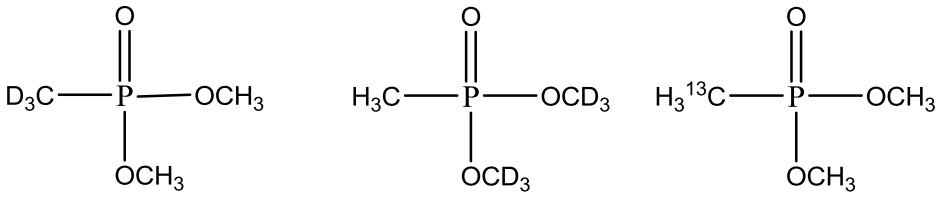

Ia **I**b **I**c

Figure 5.2 isotopomers of DMMP (figure 5.1)

this scrambling involving the isotopomers **I**a, **I**b and **I**c (figure 5.2) were made with the combined effort of the Department of Chemistry, Southampton University.[78] Subsequently, the scrambling of the methyl groups on elimination of formaldehyde (CH_2O) from **II** was investigated using quantum mechanical calculations at the B3LYP and MP2 levels, by the Diparmento di Chimica Fisica, Universita degli Studi di Palermo, in an attempt to understand the mechanism(s) of fragmentation of **II**.[79] This was proposed in the paper describing the original experimental work[78] to occur through the dimethoxyphosphenium ion $P(OMe)_2^+$ formed from $MeP(O)OMe^+$ via a 1,2-methyl migration. 1,4-H migrations in both $MeP(O)OMe^+$ and $P(OMe)_2^+$ were proposed to explain the elimination of formaldehyde. The electronic structure calculations showed that the barriers to the originally proposed 1,4-H migration steps leading to loss of CH_2O are much higher in energy than 1,3-H migrations in which a methoxy hydrogen atom migrates to the phosphorus atom. These produce the ion-dipole complexes $CH_2O.(MeP(O)H)^+$ and $CH_2O.(MePOH)^+$ which then dissociate to give the experimentally observed products. This report describes similar studies on DMEP (**III**) and its deuterated isotopomers **IIIαD** and **IIIβD** (figure 5.3). Several other organophosphorus esters were also fragmented, whose chemical formulae are given in appendix D.

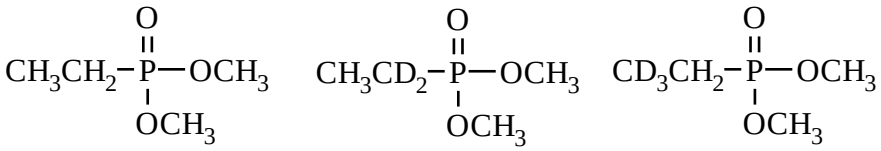

III **IIIαD** **IIIβD**

Figure 5.3 Isotopomers of dimethyl ethylphosphonate (DMEP)

5.3 Experimental methods

5.3.1 Chemical synthesis

All organophosphorus ester samples used in the ESI-ITMS studies were synthesised at dstl, Porton Down, Salisbury and shipped to the University of Birmingham. The preparation of **III**, **IIIαD** and **IIIβD** is described in the paper in appendix C .

The organophosphorus compounds were diluted to a concentration of circa 400 μg per ml in 1:1 methanol:water + 0.1% formic acid before being injected into the ESI-ITMS.

5.3.2 Instrumentation

The ITMS used for all MS analysis in this section is a commercial machine, an Esquire-LC produced by Brucker Daltonics, GmbH (figure 5.4). Liquid Chromatography (LC) is the most common form of sample delivery for this machine, but electrospray ionisation is used in this case due to its quick delivery of gas-phase sample ions. Also there is no requirement for pre-selection of sample neutrals prior to ionisation. The electrospray needle is fed by a 250 μl syringe at a controlled 'low flow rate' of 8 μl/min using the supplied syringe pump. The layout of the ESI-ITMS system is shown in figure 5.4 and the electrospray is shown in figure 5.5.

The minimum m/z detection of ions in the Esquire-LC is m/z 50. ECD grade nitrogen was used as the heated nebuliser gas for the ESI. Working conditions in the electrospray chamber were 5-10 psi at 250-300˚C and a flow rate of 5 l/min. The electrospray needle was operated at 4 kV, and subsequent voltages on the capillary and focussing system were optimised to produce a maximum stable ion count in the trap. Typical operating voltages for the Esquire-LC are shown in table 5.1.

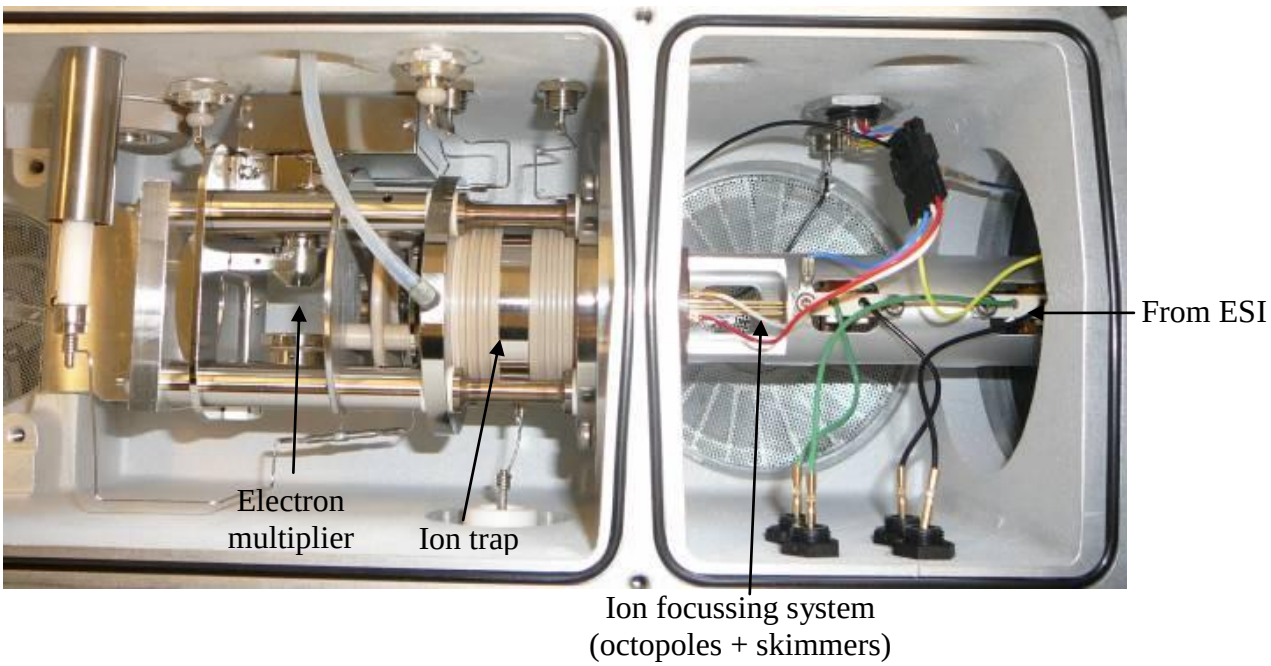

Figure 5.4 Esquire-LC system layout. Ions travel from right to left. The first chamber on the right contains ion focussing lenses and is differentially pumped to ~2 mBar, the second chamber contains the ion trap and electron multiplier and has an operational pressure of ~1 x 10^{-5} mbar.

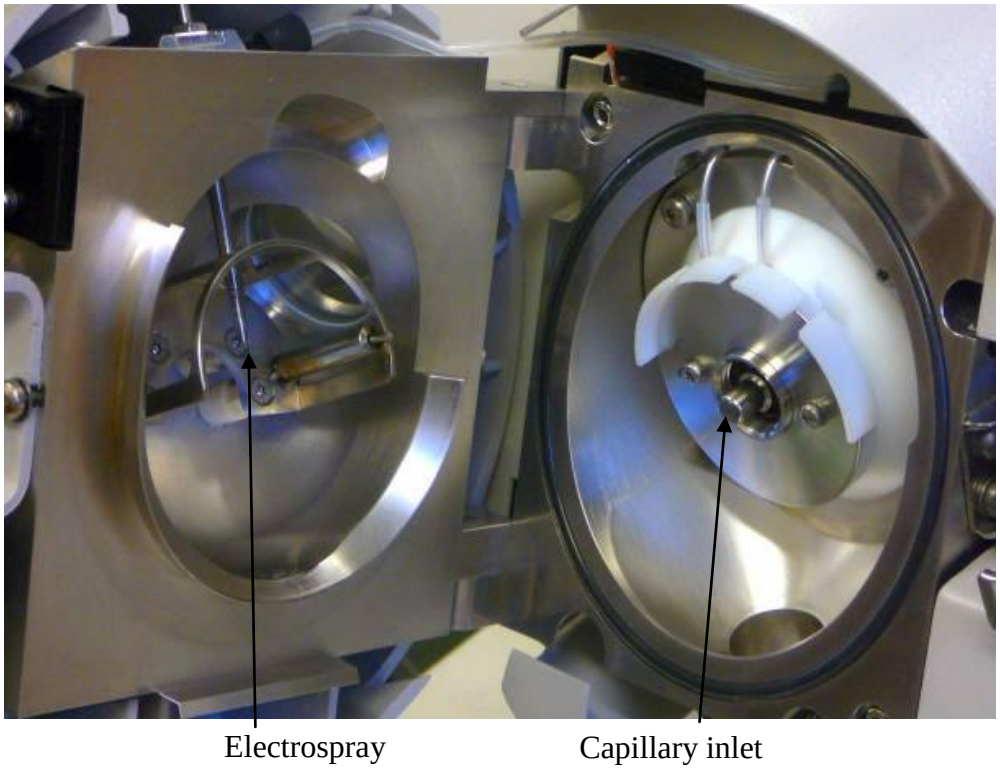

Figure 5.5 Esquire-LC ESI chamber which is clamped shut when in operation and pumped with heated ECD grade nitrogen nebuliser gas.

Parameter	Typical parameter value
ESI needle voltage	+4000 V
Capillary voltage	-4800 V
Endplate offset	-100 V
Skimmer 1	24.8 V
Skimmer 2	5 V
Capillary exit offset	60 V
Octopole	2.57 V
Octopole RF	103.3 V_{pp}
Octopole Δ	3 V
Lens 1	-2.6 V
Lens 2	-57.5 V
Trap drive	35 V
Pressure in trap region	6 x 10^{-6} mbar

Table 5.1 Operating parameters used for the ion inlet, ion optics and ion trap for the Esquire-LC

Variables of isolation and fragmentation in the Esquire-LC are fragmentation time (Frag t), fragmentation amplitude (RF Amp) and low mass cut-off (Cut-Off). The cut-off defines the lowest m/z that can be detected upon fragmentation of the parent ion. These three variables are set for each isolation and fragmentation to produce optimal ion intensities of the fragments of interest. They are displayed in the caption of each m/z spectrum in the results section. The isolation window of the parent ions is always set to m/z 1.

CID was performed in the trap with helium gas with the following consequences.

$$MH^+ + He \rightarrow m_1H^+ + m_2 + He,$$

where M is the parent ion and m_1 and m_2 are the daughter fragments.

5.3.2 Theoretical methods

Energy calculations were performed for DMEP by F. Ferrante from the Diparmento di Chimica Fisica, Universita degli Studi di Palermo. Geometry optimizations and frequency calculations of all species reported in this work were performed by using DFT with the Becke three parameters hybrid functional B3LYP.[80] Vibrational frequencies were calculated in all cases to characterize the minima and the transition states and provide zero point energies (ZPE). All total energy comparisons include ZPE corrections. Earlier studies on ions obtained from protonated DMMP[79] demonstrated that the results at the B3LYP level corresponded very well with those from the more time-consuming MP2 calculations and that all ions have a singlet electronic ground state. All electronic structure calculations were performed using the Gaussian 03 programme.[75] More details of the DFT calculations used to find the transition states for the fragmentation mechanisms of DMEP can be found in the paper in Appendix C.

5.4 Results and discussion

5.4.1 Fragmentation of dimethyl ethylphosphonate

A mass spectrum of DMEP (**III**) gives predominantly m/z 139, corresponding to protonated DMEP (MH^+). Upon isolation and fragmentation of m/z 139, as shown in figure 5.6, daughter ions at m/z 125, 107 (**IV**) and 79 are produced.

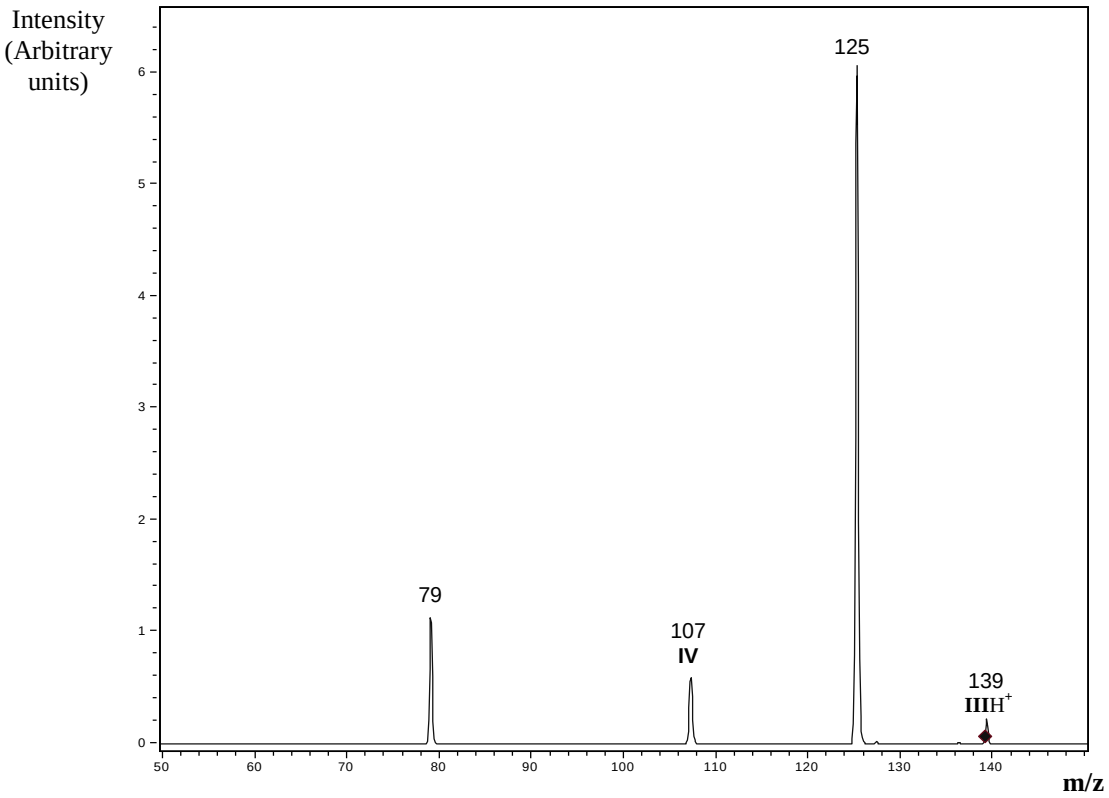

Figure 5.6 Isolation and fragmentation of m/z 139, marked with a diamond.
Frag t = 30 ms, Cut-off = m/z 50 , RF Amp = 0.9 V

Isolation of m/z 125 gives m/z 107 (**IV**) and further fragmentation gives m/z 79 as well as m/z 111, 93 (**V**) and 65 (see figure 5.7). This implies that m/z 107 (**IV**) is produced directly from m/z 125 via the loss of water. This is confirmed when trying to isolate m/z 107, when all that is produced is m/z 125.

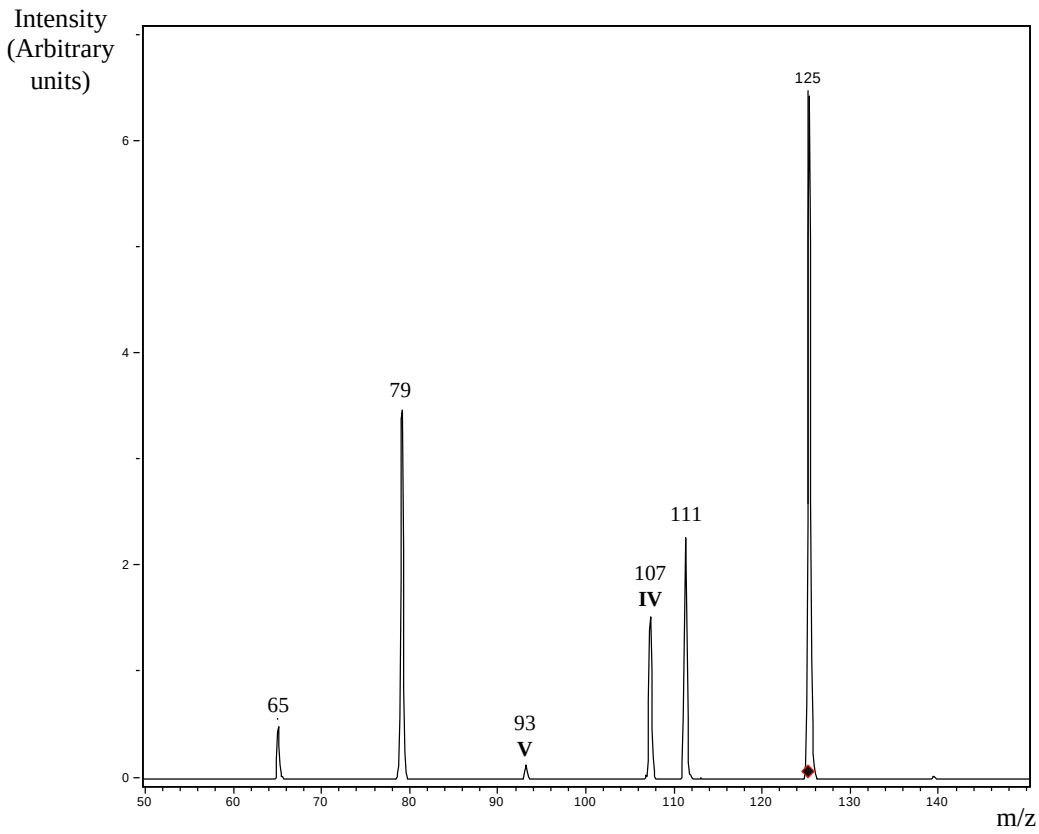

Figure 5.7 Isolation and fragmentation of m/z 125, marked by diamond. Frag t = 30 ms, Cut-off = m/z 50, RF Amp = 1.2 V

Fragmentation of m/z 107 is shown in figure 5.8, this produces m/z 79 and as expected, m/z 125. Isolation and fragmentation of m/z 111, as shown in figure 5.9, gives m/z 93 (**V**), 65 and a small amount of 125. From all these data it can be inferred that the fragmentation pathway separates into two branches, one involving m/z 139, 107 and 79 and the other m/z 139, 125, 111, 93 and 65. The reaction between m/z 125 and 107 is reversible.

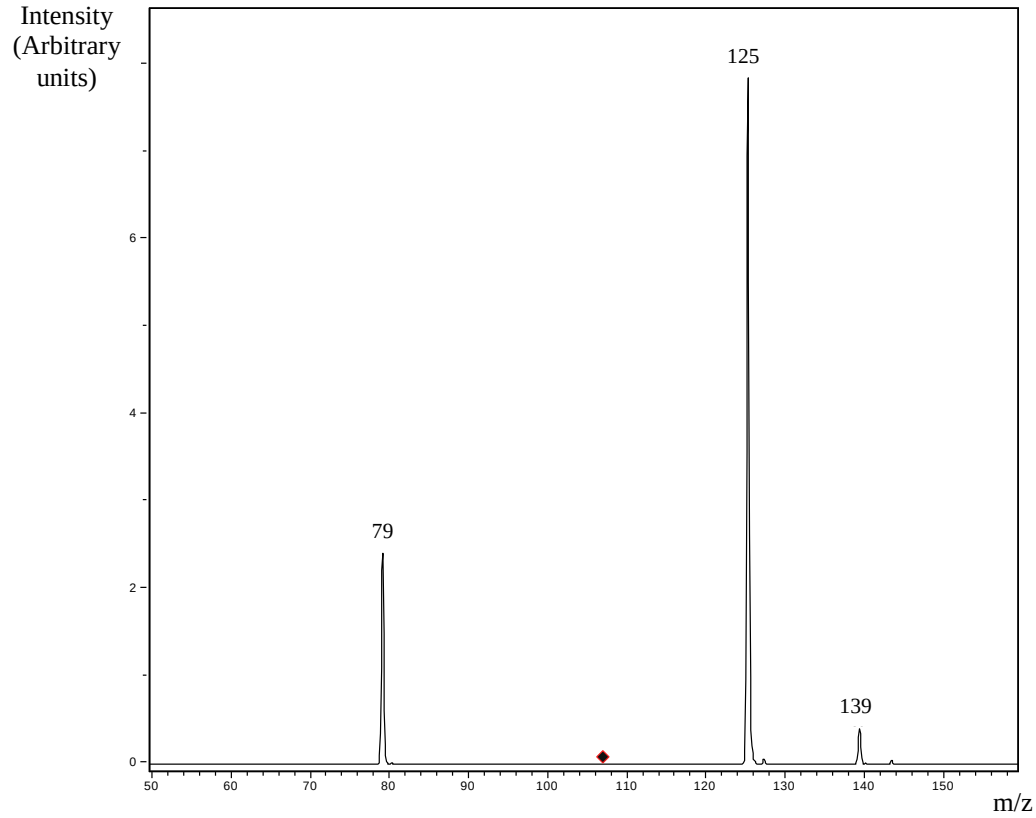

Figure 5.8 Fragmentation of m/z 107 (following on from figure 5.7), marked by a diamond. Frag t = 30 ms, Cut-off = m/z 50, RF Amp = 0.9 V

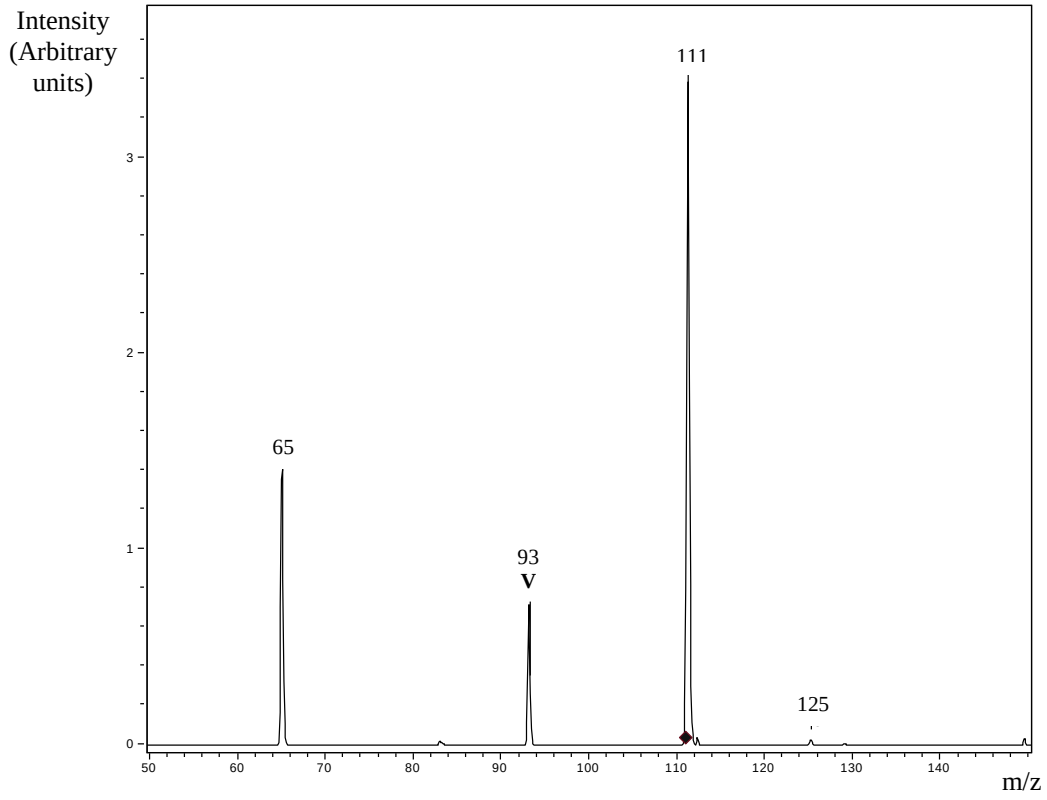

Figure 5.9 Isolation and fragmentation of m/z 111, marked by a diamond. Frag t = 30 ms, Cut-off = m/z 50, RF Amp = 1.2 V

The most likely fragmentation pathway deduced from the ITMS data and the m/z differences between the fragments is shown in figure 5.10. Common losses in this case are that of methanol which gives a m/z difference of m/z 32, ethene: m/z 28 and water: m/z 18. It is of note that formaldehyde (CH_2O) is not eliminated from any of the ions in the fragmentation of DMEP, this is in contrast to DMMP where formaldehyde is eliminated from $CH_3P(O)OCH_3^+$.

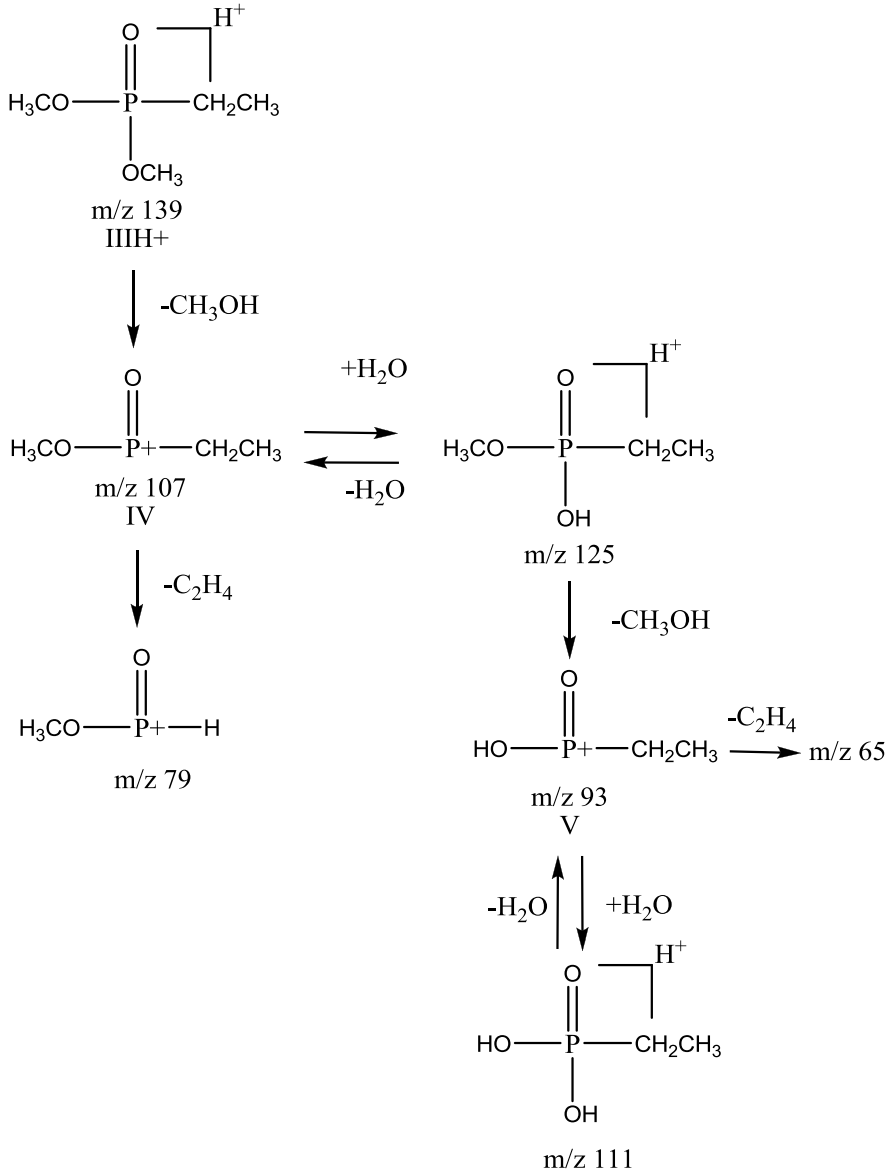

Figure 5.10 Fragmentation pathway of **III**H^+.

Corresponding fragmentations and isolations were performed for **IIIαD**H^+ and **IIIβD**H^+. The deuterated isotopomers of **IV** and **V** produced ethene with the hydrogen/deuterium loss occurring from both the α and β positions of the ethyl group. Thus fragmentation of **IVαD**, m/z 109, gave ions with m/z 79 and m/z 80 corresponding to loss of CD_2CH_2 (β loss) and $CHDCH_2$ (α loss) respectively. Fragmentation of **IVβD**, m/z 110, also gave ions with m/z 79 and m/z 80, this time corresponding to loss of CD_2CHD (α loss) and CD_2CH_2 (β loss) respectively. The fragmentations of **IVαD** and **IVβD** are shown in figure 5.11. Similar results were obtained for the fragmentations of **VαD** and **VβD**.

The mechanism for this scrambling can be considered to be similar for production of m/z 79/80 and 65/66 since both sets are formed from elimination of ethene from the same deuterated branch. Therefore the remainder of this section of the report will focus on the production of m/z 79/80 only.

Determining the branching ratios of the production of m/z 79 and 80 can be very complicated due to various factors. Firstly, when the fragmentation time is increased from 3 ms up to 40 ms, the m/z 80 peak diminishes. This is most probably due to a rapid reaction with water impurities in the trap where m/z 80 exchanges a deuterium for a hydrogen to produce m/z 79. This also occurs with m/z 65 and 66 produced from **V**. Secondly, isotope effects must be considered and it was initially thought that this would be an important factor in determining the α and β loss ratio. However, it was observed that the α/β loss ratio was dependent upon the fragmentation time and therefore the isotope effects were not considered to be the dominant reason for the observed differences. The α/β loss ratio decreased with increasing fragmentation time for the **αD** isotopomer but this loss ratio increased for the **βD** isotopomer. A summary of the fragmentations produced by α and β carbon loss from **IVαD,**

IVβD, VαD and **VβD** is shown in table 5.2, these were obtained directly from spectra such as those of figure 5.11.

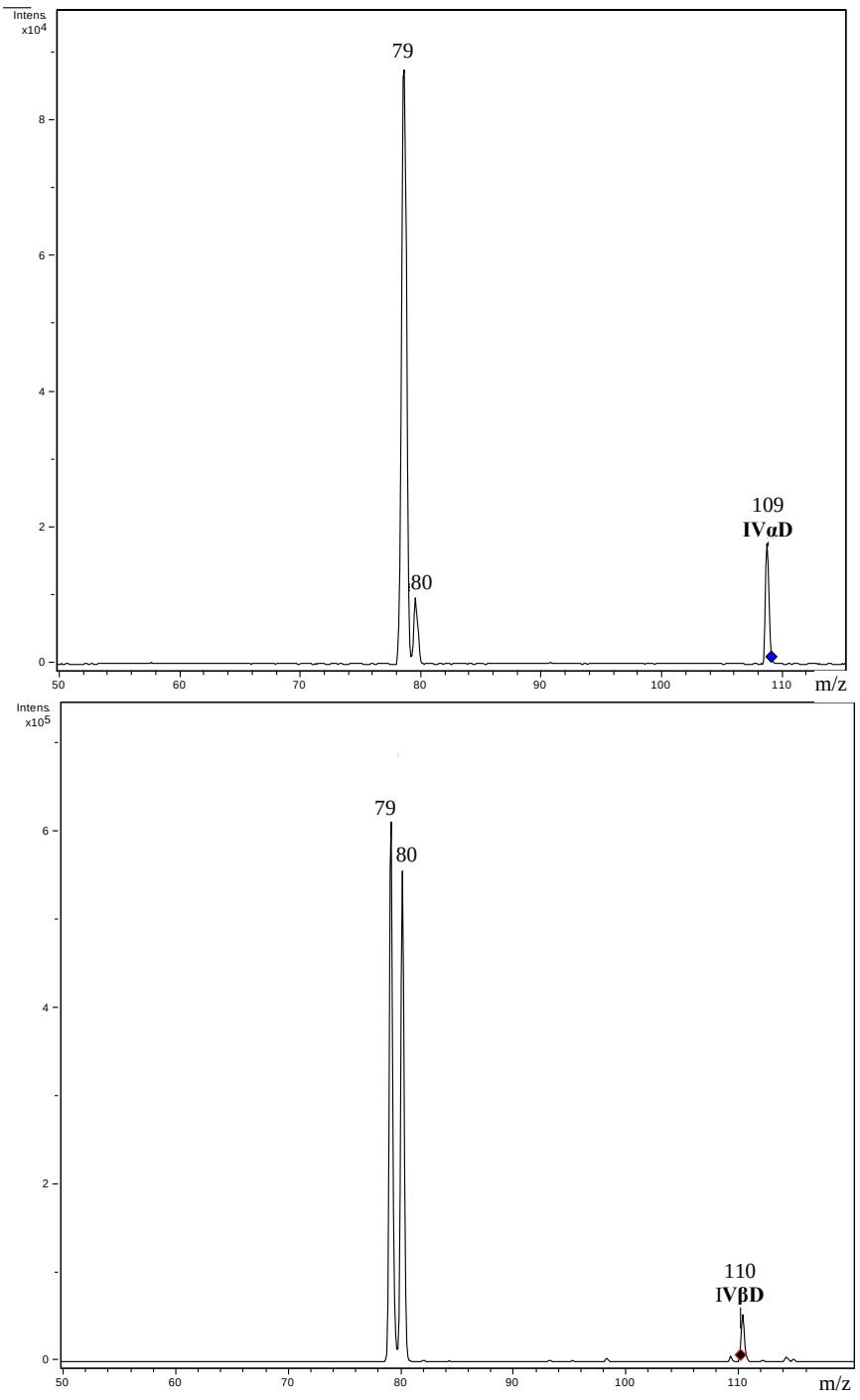

Figure 5.11 Fragmentation of a) **IVαD** Frag t = 2 ms, Cut-off = m/z 50, Amp = 1 V and b) I**VβD** Frag t =10 ms, Amp =1 V, Cut-off = m/z 50.

Ion	α loss	β loss	α/β ratio
IVαD	$CHDCH_2$	CD_2CH_2	β>>α
VαD			
IVβD	$CHDCD_2$	CD_2CH_2	α~β
VβD			

Table 5.2 fragments produced from the four chemicals **IVαD, IVβD, VαD** and **VβD** when the α or β carbon is lost from the parent ion.

Modelling of the kinetics of the eliminations from the α and β carbons using VisSim (Visual Solutions Inc., Westford, MA 01886, USA) by comparing the concentration time profiles with fragmentation spectra such as given in figure 5.11 suggests that, ignoring kinetic isotope effects, α-elimination is about five times slower than β-elimination. Assuming hydrogen/deuterium exchange occurs at the collisional rate, the water concentration in the trap is ca. 10 ppm. These calculations were performed by Peter Watts, University of Birmingham.

From DFT calculations, the most energetically feasible species for elimination of ethene is **IVa**. The possible reactions of **IVa** are shown in figure 5.12 and the transition states between these species are shown graphically in figure 5.13. The complex in figure 5.13 refers to **IVe** which is the penultimate state to ethene elimination. According to these calculations both α and β elimination have the same penultimate state **IVe**. It is assumed that the system does not lose any of its energy during the dissociation process so that it is the absolute value of enthalpy that is important and not the change in enthalpy between each chemical rearrangement. The breaking of the complex **IVe** is therefore is the rate-determining step since it has the largest transition state energy, this means that α and β elimination should be of equal probability. Of course from the above experimental results this is certainly not the case.

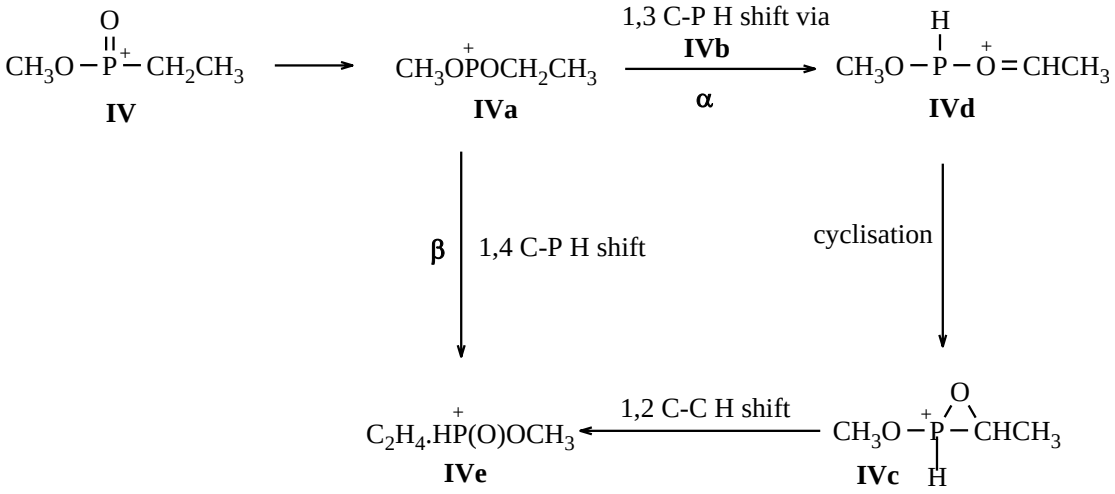

Figure 5.12 Reactions of **IV** to produce m/z 79/80 and ethene.

It is acceptable to treat the energies already calculated (figure 5.13) as enthalpies,[1] the only unknown is the temperature of the ions inside the ion trap upon excitation, which can be in excess of 1000 K.[79] However, the calculated entropy change from the complex **IVe** to the final fragments is so large that at the high temperatures in the ITMS, the overall free energy is negative and the reaction is exergonic. Therefore, it is suggested that the free energy should be considered for the final dissociation step to explain the non-unity branching ratio of α and β elimination (Free energy = Enthalpy – Temperature x Entropy). For the other transition states from **IV** to the **IVe**, the calculated entropies are lower and very similar to one another. Therefore ignoring the final dissociation step, it is clear from figure 5.13 that β-elimination is more favoured than α-elimination. The arguments for α and β elimination from **V** are very similar and are shown in full in the paper in appendix C.[1]

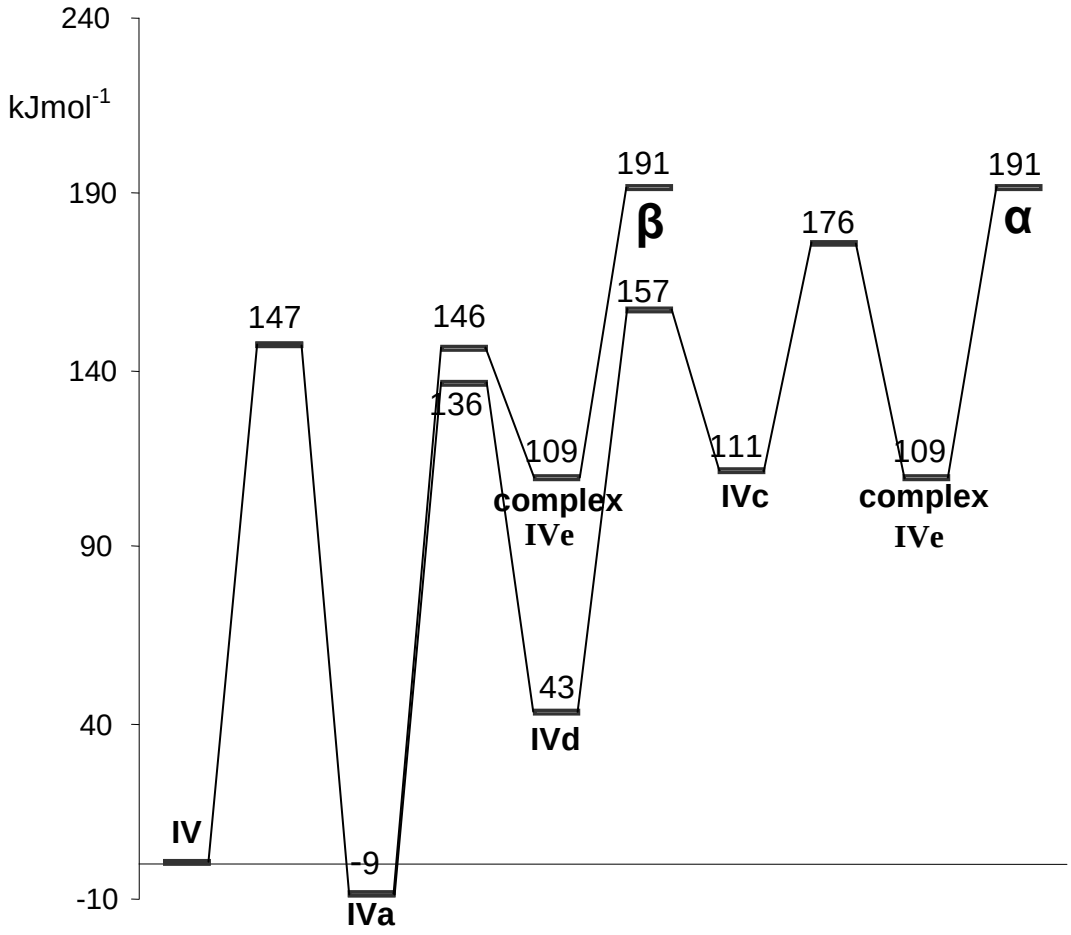

Figure 5.13 Energies of transition (enthalpies) for the reactions of **IV** to form m/z 79/80 and ethene via the elimination of hydrogen from the α or β carbon on the ethyl group.

5.4.2 Fragmentations of dimethyl *n*-propylphosphonate

The undeuterated compound DiMethyl *n*-PropylPhosphonate (DMnPP) followed the expected pathway with elimination of methanol followed by the elimination of propene. The deuterated compound is required to investigate which hydrogens are involved in the propene elimination. The fragmentation pathway for the γ isotopomer is shown in figure 5.14.

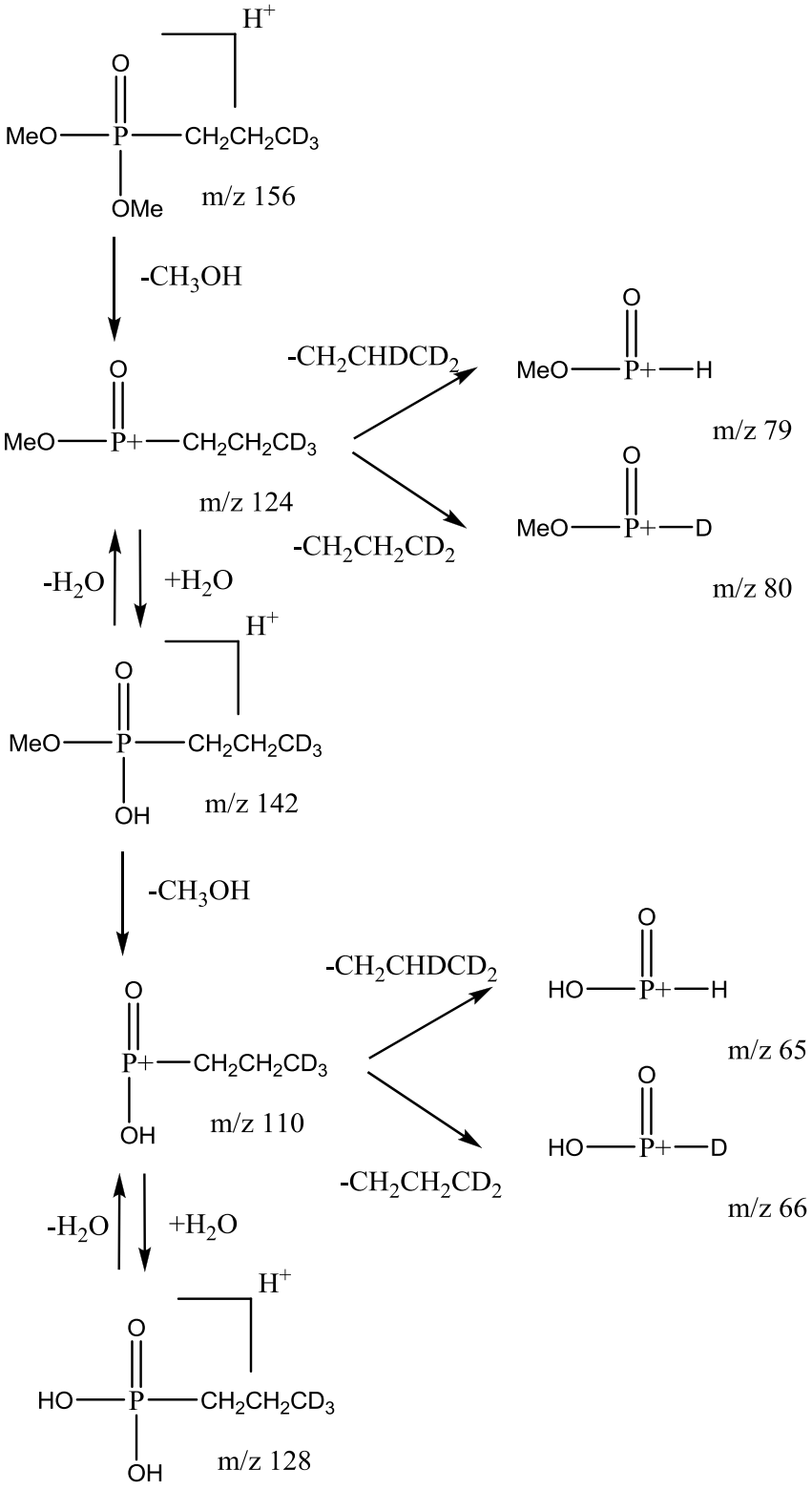

Figure 5.14 Fragmentation pathway of DMnPP.H^+

This shows that the deuterium atoms on the γ carbon of the alkyl group and either or both of the hydrogen atoms in the α and β positions are involved in the elimination of propene. Loss of the hydrogen in the α position in this mechanism is shown to occur by observing the fragmentation pathway of the α isotopomer of DMnPP. Unfortunately the β isotopomer was not available to complete the studies. Whilst hydrogen loss from the α position was expected, loss from the γ position was not. Preliminary DFT calculations in order to further explore this fragmentation mechanism have been performed by Peter Watts, the details of which are summarised in the draft paper in Appendix D.

5.4.3 Fragmentations of dimethyl isopropylphosphonate

Following preliminary work by David Mitchell (Department of Chemistry, Southampton University), a comprehensive study of DiMethyl isoPropylPhosphonate (DMiPP) was completed and the resultant fragmentation pathway is much the same as $DMnPP.H^+$ as shown in figure 5.14. Use of the α and β isotopomers of DMiPP gave no evidence for the α deuterium/hydrogen being lost in the elimination of propene. This may be due to the low ratio of 1:6 of the α to β hydrogens in the isopropyl group. It must be noted that the ion intensity for the α isotopomer was poor and isolation prior to fragmentation was not possible.

Of particular importance is the production of m/z 111 and 93 upon fragmentation of $DMiPP.H^+$. These ions are not seen in the fragmentation of $DMnPP.H^+$. The structures of m/z 111 and 93 are not known, which will, in any case, depend on the fragmentation mechanism forming them.

The ion m/z 93 does not add water on isolation, and on fragmentation it loses CH_2O to give m/z 63. Therefore, m/z 93 must be the dimethoxyphosphenium ion $P(OMe)_2^+$ in accordance with the earlier studies on DMMP.[78] This also suggests that m/z 93 is not formed from m/z

111, but directly form the parent ion via loss of propanol. Equally, the ion at m/z 111 does not lose water on isolation and fragmentation, although it does lose CH_3OH to give an ion at m/z 79.

Fragmentation of the protonated β isotopomer of DMiPP ($DMiPP_\beta.H^+$) gives ions m/z 93 and 112. When D_2O is used (as opposed to H_2O) in the ESI medium, the ion $DMiPP_\beta.D^+$ fragments to ions of m/z 93 and 113. The observation of m/z 112 and 113 confirms that m/z 111 is not primarily formed by addition of water to m/z 93 but arises from loss of propene from the parent ion.

Both the ions at m/z 112 and 113 fragment to give ions at m/z 79 and 80. An ion at m/z 112 is also formed on fragmentation of $DMiPP.D^+$ and this can be fragmented to give ions m/z 79 and 80. The possible structures for m/z 111 and 112 are given in Appendix D along with the DFT calculations (performed by Peter Watts, University of Birmingham) of the mechanisms to form m/z 111, 93, and 79. The fragmentation pathways of interest are shown in figure 5.15.

The elimination of propene rather than propanol, is expected since larger side groups tend to fragment at the PO-C bond, whereas methyl groups tend to fragment at the P-O bond.[77, 81, 82] The mechanism for the elimination of propene may have similarities to the elimination of ethene in DMEP.

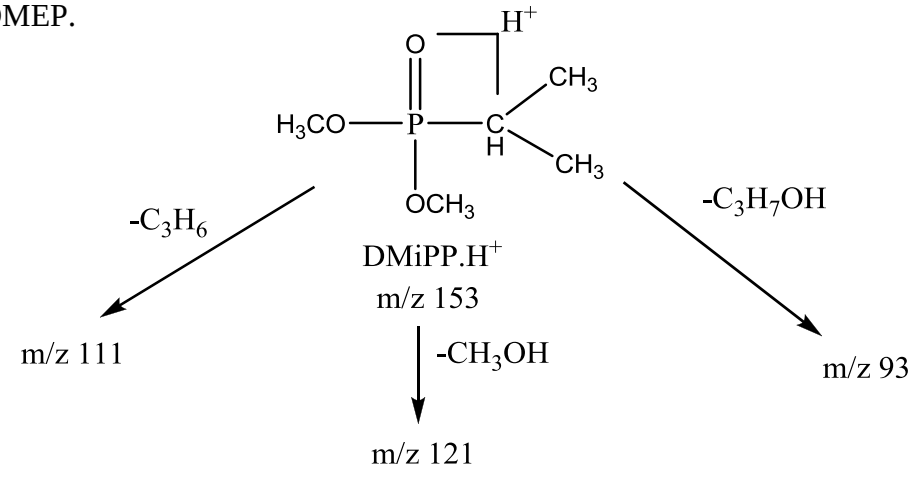

Figure 5.15 Additional fragmentation pathways of $DMiPP.H^+$ to that of $DMnPP.H^+$

5.4.4 Fragmentations of nitrogen-containing organophosphorus esters

The compounds JLM165, JLM155, JLM154, JLM159, JLM139, JLM148 and JLM131 are all nitrogen containing organophophates (structures are shown in Appendix E and in the relevant fragmentation pathway diagrams). The fragmentation pathways of JLM155, 154 and 131 were already proposed by Jo Mundy of dstl, Porton Down, Salisbury. These were simply checked for agreement and are shown in figures 5.16-5.18. The fragmentation pathways are as expected from previous results.

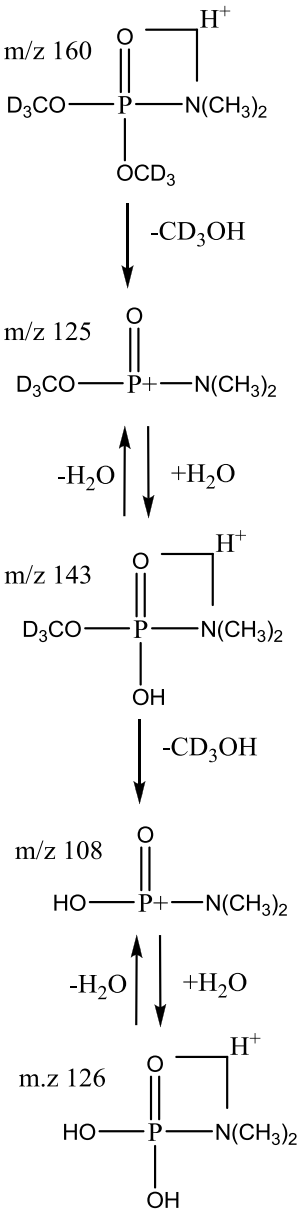

Figure 5.16 Fragmentation pathway of JLM155

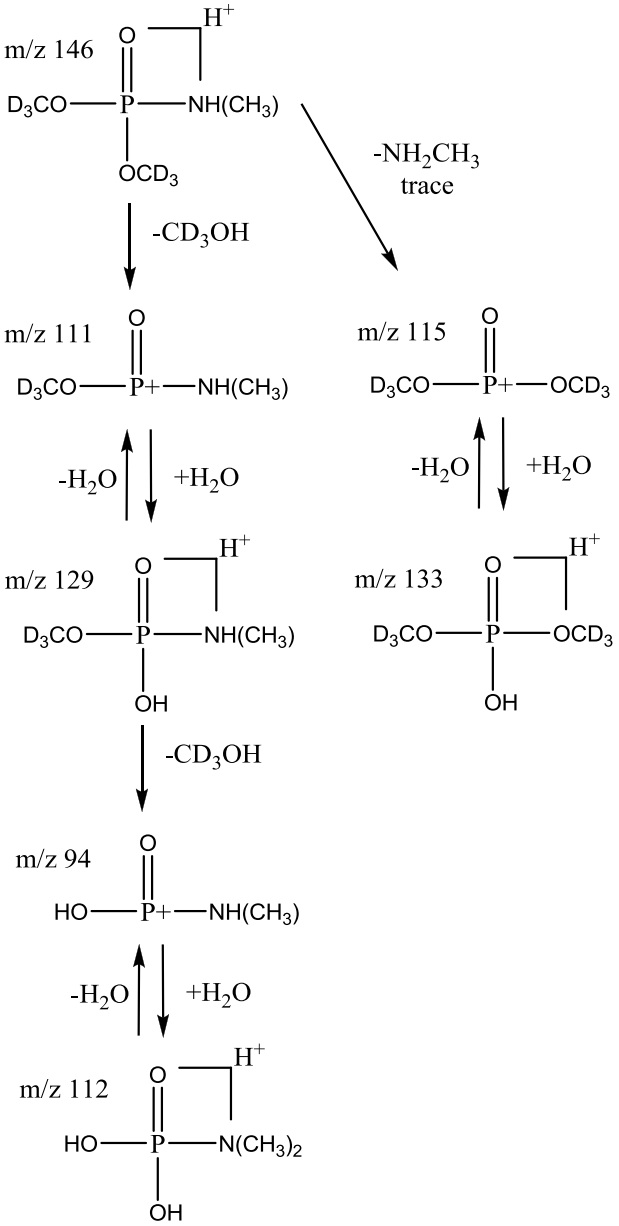

Figure 5.17 Fragmentation pathway of JLM154

The compounds JLM 155 and JLM 154 (figures 5.16 & 5.17) showed no unusual fragmentations. Mass spectral runs of both these chemicals were repeated with D_2O in solution in place of H_2O. This produced a parent ion of MD^+, and the fragmentation pathways appeared to be the same for JLM155. In JLM154, the labile hydrogen on the nitrogen atom appeared to be replaced in a certain percentage of ions by deuterium, as expected. It is not clear what this percentage is or whether it varies with the ion fragment. For example, it appears that the majority of the parent ion becomes m/z 148 with deuterium on the nitrogen atom. However, the appearance of m/z 111, 112 and 113 in the mass spectrum obtained in D_2O solution confuses matters. The peak at m/z 112 could either be the ion in the original fragmentation pathway (figure 5.17) or it could be a deuterated version of m/z 111.

For the compound JLM131 (figure 5.18) it is clear that the hydrogen is lost from the β-carbon of the deuterated ethyl groups to create m/z 184 and 154 and no scrambling is observed. It would be interesting to deuterate the ethyl groups on the nitrogen atom to confirm whether the hydrogen is lost from the α or β carbon, or even both, when fragmenting to m/z 126 and 98.

Fragmentations of JLM165, JLM159, JLM139 and JLM148 were investigated for the first time in this project and their fragmentation pathways are given in figures 5.19-5.21. The JLM165 and JLM159 fragmentations are extensive, yet straightforward. In figure 5.19 for the fragmentation pathway of JLM165, about half of the fragments produced are only present in trace quantities. This means that the ion peaks are present from scan to scan, but that they are significantly lower than any of the other fragments.

The red numbers on the fragmentation pathway of JLM159 (figure 5.20) correspond to the branching ratios of the various pathways. These are simply the ratio of peak intensities of the daughter ions. The loss of ethene from the nitrogen atom consistently has a higher probability (~10:1) of occurrence than the loss of methanol from the phosphorus atom.

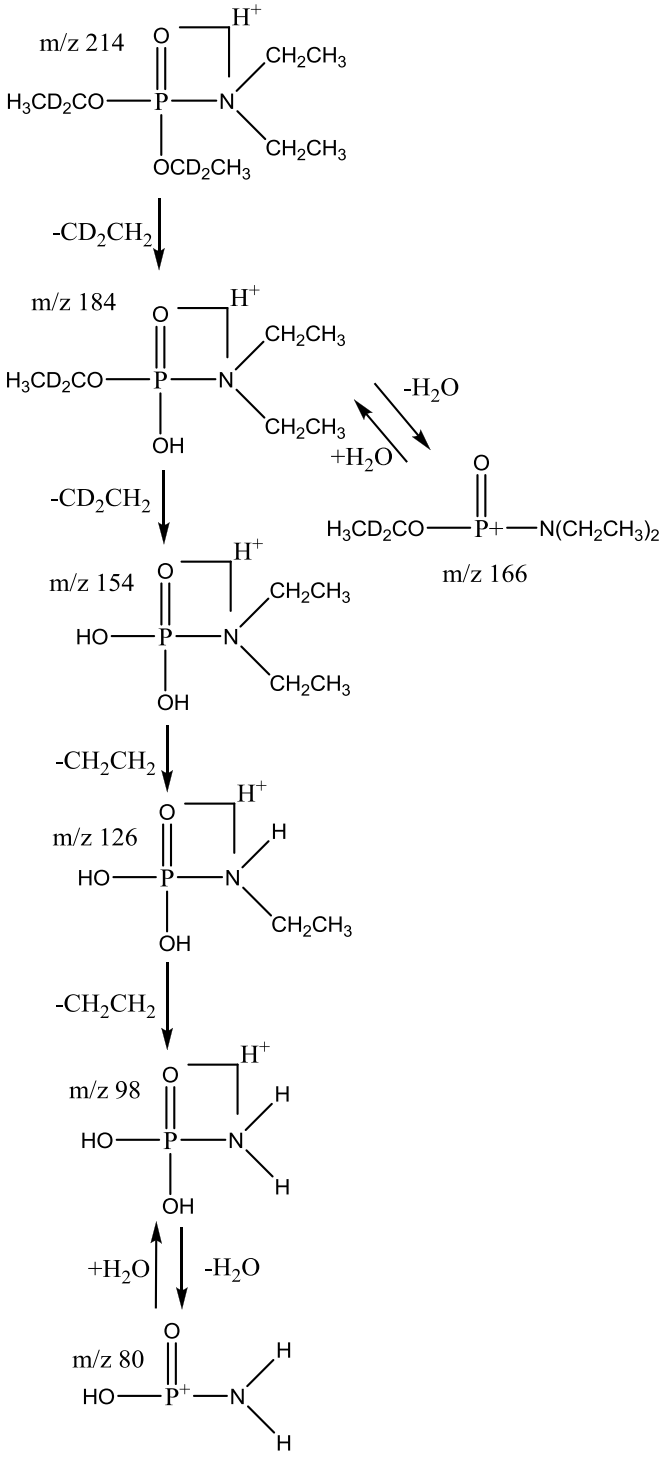

Figure 5.18 Fragmentation pathway of JLM131

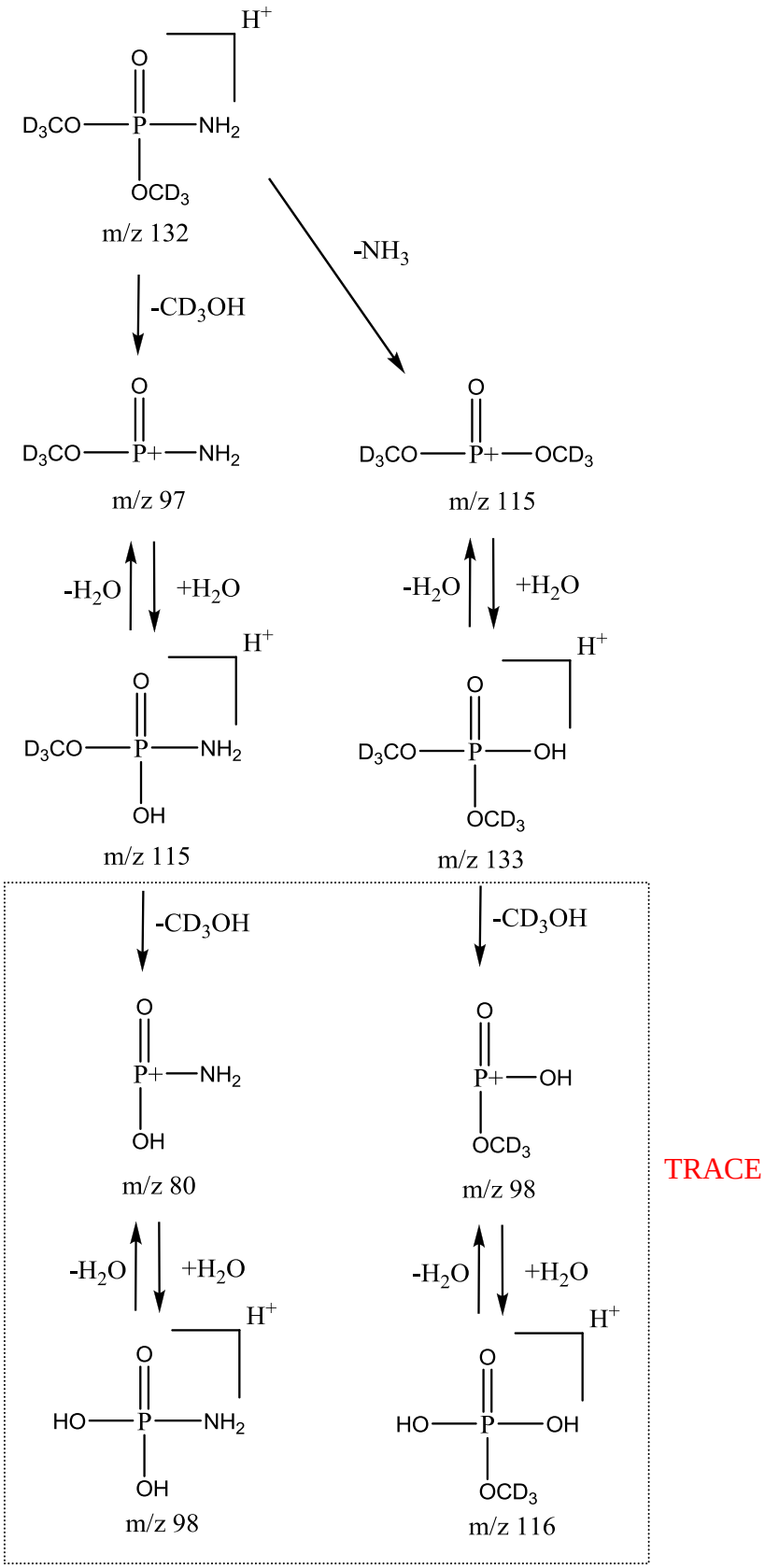

Figure 5.19 Fragmentation pathway of JLM165

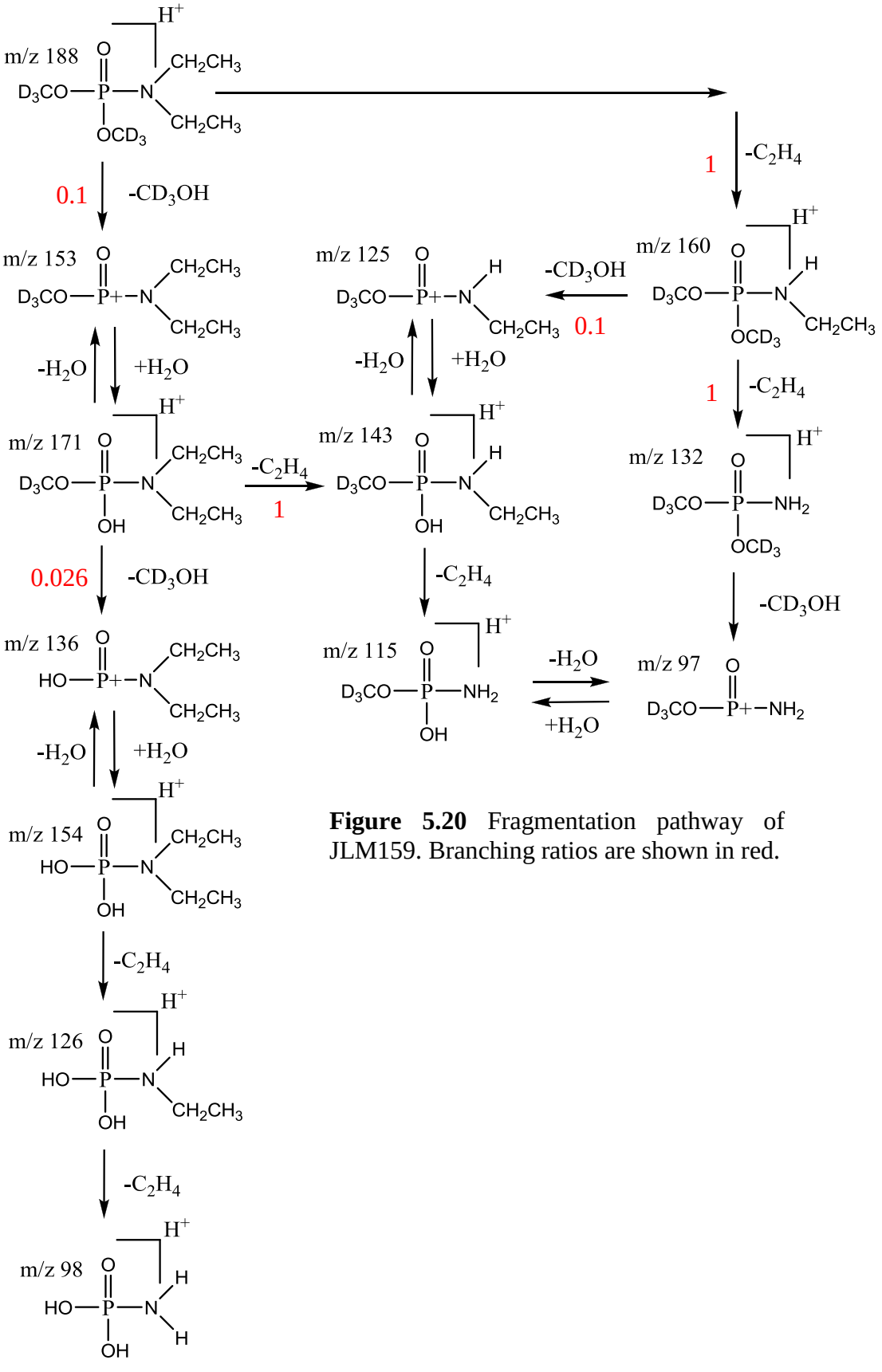

Figure 5.20 Fragmentation pathway of JLM159. Branching ratios are shown in red.

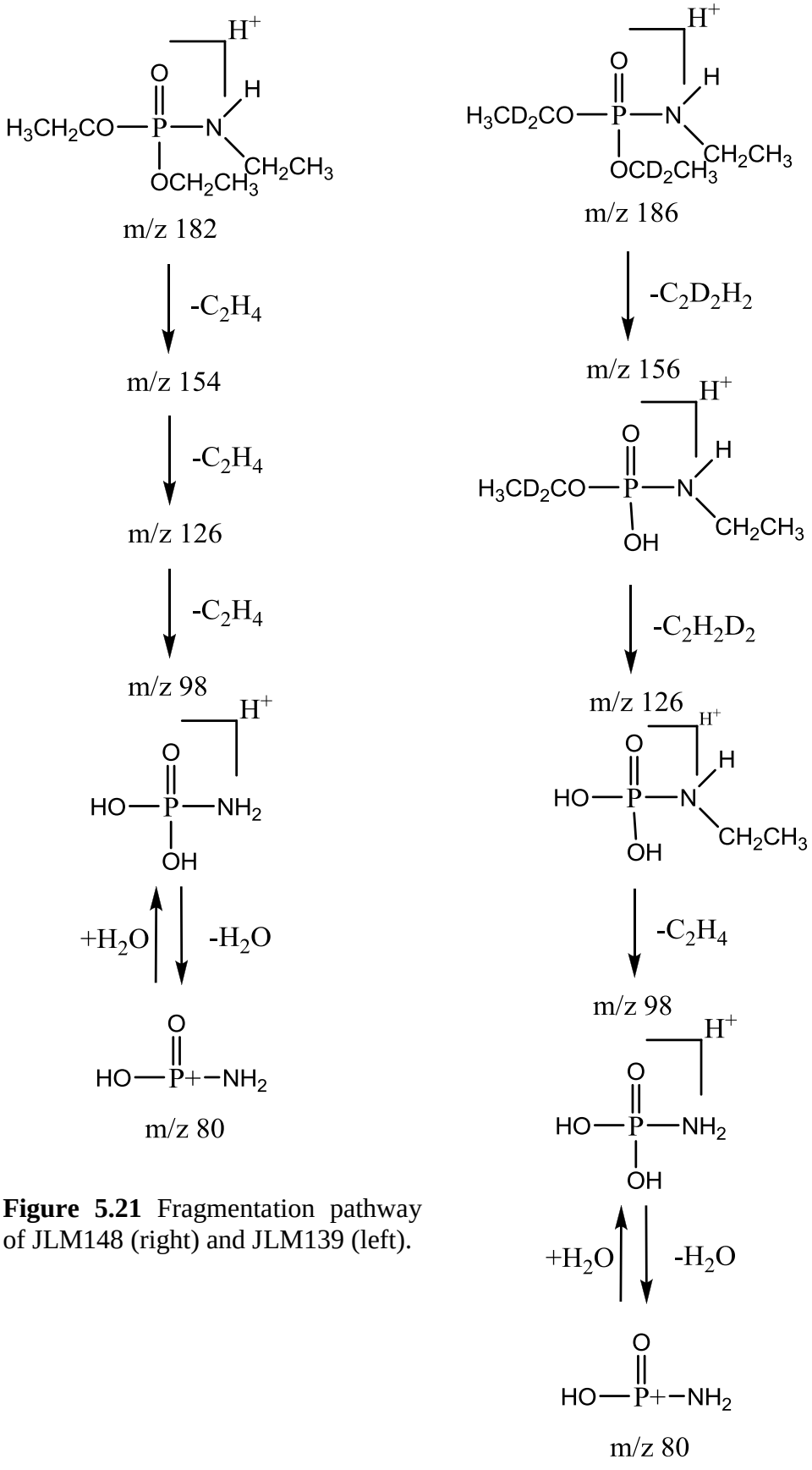

Figure 5.21 Fragmentation pathway of JLM148 (right) and JLM139 (left).

Fragmentations of JLM139 (figure 5.21 left) show the loss of each of the ethene groups one by one, although it is not clear in which order. JLM148 (figure 5.21 right) has deuterated ethyl groups on the oxygen and fragmentations are as expected. It is apparent that the hydrogen is eliminated from the β-carbon on the P-ethyl groups, and therefore there is no scrambling.

5.4.5 Fragmentations of some further organophosphorus esters

The compounds MB594, MB45, MB48, MB51, MB53, MB54, MB59, MB61 and MB63 are all alkyl methyl methylphosphonates (chemical structures are shown in appendix E). Upon fragmentation, all these chemicals eliminated the alkene from the alkyl group to produce the same daughter fragment at m/z 111, which is equivalent to protonated methyl hydrogen methylphosphonate as shown in figure 5.22. This implies that all side groups broke between the C-O bond, and left a hydrogen to form the hydroxyl group. It was anticipated that by varying the fragmentation conditions some measure of the relative reaction rates of fragmentation may be obtained. However, this was not the case. The relative peak intensities of the fragment ions did not appear to differ greatly from compound to compound under the same fragmentation conditions. Reaction kinetics for each compound were hard to measure due to instabilities in the peak signal.

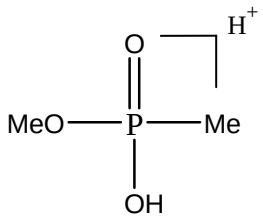

Figure 5.22 Protonated methyl methylphosphonate

5.5 Conclusions and further work

Deuterated DMEP.H^+ shows elimination of methanol followed by ethene. Both α and β hydrogens are eliminated from the ethyl group, the β-elimination being the dominant fragmentation pathway. From DFT calculations, possible mechanisms for this elimination have been elucidated; considering the enthalpies of the most energetically favourable mechanism, it is implied that the branching ratio for α and β elimination should be unity. Only upon taking entropy into consideration can the preference for β elimination be explained. The large entropy change of the final, and otherwise rate-determining, step reduces the free energy of the transition so that previous transitions in the fragmentation mechanism become the rate-determining steps. Therefore, when ignoring the final dissociation step, the calculated energetics show a preference for β elimination.

A similar fragmentation pathway is seen in DMnPP.H^+, methanol is eliminated followed by propene. Upon fragmenting the isotopomers with deuterium on the α and γ-hydrogen of the propyl group, it is clear that several fragmentation pathways are available involving γ- and α- hydrogen elimination and possibly β elimination. This can only be interrogated properly with further DFT calculations and deuterated isotopomers of the β hydrogens. Fragmentation of DMiPP.H^+ also shows elimination of methanol followed by elimination of propene, similar to DMnPP. However, DMiPP shows an interesting and unexpected elimination of propene and propanol from the parent ion, the mechanism and structures of the fragments of which also require further investigation. The DFT calculations and discussions for these mechanisms are a work in progress and are summarised in the draft paper in Appendix D.

The nitrogen-containing organophosphorus esters show expected fragmentations with little signs of scrambling. It may be interesting to repeat the experiments for JLM131,

particularly with deuterium labelling of the α and β carbons of the ethyl groups on the nitrogen atom.

Other organophosphorus esters with large side groups all fragment to form methyl methylphosphonate, therefore cleaving at the PO-C bond. No further work needs be undertaken for this group of chemicals.

From these experiments, further understanding has been gained of the nature of nerve gas derivatives. In particular, fragmentation pathways help to increase knowledge of the possible degradation products that may occur once these toxic chemicals have been released into the atmosphere. This can aid in the detection of these chemicals and points to potential longer term risks of the use of nerve gas agents and insecticides.

References

1. Bell, A. J., Ferrante, F., Hall, S. E., Mikhailov, V., Mitchell, D., Timperley, C. M., Watts, P., and Williams, N., *Fragmentations and reactions of protonated O,O-dimethyl ethylphosphonate and some isotopomers produced by electrospray ionisation in an ion trap mass spectrometer.* International Journal of Mass Spectrometry, 2008. **269**(1-2): p. 46-54.
2. Smiths Detection Ltd., *The GID-3 chemical agent detector*. [cited 2010; http://www.smithsdetection.com/eng/GID-3.php].
3. Smiths Detection Ltd., *IONSCAN 500DT Simultaneous Explosives and Narcotics Trace Detector*. [cited 2007; http://www.smithsdetection.com/eng/1526.php].
4. Li, F., Xie, Z., Schmidt, H., Sielemann, S., and Baumbach, J. I., *Ion mobility spectrometer for online monitoring of trace compounds.* Spectrochimica Acta Part B-Atomic Spectroscopy, 2002. **57**(10): p. 1563-1574.
5. Committee on Assessment of Security Technologies for Transportation, National Materials Advisory Board, Division of Engineering and Physical Sciences, National Research Council, *Opportunities to Improve Airport Passenger Screening with Mass Spectrometry*. 2004: National Academic Press.
6. Hill, H.H., and Martin, S.J., *Conventional analytical methods for chemical warfare agents.* Pure Applied Chemistry, 2002. **74**(12): p. 2281-2291.
7. Williams, D. and Pappas, G., *Rapid Identification of Nerve Agents Sarin (GB) and Soman (GD) with the Use of a Field-Portable GC/SAW Vapor Detector and Liquid Desorption Front-End Device.* Field Analytical Chemistry and Technology, 1999. **3**(1): p. 45-53.
8. Grate, J.W., Rose-Pehrsson, S.L., Venezky, D.L., Klusty, M., and Wohltjen, H., *Smart Sensor System for Trace Organophosphorus and Organosulfur Vapor Detection Employing a Temperature-Controlled Array of Surface Acoustic Wave Sensors, Automated Sample Preconcentration, and Pattern Recognition.* Analytical Chemistry, 1993. **65**(1868-1881).
9. Smith, S. J., *Detection methods for highly toxic organophosphonates : A literature survey.* Talanta, 1983. **30**(10): p. 725-739.

10. Gupta, A.K., Shakya, P.D., Pardasani, D., Palit, M., and Dubey, D.K., *Mass spectral analysis of synthones of nerve agents for verification of the Chemical Weapons Convention.* Rapid Communications in Mass Spectrometry, 2005. **19**: p. 975-983.
11. Smith, P.A., Sng, M.T., Eckenrode, B.A., Leow, S.Y., Koch, D., Erickson, R.P., Jackson Lepage, C.R., and Hook, G.L.,, *Towards smaller and faster gas chromatography–mass spectrometry systems for field chemical detection.* Journal of Chromatography A, 2005. **1067**: p. 285-294.
12. Lei, M., Xi, H., Xu, D., and Chen, Z., *Identification of certain chemical agents in complex organic solutions by gas chromatography/tandem mass spectrometry.* Journal of Mass Spectrometry, 2006. **41**: p. 1453-1458.
13. Sferopoulos, R., *A Review of Chemical Warfare Agent (CWA) Detector Technologies and Commercial-Off-The-Shelf Items*, Australian Government Department of Defence, 2009, Human Protection and Performance Division, DSTO Defence Science and Technology Organisation
14. Bajgar, J., *Complex View on Poisoning with Nerve Agents and Organophosphates.* Acta Medica, 2005. **48**(1): p. 3-21.
15. Frishman, G. and Amirav, A., *Fast GC-PFPD System for Field Analysis of Chemical Warfare Agents.* Field Analytical Chemistry and Technology, 2000. **4**(4): p. 170-194.
16. Eiceman, G.A., and Karpas, Z., *Ion Mobility Spectrometry*. 2005, Taylor & Francis Group: Boca Raton.
17. Puton, J., Nousiainen, M., and Sillanpaa, M., *Ion mobility spectrometers with doped gases.* Talanta, 2008. **76**(5): p. 978-987.
18. Bradbury, N. E. and Nielsen, R. A., *Absolute values of the electron mobility in hydrogen.* Physical Review, 1936. **49**(5): p. 0388-0393.
19. Rutherford, E., Phil. Mag., 1897. **44**: p. 422-440.
20. Roentgen, W.C., Nature, 1895. **53**: p. 274-276.
21. Lattey, R.T. and Tizard, H.T., *The velocity of ions in dried gases.* Proceeedings of the Royal Society of London (A), 1913. **86**: p. 349-357.
22. Cohen, M.J. and Karasek, F.W., *Plasma Chromatography - A new dimension for gas chromatography and mass spectrometry.* Journal of Chromatographic Science, 1970. **8**(6): p. 330-337.

23. Karasek, F.W. and Tatone, O.S., *Plasma Chromatography of the Mono-Halogenated Benzenes.* Analytical Chemistry, 1972. **44**(11): p. 1758-1763.
24. Karasek, F.W., *Qualitative Studies of Trace Constituents by Plasma Chromatography.* Analytical Chemistry, 1971. **43**(11): p. 1441-1447.
25. Karasek, F.W., *Plasma Chromatography of the PolychIorinated BiphenyIs.* Analytical Chemistry, 1971. **43**(14): p. 1982-1986.
26. Baim, M.A. and Hill, H.H., *Tunable Selective Detection for Capillary Gas Chromatography by Ion Mobility Monitoring.* Analytical Chemistry, 1982. **54**(1): p. 38-43.
27. Collins, D.C. and Lee, M.L. , *Developments in ion mobility spectrometry-mass spectrometry.* Analytical and Bioanalytical Chemistry, 2002. **372**(1): p. 66-73.
28. Sysoev, A., Adamov, A., Viidanoja, J., Ketola, R.A., Kostiainen, R., and Kotiaho, T., *Development of an ion mobility spectrometer for use in an atmospheric pressure ionization ion mobility spectrometer/mass spectrometer instrument for fast screening analysis.* Rapid Communications in Mass Spectrometry, 2004. **18**: p. 3131-3139.
29. Hill, C.A. and Thomas, C.L.P., *A pulsed corona discharge switchable high resolution ion mobility spectrometer-mass spectrometer.* The Analyst, 2003. **128**: p. 55-60.
30. McDaniel, E.W. and Mason, E.A., *Transport properties of ions in gases*. 1987, New York: John Wiley & Sons.
31. Yamashita, M. and Fenn, J.B., *Electrospray Ion Source. Another Variation on the Free-Jet Theme.* Journal of Physical Chemistry, 1984. **88**: p. 4451-4459.
32. Barr, J.D., Bell, A.J., Bird, M., Mundy, J.L., Murrell, J., Timperley, C.M., Watts, P., and Ferrante, F., *Fragmentations and Reactions of the Organophosphate Insecticide Diazinon and its Oxygen Analog Diazoxon Studied by Electrospray Ionization Ion Trap Mass Spectrometry.* American Society for Mass Spectrometry, 2005. **16**: p. 515-523.
33. Zhu, Z., Zhang, H., Zhao, L., Dong, X., Li, X., Chai, Y., and Zhang, G., *Rapid separation and identification of phenolic and diterpenoid constituents from Radix Salvia miltiorrhizae by high-performance liquid chromatography diode-array detection, electrospray ionization time-of-flight mass spectrometry and electrospray ionization quadrupole ion trap mass spectrometry.* Rapid Communications in Mass Spectrometry, 2007. **21**: p. 1855-1865.

34. Paul, W. and Steinwedel, H., *Apparatus for separating charged particles of different specific charges*, US Patent number 1960
35. Bonner, R.F., Fulford, J.E., March, R.E., and Hamilton, J.F. , *The cyclindrical Ion Trap. Part I. General Introduction.* International Journal of Mass Spectrometry and Ion Processes, 1977. **24**: p. 255-269.
36. Bier, M.E. and Syka, J.E.P., *Ion trap mass spectrometer system and method* Finnigan Corporation, US Patent number 5420425, 1995
37. Dawson, P.H. and Whetten, N.R., *Three-dimensional quadrupole mass spectrometer and gauge*, US Patent number 3527939, 1970
38. Stafford, G.C., Kelley, P.E., Syka, J.E.P., Reynolds, W.E., and Todd, J.F.J., *Recent Improvements in and Analytical Applications of Advanced Ion Trap Technology.* International Journal of Mass Spectrometry and Ion Processes, 1984. **60**: p. 85-98.
39. Black, D. M., Payne, A. H., and Glish, G. L., *Determination of cooling rates in a quadrupole ion trap.* Journal of the American Society for Mass Spectrometry, 2006. **17**(7): p. 932-938.
40. Louris, J.N., Cooks, R.G., Syka, J.E.P., Kelley, P.E., Stafford, G.C., and Todd, J.F.J., *Instrumentation, Applications, and Energy Deposition in Quadrupole Ion-Trap Tandem Mass Spectrometry.* Analytical Chemistry, 1987. **59**: p. 1677-1685.
41. Morand, K.L, Cox, A.K. and Cooks, R.G., *Efficient trapping and collision-induced dissociation of high-mass cluster ions using mixed target gases in the quadrupole ion trap.* Rapid Communications in Mass Spectrometry, 1992. **6**: p. 520-523.
42. Dehmelt, H.G., *Radiofrequency spectroscopy of stored ions I: Storage*, in *Advances in Atomic and Molecular Physics*, D.R. Bates, Editor. 1967, Academic: New York. p. 53-72.
43. March, R.E., and Todd, J. F. J., *Quadrupole Ion Trap Mass Spectrometry*. Second ed. Chemical Analysis: A series of Monographs on Analytical Chemistry and it's Applications, ed. J D Winefordner. Vol. 165. 2005, Hoboken: John Wiley & Sons Inc. .
44. Mathieu E, *The vibrational movement of a membrane in the shape of an ellipse.* Journal of applied and pure mathematics, 1868. **13**(2): p. 137-203.
45. McLachan, N.W., *Theory and Applications of Mathieu Functions*. 1947, Oxford: Clarendon.

46. Titov, V.V., *Detailed Study of the Quadrupole Mass Analyzer Operating Within the First, Second, and Third (Intermediate) Stability. I Analytical Approach.* American Society for Mass Spectrometry, 1998. **9**: p. 50-69.
47. Nie, Z. X., Lin, C.W., Peng, W. P., Lee, Y. T. , and Chang, H. C., *Frequency Scan of a Quadrupole Mass Analyzer in the Third Stability Region for Protein Analysis.* Journal of the Chinese Chemical Society, 2006. **53**: p. 47-52.
48. Ltd., Smiths Detection, *The GID-M chemical agent detector*. 2007, Smiths Detection Ltd.
49. Kim, S. H., Karasek, F. W., and Rokushika, S., *Plasma Chromatography with Ammonium Reactant Ions.* Analytical Chemistry, 1978. **50**(1): p. 152-155.
50. Cao, L., Harrington, P. D., Harden, C. S., McHugh, V. M., and Thomas, M. A., *Nonlinear wavelet compression of ion mobility spectra from ion mobility spectrometers mounted in an unmanned aerial vehicle.* Analytical Chemistry, 2004. **76**(4): p. 1069-1077.
51. Proctor, C. J. and Todd, J. F. J., *Alternative Reagent Ions for Plasma Chromatography.* Analytical Chemistry, 1984. **56**(11): p. 1794-1797.
52. Munro, W. A., Thomas, C. L. P., and Langford, M. L., *Characterisation of the molecular ions produced by a dinitroalkane in positive mode ion mobility spectrometry with water, dichloromethane and ammonia reactant ion chemistries.* Analytica Chimica Acta, 1998. **374**(2-3): p. 253-267.
53. Khayamian, T., Tabrizchi, M., and Jafari, M. T., *Quantitative analysis of morphine and noscapine using corona discharge ion mobility spectrometry with ammonia reagent gas.* Talanta, 2006. **69**(4): p. 795-799.
54. Kanu, A. B., Dwivedi, P., Tam, M., Matz, L., and Hill, H. H., *Ion mobility-mass spectrometry.* Journal of Mass Spectrometry, 2008. **43**(1): p. 1-22.
55. Steiner, W.E., Klopsch, S.J., English, W.A., Clowers, B.H., and Hill, H.H., *Detection of a Chemical Warfare Agent Simulant in Various Aerosol Matrixes by Ion Mobility Time-of-Flight Mass Spectrometry.* Anal. Chem., 2005. **77**: p. 4792-4799.
56. Steiner, W. E., Clowers, B. H., Fuhrer, K., Gonin, M., Matz, L. M., Siems, W. F., Schultz, A. J., and Hill, H. H., *Electrospray ionization with ambient pressure ion mobility separation and mass analysis by orthogonal time-of-flight mass spectrometry.* Rapid Communications in Mass Spectrometry, 2001. **15**(23): p. 2221-2226.

57. Giles, K. and Grimsrud, E. P., *The Kinetic Ion Mobility Mass-Spectrometer - Measurements of Ion Molecule Reaction-Rate Constants at Atmospheric-Pressure.* Journal of Physical Chemistry, 1992. **96**(16): p. 6680-6687.
58. Eiceman, G. A., Shoff, D. B., Harden, C. S., and Snyder, A. P., *Fragmentation of butyl acetate isomers in the drift region of an ion mobility spectrometer.* International Journal of Mass Spectrometry and Ion Processes, 1988. **85**(3): p. 265-275.
59. Clowers, B.H. and Hill, H.H., *Mass Analysis of Mobility-Selected Ion Populations Using Dual Gate, Ion Mobility, Quadrupole Ion Trap Mass Spectrometry.* Anal. Chem., 2005. **77**: p. 5877-5885.
60. Blake, R. S., Monks, P. S., and Ellis, A. M., *Proton-Transfer Reaction Mass Spectrometry.* Chemical Reviews, 2009. **109**(3): p. 861-896.
61. Wong, P.H. and Cooks, R. G., *Ion Trap Mass Spectrometry.* Current Separations and Drug Development, 1997. **16**(3).
62. Dain, R. P. and Van Stipdonk, M. J., *Generation and collision-induced dissociation of ammonium tetrafluoroborate cluster ions.* Rapid Communications in Mass Spectrometry, 2008. **22**(13): p. 2044-2052.
63. Traldi, P., Catinella, S., March, R.E., and Creaser, C.S., *Chapter 7: Boundary excitation*, in *Practical Aspects of Ion Trap Mass Spectrometry*, R.E. March and J. F. J. Todd, Editors. 1995, CRC Press.
64. *IUPAC Compendium of Chemical Terminology, resolution (mass spectrometry)*. [cited 2010; http://old.iupac.org/goldbook/R05318.pdf].
65. Tabrizchi, M., *Temperature effects on resolution in ion mobility spectrometry.* Talanta, 2004. **62**(1): p. 65-70.
66. Kanu, A. B., Gribb, M. M., and Hill, H. H., *Predicting optimal resolving power for ambient pressure ion mobility spectrometry.* Analytical Chemistry, 2008. **80**(17): p. 6610-6619.
67. Watts, P. and Wilders, A., *On the Resolution Obtainable in Practical Ion Mobility Systems.* International Journal of Mass Spectrometry and Ion Processes, 1992. **112**(2-3): p. 179-190.
68. Khayamian, T. and Jafari, M. T., *Design for electrospray ionization-ion mobility spectrometry.* Analytical Chemistry, 2007. **79**(8): p. 3199-3205.

69. Rokushika, S., Hatano, H., Baim, M. A., and Hill, H. H., *Resolution Measurement for Ion Mobility Spectrometry.* Analytical Chemistry, 1985. **57**(9): p. 1902-1907.

70. *Signal-to-noise ratio*. [cited 2010; http://en.wikipedia.org/wiki/Signal-to-noise_ratio].

71. Fehsenfeld, F.C. and Ferguson, E. E., *Thermal Energy Positive-Ion Reactions in a Wet Atmosphere Containing Ammonia.* Journal of Chemical Physics, 1973. **59**(12): p. 6272-6276.

72. Karpas, Z. and Pollevoy, Y., *Ion Mobility Spectrometric Studies of Organophosphorus Compounds.* Analytica Chimica Acta, 1992. **259**(2): p. 333-338.

73. Goeringer, D. E. and McLuckey, S. A., *Evolution of ion internal energy during collisional excitation in the Paul ion trap: A stochastic approach.* Journal of Chemical Physics, 1996. **104**(6): p. 2214-2221.

74. Vautz, W., Zimmermann, D., Hartmann, M., Baumbach, J. I., Nolte, J., and Jung, J. , *Ion mobility spectrometry for food quality and safety* Food Additives and Contaminants, 2006. **23**(11): p. 1064-1073.

75. Frisch, M.J., Trucks, G.W., Schlegel, H.B., G.E. Scuseria, M.A. Robb, J.R., Cheeseman, J.A. Montgomery Jr., T. Vreven, K.N. Kudin, J.C. Burant, J.M., Millam, S.S. Iyengar, J. Tomasi, V. Barone, B. Mennucci, M. Cossi, G. Scalmani,, N. Rega, G.A. Petersson, H. Nakatsuji, M. Hada, M. Ehara, K. Toyota,, R. Fukuda, J. Hasegawa, M. Ishida, T. Nakajima, Y. Honda, O. Kitao, H., Nakai, M. Klene, X. Li, J.E. Knox, H.P. Hratchian, J.B. Cross, C. Adamo, J., Jaramillo, R. Gomperts, R.E. Stratmann, O. Yazyev, A.J. Austin, R. Cammi,, C. Pomelli, J.W. Ochterski, P.Y.Ayala, K. Morokuma, G.A.Voth, P. Salvador,, J.J. Dannenberg, V.G. Zakrzewski, S. Dapprich, A.D. Daniels, M.C. Strain,, O. Farkas, D.K. Malick, A.D. Rabuck, K. Raghavachari, J.B. Foresman, J.V., Ortiz, Q. Cui, A.G. Baboul, S. Clifford, J. Cioslowski, B.B. Stefanov, G., Liu, A. Liashenko, P. Piskorz, I. Komaromi, R.L. Martin, D.J. Fox, T. Keith,, M.A. Al-Laham, C.Y. Peng, A. Nanayakkara, M. Challacombe, P.M.W. Gill,, and B. Johnson, W. Chen, M.W. Wong, C. Gonzalez, J.A. Pople, *Gaussian 03*. 2004, Gaussian Inc., Wallingford CT.

76. Asano, K. G., Goeringer, D. E., and McLuckey, S. A., *Thermal dissociation in the quadrupole ion trap: ions derived from leucine enkephalin.* International Journal of Mass Spectrometry, 1999. **187**: p. 207-219.

77. Bell, A.J., Despeyroux, D., Murrell, J., and Watts, P., *Fragmentation and reactions of organophosphate ions produced by electrospray ionization.* International Journal of Mass Spectrometry and Ion Processes, 1997. **165/166**: p. 533-550.

78. Barr, J.D., Bell, A.J., Konn, D.O., Murrell, J., Timperley, C.M., Waters, M.J., and Watts, P., *Fragmentations and reactions of three isotopically labelled dimethyl methylphosphonate ions produced by electrospray ionisation in an ion trap mass spectrometer.* PHYSICAL CHEMISTRY CHEMICAL PHYSICS, 2002. **4**(11): p. 2200-2205.

79. Bell, A.J., Citra, A., Dyke, J.M., Ferrante, F., Gagliardi, L., and Watts P., *An ab initio and DFT study of the fragmentation and isomerisation of MeP(O)(OMe).* PHYSICAL CHEMISTRY CHEMICAL PHYSICS, 2004. **6**: p. 1213-1218.

80. Becke, A.D., *Density functional thermochemistry 3. The role of exact exchange.* Journal of Chemical Physics, 1993. **98**: p. 5648.

81. Snyder, A.P., and Harden, C.S. , *Part 1: Determination of the fragmentation mechanisms of organophosphorus ions by H2O and D2O atmospheric-pressure ionization tandem mass spectrometry.* Organic Mass Spectrometry, 1990. **25**(1): p. 53-60.

82. Snyder, A.P. and Harden, C.S. , *Part 2: Determination of the fragmentation mechanisms of organophosphorus ions by H2O and D2O atmospheric-pressure ionization tandem mass spectrometry II - dialkyl alkylphosphonate ions.* Organic Mass Spectrometry, 1990. **25**(6): p. 301-308.

APPENDIX A

Chemical structures of some common organophosphate chemicals warfare agents and pesticides

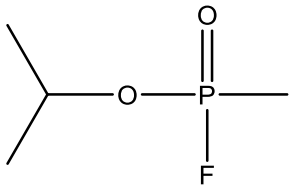

Sarin
Nerve gas (GB)
Highly toxic
CWC Schedule 1

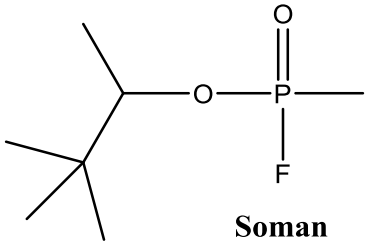

Soman
Nerve gas (GD)
Highly toxic
CWC Schedule 1

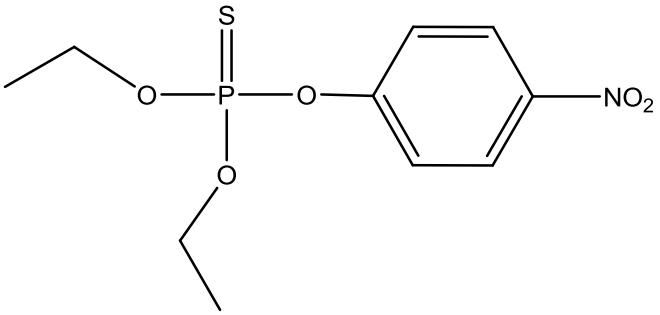

Parathion
Potent insecticide
Now banned and restricted in many countries.
Toxic to humans

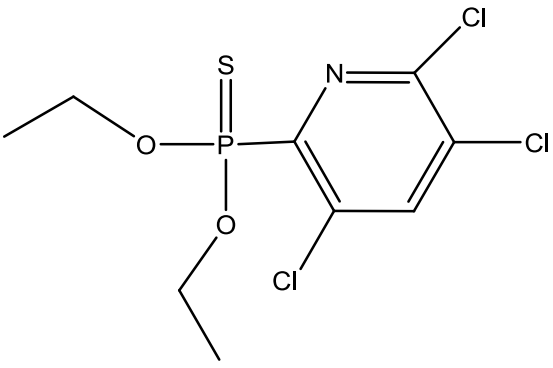

Chlorpyrifos
One of the most widely used
OP insecticides in the US.
Moderatly toxic to humans.

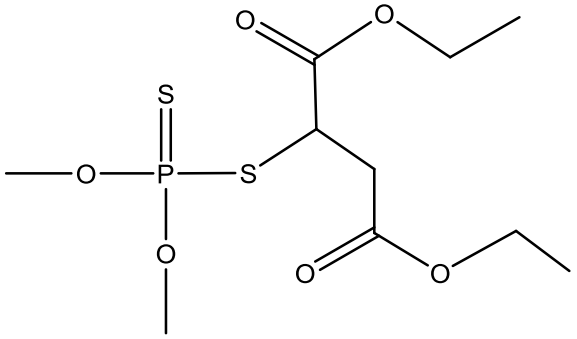

Malathion
Insecticide
Used to combat Mediterranean fruit fly in Australia and
Canada & the West Nile virus-transmitting mosquito.
Low toxicity to Humans

APPENDIX B

The development of an ion mobility spectrometer-ion trap mass spectrometer to investigate ion chemistry occurring in ion mobility systems used in the detection of threat agents

Submitted to Analytical Chemistry

June 2010

Sarah Price,* Peter Watts and Chris A. Mayhew

* Corresponding Author

APPENDIX C

Fragmentations and reactions of protonated *O,O*-dimethyl ethylphosphonate and some isotopomers produced by electrospray ionisation in an ion trap mass spectrometer

International Journal of Mass Spectrometry

2008

A.J. Bell, F. Ferrante , S.E. Hall*, V. Mikhailov, D. Mitchell,

C.M. Timperley, P. Watts and N. Williams.

* NB My maiden name

APPENDIX D

Preliminary discussions and density functional theory calculations of the fragmentation pathways of protonated dimethyl *n*-propylphosphonate and dimethyl isopropylphosphonate[§]

S Price, C A Mayhew and P Watts*

School of Physics and Astronomy, University of Birmingham, Edgbaston, UK

([§]this is a research paper in preparation for submission to International Journal of Mass Spectrometry)

* Corresponding Author

Comment: I have decided not to present this work in the main section of the thesis as an additional chapter, because Dr. P Watts has been the key author of the written material presented here. My contribution has been to take the data and discuss the reactions schemes with Dr. P Watts.

APPENDIX E

Chemicals used in the electrospray ionisation-ion trap mass spectrometry studies in Section 2

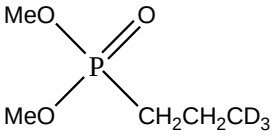

deuterated dimethyl n-propylphosphonate

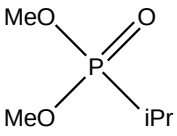

dimethyl i-propylphosphonate

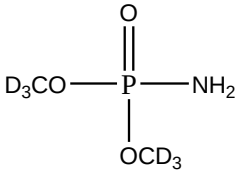

JLM165

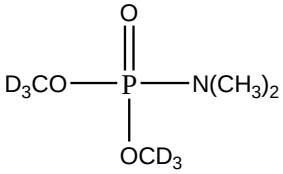

JLM155

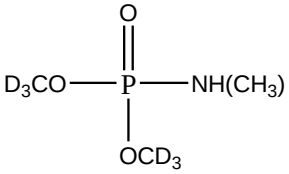

JLM154

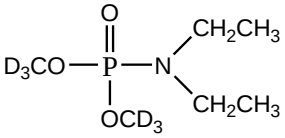

JLM159

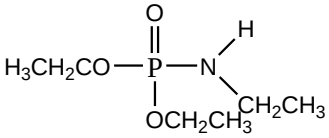

diethyl ethylphosphoramidate
JLM139

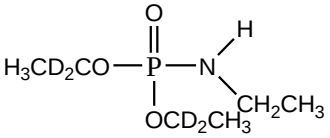

diethyl ethylphosphoramidate
JLM148

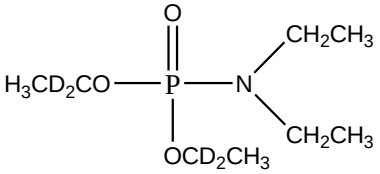

JLM131

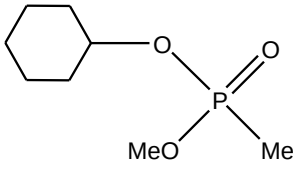

cyclohexyl methyl
methylphosphonate
MB594

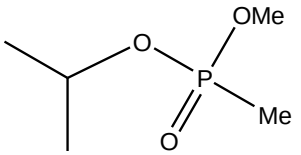

isopropyl methyl methylphosphonate
MB59

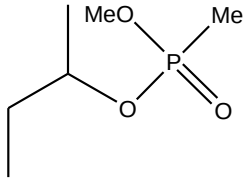

(1*R*)-*sec*-butyl methyl methylphosphonate
MB53

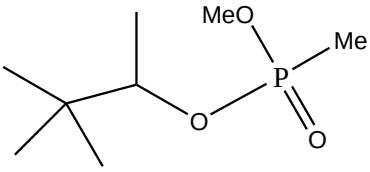

3,3-dimethylbutan-2-yl
methyl methylphosphonate
MB45

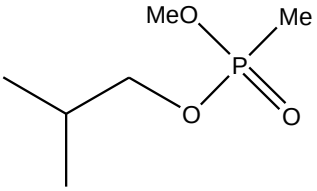

(*R*)-isobutyl methyl
methylphosphonate
MB51

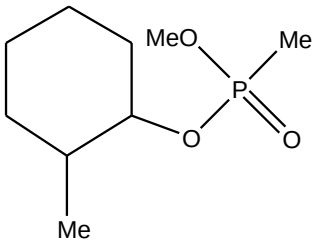

(7*R*)-methyl 2-methylcyclohexyl
methylphosphonate
MB54

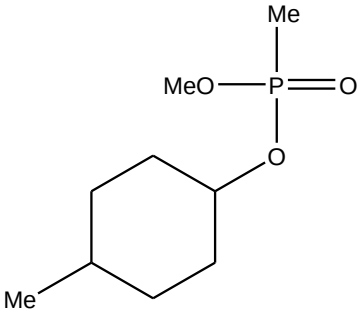

methyl 4-methylcyclohexyl
methylphosphonate
MB48

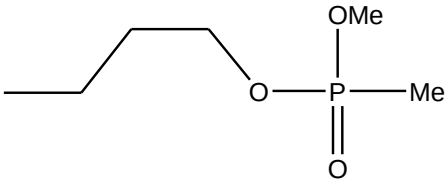

butyl methyl methylphosphonate
MB61

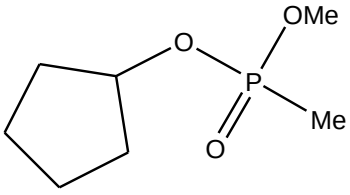

cyclopentyl methyl methylphosphonate
MB63